Ph.D. Dissertation of Agriculture

Cellulose nanocrystal Pickering emulsion of lipophilic liquids and its larvicidal and antimicrobial activities

셀룰로오스 나노결정 기반 친유성 액체 피커링 에멀젼 제조와 살충 및 항균 활성

February 2022

Seoul National University
Department of Agriculture, Forestry and Bioresources

Shin, Jonghyun

Cellulose nanocrystal Pickering emulsion of lipophilic liquids and its larvicidal and antimicrobial activities

Advised by Prof. Hyun, Jinho

Submitting a Ph.D. Dissertation of Agriculture
December 2021

Seoul National University
Department of Agriculture, Forestry and Bioresources

Shin, Jonghyun

Confirming the Ph.D. Dissertation written by
Shin, Jonghyun
December 2021

Chair	Lee, Ki Hoon	(Seal)
Vice Chair	Hyun, Jinho	(Seal)
Examiner	Kim, Tae-il	(Seal)
Examiner	Ki, Chang Seok	(Seal)
Examiner	Yun, Kyusik	(Seal)

Abstract

Ionic cellulose nanocrystals (CNCs) are an interesting surface-active particle for encapsulating oils. A CNC is modified chemically into negatively sulfated CNCs (S-CNCs) by surface treatment with sulfuric acids. Despite the amphiphilic nature of S-CNCs, it is difficult to determine the degree of substitution for emulsification of oils especially whose surface energy is low and polarity is high. Here, the degree of substitution is controlled by desulfation of S-CNCs (dS-CNC) using a low concentration of hydrochloric acid solution. dS-CNC shows the decreased surface charge and the increased hydrophobic affinity compared with S-CNC. Six different oils are selected for determination of the surface tension effect of charged CNCs on the emulsification. The stability of emulsion is evaluated by emulsion fraction, emulsion particle size, and surface tension of emulsified solutions from dS-CNCs and oils.

After the confirming of the surface charge effect of CNCs, highly volatile and hydrophobic essential oils are encapsulated with the amphiphilic CNCs. Pickering emulsion of various essential oils in CNC shell is determined by confocal microscopy with distinct fluorescent labelling. The amount of CNC affects the size distribution of Pickering emulsion and the emulsion stability is confirmed by rheological property and surface tension. The antimicrobial activity of the emulsion is evaluated against *E. coli* and *S. aureus* by minimal inhibitory concentration and minimum bactericidal concentration. The larvicidal activity is also investigated against *Ae. albopictus* by dispersing the emulsion in water. Moreover, the retrieval of the Pickering emulsion carrier of the essential oil is crucial to reduce the

environmental load in the essential oil delivery system. To retrieve the essential oil carrier, the micron-scale Pickering emulsions are embedded in SA to form macroscale hydrogel beads. The structure of the composite hydrogel bead is characterized to confirm the incorporation of SA-Pickering emulsion, and the release behavior is monitored to understand the time-dependent biological activity of the essential oils. The larvicidal performance of the SA-Pickering emulsion composite hydrogel beads is investigated with *Ae. albopictust* larvae.

Keyword: Cellulose nanocrystals, Surface charge effect, Desulfation, Pickering emulsion, Essential oil, Larvicidal effect, Antimicrobial activity

Student Number: 2017-21230

Table of Contents

List of Tables

Lists of Figures

Lists of Abbreviations

Ae. albopictus ..... *Aedes albopictus* Skuse

CHIKV ..... Chikungunya virus

CMC ..... Critical micelle concentration

CNC ..... Cellulose nanocrystal

CNF ..... Cellulose nanofiber

CNM ..... Cellulose nanomaterial

***C. officinale* RE** ..... *Cnidium officinale* root extract

DENV ..... Dengue virus

dS-CNC ..... Desulfated cellulose nanocrystal

E. coli ..... *Escherichia coli*

MBC ..... Minimum bactericidal concentration

MFC ..... Microfibrilled cellulose

MIC ..... Minimal inhibition concentration

NFC ..... Nanofibrilled cellulose

***P. kadsura* SE** ..... *Piper kadsura* stem extract

S. aureus ..... *Staphylococcus aureus*

SA ..... Sodium alginate

S-CNC ..... Sulfated cellulose nanocrystal

I. Introduction

Pickering emulsions are based on the amphiphilic solid particles adsorbed at the interface of the different phase of liquids [1-3]. The amphiphilic particles enhance the oil solubility and dispersibility to the aqueous solution and prevent loss of critical component of oil. In recent, Pickering emulsion has been attracted in cosmetic, food, and pharmaceutical areas for long term storage of phenolic antioxidant compounds and aromatic materials of functional oil [4-6], protection from microbial or food aging [7-9], and sustainable encapsulation of drug [10, 11].

The surface charge of surface active particles is one of the critical factors in Pickering emulsion [12, 13]. Especially, it is difficult for charged surfactant particles to form emulsion droplets due to the repulsive force comprising from Coulomb's law against oils with high polarity [14]. In order to form stable emulsion droplets and introduce thermodynamically stable colloidal dispersion between the droplets, it is necessary to control charge of the surface-active materials.

The amphiphilicity of CNMs comes from its crystalline structures, which are determined by the difference in density between the hydroxyl group and the pyranose ring exposed on the surface of crystalline edges at the stacking process of linearly linked cellobios polymer chain [15, 16]. The covered with abundant layer of CH methane groups (200) crystalline edge plays an important role to adsorbing the cellulose to the oil surface [17]. Among them, CNCs, in particular, are a potential candidate for Pickering particles applicable in biological technology because of their excellent amphiphilicity derived from highly crystalline structures [18-23]. Moreover, the CNC particles can form various oil-encapsulated emulsions by controlling

functional groups at the surface [24, 25]. Since the sulfonate group on S-CNC derived from sulfuric acid hydrolysis [26-29] can be substituted to the hydroxyl group in the presence of hydroxide ion, a diverse functionality can be introduced to the CNC surface [30-32]. Researchers have controlled the surface charge of S-CNC using hydrochloric acid and trifluoroacetic acid [17, 33, 34]. The highly acidic reaction, however, also results in additional acidic hydrolysis of CNCs. To prevent the hydrolysis of CNCs, Tiffany et al. conducted modification of the S-CNC to dS-CNC under the low concentration of acid [35].

Here, S-CNC hydrolyzed with sulfuric acid and dS-CNCs desulfurized with HCl at the difference reaction time were used for the emulsification of nonpolar oils and polar oils. Pickering emulsions prepared with the CNCs are evaluated by the emulsion fraction, emulsion droplet size and surface tension, which are parameters to evaluate the stability of the Pickering emulsions. It will provide a generic idea on the surface charge effect for CNC-based Pickering emulsions.

After the confirming the effect of the surface charge of CNCs on the six oils, the 5 different highly volatile and hydrophobic essential oils are encapsulated by the amphiphilic CNCs for enhancing efficiency of antimicrobial and larvicidal activity. Plant essential oils are secondary metabolic compounds of aromatic plants that have antimicrobial, and larvicidal activity [36-38]. Essential oils extracted by steam distillation or solvent extraction are composed of alcohols, aldehydes, ketones, esters, aromatic phenols, lactones, monoterpenes, and sesquiterpenes [39, 40]. It is considered that essential oils do not evolve harmful side effects because, in general, their components are highly volatile and have short residence times in natural environments such as clear water and soil. However, their volatility

also means that essential oils need to be released in a controlled, steady manner to have the desired larvicidal effect without being wasted by evaporation The S-CNCs closely packed at the surface of an oil can reduce its ability to evaporate and can enable the sustained release of the oil through pores at the nanoscale. In addition, the enhanced solubility of essential oil-Pickering emulsions in water effectively improves their mosquito larvicidal performance [41-43].

Despite the sustained release of essential oils and the high water solubility of Pickering emulsions, it is difficult to remove the S-CNC emulsion carriers have been dispersed in water and used, it is difficult to remove them from the water. The association of Pickering emulsions with a retrievable macroscale hydrogel is a potential solution to this problem. A hydrogel can easily control the release of chemicals entrapped within it by controlling the degree of gelation and pore size. SA hydrogels incorporated with essential oil-Pickering emulsions can be retrieved after the complete release of essential oils to water, which will reduce the environmental load [19, 44-47]. The eco-friendly SA-Pickering emulsions hydrogels are one potential method to control the global disease problems by preventing the growth of mosquito larvae in the future.

II. Literature Survey

2.1. Emulsion

Emulsion is a colloidal dispersion system consisting of two deference immiscible liquids [48, 49]. This metastable solution can be encapsulated by amphiphilic emulsifier. Once an external force is applied to the system, the emulsifier is located at the interface of the two liquids in order to be thermodynamically stable. As more emulsifier is added to the system, the emulsifier continues to reduce the interfacial tension to form stable spherical droplets. Adding an emulsifier manufactures more spherical droplets called micelles in the unstable solution and adding an appropriate amount of emulsifier stabilizes the emulsion.

Emulsion stability implies that the size and spatial arrangement of the droplets do not change over time. The unstable droplets of the emulsion show five different agglomeration patterns depending on the state of the fluid and the kinetic properties of the emulsion (Figure 1) [48, 50, 51].

Creaming and sedimentation states of emulsion results from the different densities between the ambient liquid and the incompletely enclosed liquid by the emulsifier. The droplets in these states keep their droplet size distribution but a vertical concentration gradient of droplets builds up in whole of solution. The exposed large droplets rapidly go up to the top layer (density of liquids: ambient liquid > enclosed liquid) or go down to the bottom layer (density of liquids: ambient liquid < enclosed liquid) [48, 52].

Flocculation state of emulsion is resulted from aggregation of the droplets. The droplets in this state maintain their original size after aggregation. The deficient of repulsive force between droplets causes the van der Waals attraction on the each of droplets. These droplets produce of larger

family of droplets unit in the medium. The family of droplets can be easily broken or strongly aggregated by the external force depending on the magnitude of attractive force on each droplet [49].

Ostwald ripening of the droplets is attributed from small droplets which has unstable surface composition. Over addition of emulsifiers is induced lots of interface area between two liquids. The increase of too much interfacial area makes the interface rather thermodynamically unstable, and the droplets smaller by the unstable interface tend to agglomerate over time and go to a larger family of small droplets or one large droplet to be a stable state [49].

Coalescence state of emulsion implies that collapse of interfacial structure of droplets and forming irreversible liquid film at the top or bottom of solution. Fluctuations of film or surface are the driving force of manufacturing coalescence layer. The van der Waals attraction, which outperforms the colloidal dispersive force attributed by emulsifiers, ensures the layer to remain unseparated [48, 53].

2.1.1. Emulsifier

Emulsifier is the surface-active agents on the emulsion system. This small material is comprised of a hydrophilic head group and a hydrophobic tail group. The water-soluble head group usually has a charge on the surface of structure. The simplest classification of head groups attributed by their polar properties; anionic, cationic, zwitterionic or non-ionic. The polarity of the head group induces a continuous electrical repulsive force on the surface of the droplet, and the properly existed surface ions are effective in manufacturing uniform and well-dispersed colloids. However, too much surface ion concentration increases the repulsive force between the emulsifiers, which increases the minimum area between the emulsifiers,

resulting in a large droplet size. In addition, in the encapsulation of high polar-oils, the surface ions of the emulsifier are maximized by the polar oil and the oil cannot be encapsulated because the polarity of the oil further increases the minimum adsorption area between the emulsifiers. On the other hand, the non-polar head group of emulsifiers can encapsulate liquids with a relatively small amount, and they are easy to manufacture emulsion droplets even if the oil has high polarity. The low repulsive force between the droplets, however, can occur flocculation or coalescence states on the emulsion system. The tail group of emulsifier usually composed of hydrocarbon, fluorocarbon and siloxane. The length of tail group can be controlled hydrophobicity of emulsifier and it also affects to the droplet size. To manufacture the clear droplets at the various conditions, these factors of emulsifier have to be controlled by mixing of various emulsifiers [48, 49, 54].

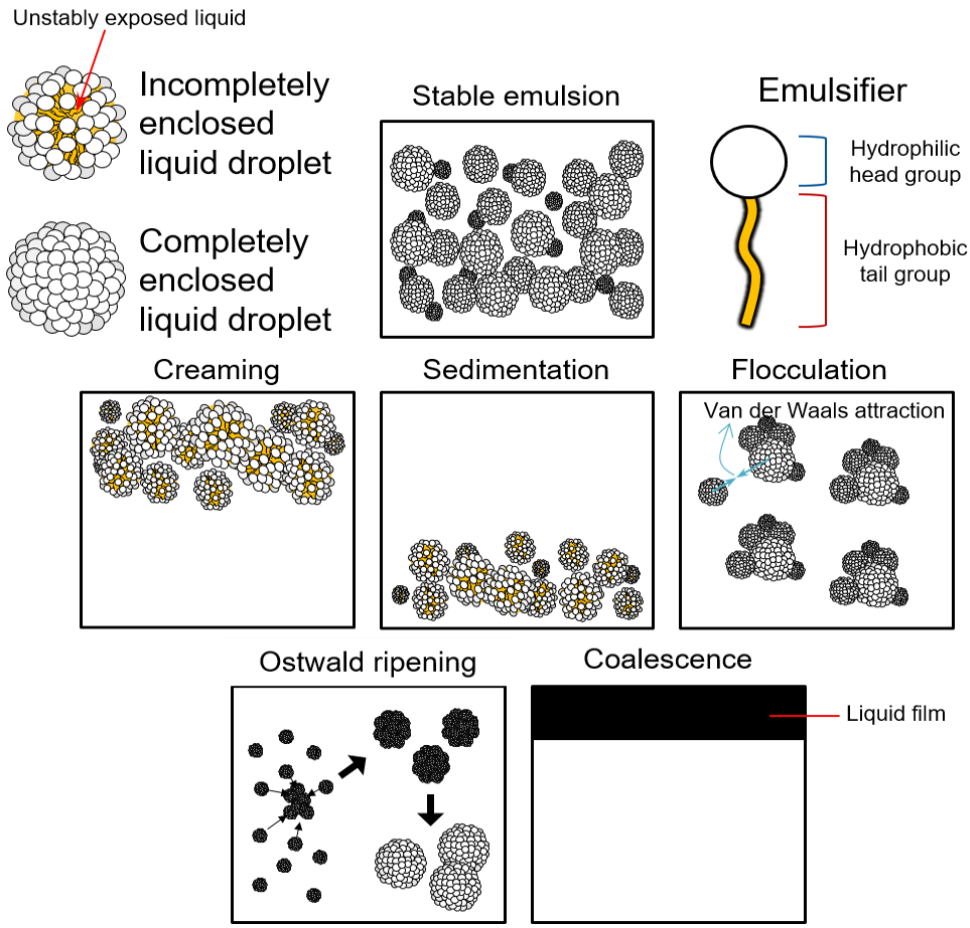

Figure 1. Schematic illustration of emulsifier, micelle and time dependent physical property changes of emulsion droplets at the stable and unstable emulsion (Creaming, sedimentation, flocculation, Ostwald ripening and coalescence).

2.1.2. Critical micelle concentration (CMC)

When the emulsifier added to an aqueous solution, they fill the water/air interface in order to be thermodynamically stable, and after forms micelles in the solution once it has completely filled the interface (Figure 2A). The concentration of emulsifier at this time is called critical micelle concentration (CMC). The CMC is principle parameter in various fields of application involving emulsifier adsorption at the interface, such as cosmetics, foam, emulsion, suspension, and paint. The aqueous solution containing the emulsifier changes several physical properties once it reaches the CMC of the emulsifier [48, 49].

First, the turbidity of solution increases rapidly (Figure 2B). Because emulsifiers exist as a single molecule, the transparency of aqueous solutions does not change below the CMC. However, upon above the CMC, the emulsifier forms micelles and these supermolecular structures reflect all the visible light applied from the outside [55, 56].

Above the CMC, the equilibrium surface tension of the solution can be also obtained (Figure 2C). The surface tension is only changed by the surface-active emulsifiers present on the surface of water materials and the micelle in the bulk does not be concerned with change of surface tension. So, if there are impurities on the surface of solution, they can easily affect to the value of surface tension [31, 57].

As the emulsifier increases in the solution, osmotic pressure also increases because of the free energy of the monomolecular emulsifier in the system (Figure 2D). However, the amphiphilic emulsifiers above the CMC stick together to form micelles and minimize the free energy for thermodynamically stability of system. Hence, the micellar-emulsifier

equilibrium is maintained even when the emulsifier is continuously added, which causing the constant osmotic pressure [58-60].

The preceding factors are important physical properties that determine the CMC in aqueous solution. All the CMC determination factors are recommended that being presented along with other methods for accuracy of the CMC.

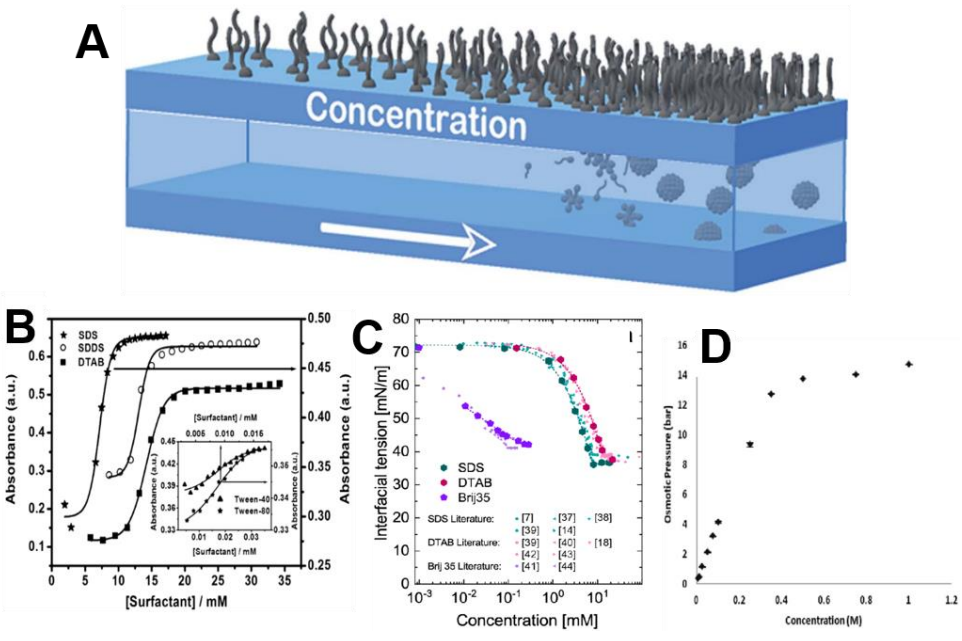

Figure 2. Formation of micelle as a function of emulsifier concentration and critical micelle concentration (CMC). (A) Schematic illustration of micelle formation at the concentration of emulsifier at the surface increases [55]. (B) Dependence of absorbance on surfactant concentration profile for emulsifiers [56], (C) interfacial tension at the A/W interface as a function of emulsifier concentration [57] and (D) measured osmotic pressure in terms of the molar concentration of emulsifier [58].

2.2. Pickering emulsion

A Pickering emulsion is coacervate solution between the two immiscible phases stabilized by amphiphilic particles [61]. Pickering emulsion has a relatively weak hydrophobic interaction of the emulsified polymer than monomolecular surfactant, but once a sufficient amount of particles is adsorbed on the surface at the O/W interface, an irreversible emulsion is formed due to the attraction between the particles. The particles form a porous spherical film at the interface of the two phases, and the formed film not only enhances the dispersibility of the hydrophobic liquid in aqueous solution, but also enables sustained release.

The physical stability of Pickering emulsion determines by the size, shape, rheology and morphology of the fabricated droplets. At the unstable emulsion, the state of droplets is gradually changed over time like droplets stabilized by surfactant [62, 63].

Incompletely adsorbed amphiphilic particles on the O/W interface induce the creaming or sedimentation state of emulsion. In this states, the droplets stick together to reduce the instability of exposed liquid part. The aggregated droplets on the top or bottom of the solution are formed fluctuation each other resulted coalescence film structure over time [64].

The flocculation usually induces by the deficiency of repulsive force between each droplet. At the Pickering emulsions, the surface-active particles can attract because of their structural similarity. Thus, the polar on the surface of droplets plays an important role to prevent flocculation. However, insufficient of polarity on the droplets generates aggregation of droplets resulted by Van der Waals attraction and it produces flocculation of droplets in the Pickering emulsion.

The Ostwald ripening, the coalescence or flocculation state of the Pickering emulsion, occurs because the incompletely absorbed emulsion aggregate each other or the fabrication of too small droplets manufactured by Pickering particles. At the flocculation states, the continuously stacked particles on the O/W interface cause the surface of the droplet to become unstable state. These small droplets with increased free energy aggregate together to form flocculation for the energy benefit of the system. The flocculation of small droplets, however, does not grow a single large droplet at the stable Pickering emulsions since the particles are irreversibly absorbed on the surface of liquid. Therefore, they maintain a congregate consists of small droplets unlike unstable Pickering emulsions.

2.2.1. Surface-active particles

Their amphiphilicity is caused selective surface modification or unique naturally derived structure on their surface. The selectively surface modified particles are called Janus particles. Janus particles can control the hydrophobic and hydrophilic surface regions by various synthesize technic and with this method their emulsified droplets. Although it is difficult to accurately synthesize Janus particles, the Janus particle synthesis method, which can give clear amphiphilicity to the polymer particles, is widely used in various emulsion field [65].

Some kinds of particles have amphiphilicity by itself. The difference in exposure of side groups caused by structural specificity imparts amphiphilicity to polymer particles [66, 67]. For example, in a structure stacked in a certain direction, a part with a relatively large amount of hydrophilic surface exposed and a part with a large amount of hydrophobic

surface exposed occur depending on the crystal direction. Therefore, these particles can form a Pickering emulsion without any other treatment. However, depending on the type of fluid, it may be difficult to prepare an emulsion with a liquid having a weak adsorption affinity (Figure 3).

In early years, the sphere-like Pickering particles were studied to stabilize the two immiscible liquids (Figure 3A-3E) [68-70]. The particles on the surface of droplets compose mono-layer by dual attracted adsorption at the liquids interface. The homogeneously formed spherical particles fabricate a uniformly connected layer on the surface of the droplet, and the continuously induced space between the particles occurs strong capillary adsorption of the liquid. Although it is difficult for the surface layer to be densely fabricated due to the steric hindrance of the particles, the particles can form a triangular mesh structure on the surface of the droplets to inhibit the droplet coalescence [71-73].

Recently, the rod-like Pickering particles used in various fields (Figure 3F-3J) [74-76]. Their high aspect ratio and thin thickness more efficient in stabilizing emulsions than the other shape ones. Fabricated monolayers by rod-like particles has buckling capacity under compression on the surface of droplets and this capacity induces highly attracted adsorption ability. In addition, the additional bridge structure between the particles keeps the surface particles more rigid, which leads to a super-stable Pickering droplets [77].

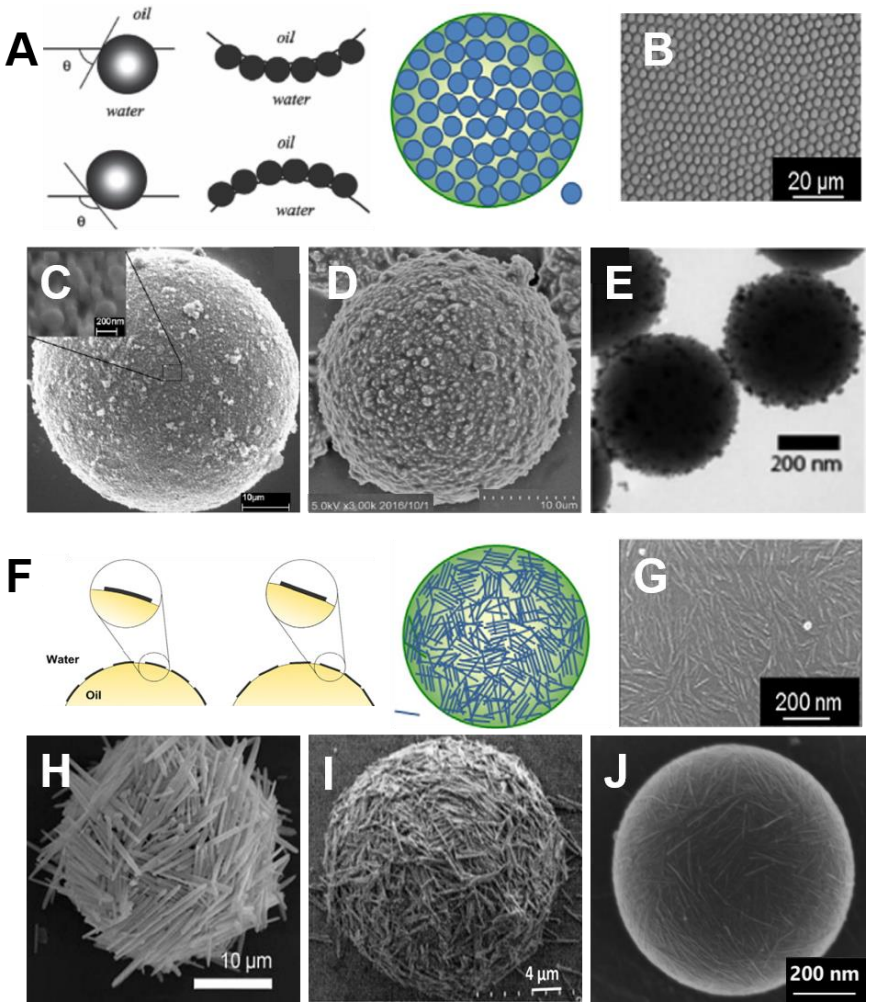

Figure 3. Pickering emulsion stabilized by (A-E) sphere-like particles and (F-J) rod-like particles. (A) Schematic illustration of surface-active spherical particles at the O/W interface [73]. (B) SEM images of Pickering emulsion's surface stabilized by spherical particles [78]. Pickering emulsion stabilized by (C) sphere TiO_2 [68], (D) sphere SiO_2-TiC [69] and (E) sphere silica [70]. (F) Schematic illustration of surface-active rod-like particles at the O/W interface [78]. (G) SEM images of Pickering emulsion's surface stabilized by rod-like particles [78]. Pickering emulsion stabilized by (H) rod-like $CaCO_3$ particles [74], (I) silica micro-rods [75] and (J) chitin nanocrystals [76].

2.2.2. Colloidal stability of Pickering emulsion

The colloidal stability of Pickering emulsion can be observed by various physical properties (Figure 4). Stable Pickering emulsion is composed of irreversible droplets, so the overall properties do not change over time. Stable Pickering emulsion can be shown by its phase stability, droplet size, rheological properties and surface tension measurements.

Phase stability can be obtained by observing the phase separation of the Pickering emulsion over time (Figure 4A). Unstable Pickering emulsion due to a small amount of Pickering particles causes phase separation such as creaming or segmentation in solution. The phase of unstable Pickering emulsion separates within minutes to days depending on the state of the droplet. The stable emulsion maintains the emulsion fraction at 100% if the oil inside the droplet does not release even after a long time [79-85].

The droplet size distribution of the emulsion is a parameter that determines whether a sufficient amount of surface-active particles has been used for encapsulation (Figure 4B). When there is a small amount of Pickering particles, the droplets, which were distributed in various sizes, gradually form droplets of a uniform size as the particles are added. Pickering particles are thermodynamically stable when forming the most stable droplet size depending on the encapsulating liquid, so if enough particles are included in the solution, the overall droplet size will be distributed homogeneously [81, 83, 84, 86].

The rheological properties of Pickering emulsion are depicted colloidal stability (Figure 4C). The small amplitude oscillatory shear (SAOS) flow of stable Pickering emulsion show that the elastic storage modulus (G') has a higher value than the loss storage modulus (G''). The frequency dependence

of G' and G" indicates whether the fabricated Pickering emulsion has gel or sol behavior. If G' is larger than G", Pickering emulsion has a gel behavior, and if G" is larger than G', Pickering emulsion has a sol behavior. The gel behavior of Pickering emulsion means that the enough amount of Pickering particles are used to emulsify two immiscible liquids. The loss factor ($\tan\delta = G''/G'$) present lost and stored deformation energy of SAOS flow in Pickering emulsion at a specific frequency [87]. As previously described, the loss factor also indicates the sol-gel behavior of Pickering emulsion at the different content of Pickering particle, and when the loss factor is less than 1, it means that the prepared Pickering emulsion has colloidal stability [32, 82-84, 86].

Amphiphilic particles added to two immiscible liquid solution form droplets through Pickering encapsulation (Figure 4D). After forming enough droplets, the remaining particles move to the A/W interface for thermodynamic stability. As the amount of particles at the interface increases, the A/W interface is activated, and when the particles completely fill the interface, the surface tension of the solution with respect to air becomes an equilibrium state. The equilibrium surface tension of the Pickering emulsion thus indicates the colloidal stability of the Pickering emulsion [85, 88].

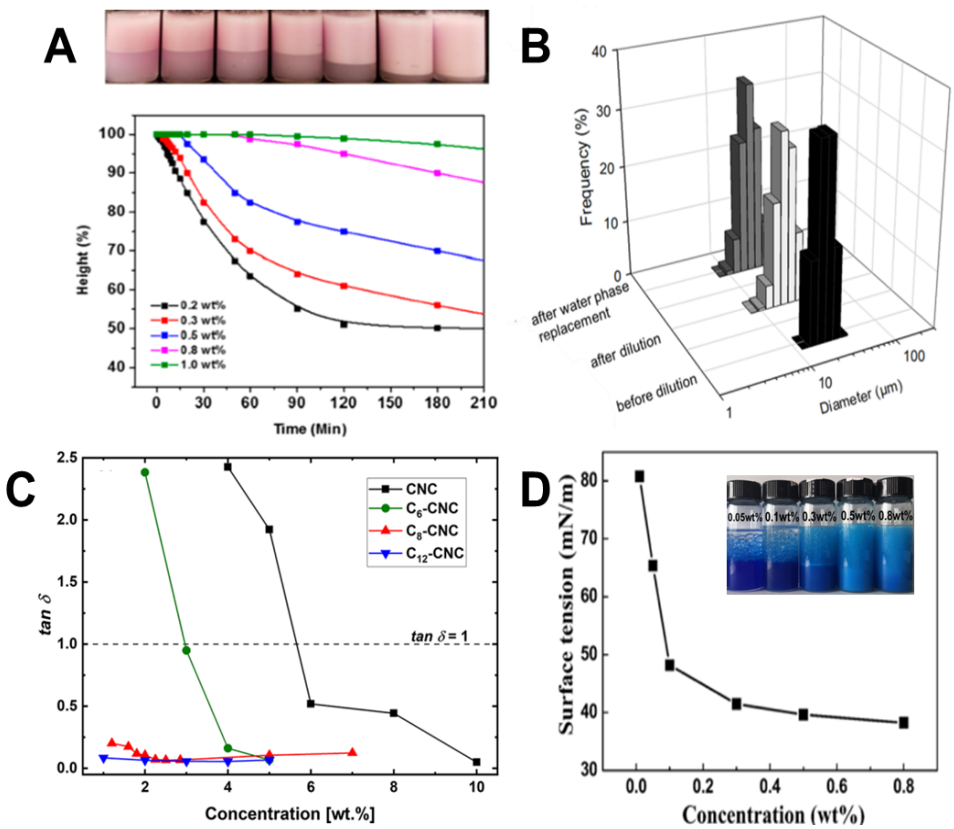

Figure 4. Colloidal stability of Pickering emulsion. (A) Optical appearance of Pickering emulsions and creaming profile of Pickering emulsion [81], (B) Size distribution of Pickering emulsion droplets before dilution, after dilution and after water phase replacement [89], (C) Loss factor changes as a function of Pickering particles concentration [32], and (D) Surface tension profile as a Pickering particles concentration [88].

2.3. Cellulose

Cellulose is the most abundant polysaccharide that biosynthesized from plant, algae and bacteria by carbon dioxide fixation in the photosynthetic cycle. Its chemical simplicity derived from β-D-glucosidic linkage of linear glucose chain are given it high elastic modulus and low thermal expansivity. Despite of their strong physical properties, its structural low density makes them light. In addition, its low carbon footprint, renewability and sustainability of cellulose have drawn attention in many studies as eco-friendly materials [17, 90, 91].

Recently, the extracted cellulose from various sources is widely studied for biological application (Figure 5A and 5B). Plants are the general source of cellulose. They synthesize the cellulose at the surface of plant cell for their structural robustness. As plants grow, they produce more cellulose to support their bodies, so cellulose can be extracted in large amounts from most woody plants [92]. Although cotton is a herbaceous plant, it is also a major source of cellulose, as it produces large amounts of cellulose in a short period of time [93]. Plant cellulose usually contains other substances such as lignin, hemicellulose, pectin, xylene and so on. Therefore, plant-derived cellulose has to go through many purification processes to remove other substances, and it is difficult to separate only cellulose even in numerous purification processes [93-95].

Cellulose can be also extracted from algae. Algal cellulose is synthesized on the surface of cell for manufacturing cell wall like land plant cellulose, however, the synthesize enzyme more diverse than land plants. Because algae do not require xylem to support the structure of land plants, algae have more linear terminal complexes cellulose synthase (TCs) than the rosette structured

cellulose synthase which forms strong cellulose. The linear TCs in algae synthesizes small and thin cellulose fibers that allow the algae to move flexibly [96]. Therefore, the structure of algal cellulose in the cell wall has lots of pores that can increase surface area of inner surface. The algal cellulose does not require as much purification as woody cellulose, but in the case of brown or red algae require some purification to remove lignin [94, 96-98].

High-purity cellulose can be obtained by bacteria. The bacterial cellulose is synthesized by static cultivation of cellulose-synthesizing bacteria on the surface of nutrient solution. All the bacteria on the surface form highly packed BC film without any impurities. So, the bacterial cellulose has high Young's modulus and porosity in their structures. Unlike the plant cellulose and algal cellulose, bacterial cellulose does not require extra purification process [99]. However, since cellulose-synthesizing bacteria are aerobic bacteria, they can only synthesize bacterial cellulose at the A/W interface. Therefore, there are spatial and temporal constraints in order to synthesize high-purity bacterial in large quantities like plant cellulose and algal cellulose [94, 95].

All celluloses generally have excellent mechanical properties. Abundant hydroxyl groups on the cellulose surface induce strong hydrogen bonds between each linear chain, and cellulose constitutes a dense and strong crystalline structure. The hydroxyl groups in cellulose can strongly interact with other biopolymers as well as inter-chain bonds. In the field of biocomposites, due to the interactions between the materials, cellulose is sometimes added as a filler to enhance the physical properties of the matrix [100]. The hydroxyl group can be easily substituted also through chemical methods.

2.3.1. Cellulose nanomaterials (CNM)

Cellulose nanomaterials (CNMs) are cellulose-derived materials that have a nanosize scale (1-100 nm) in at least one dimension. CNMs are classified into cellulose nanofiber (CNF) and cellulose nanocrystal (CNC) according to the presence or absence of amorphous region on their structure. Cellulose can be nanoized by several methods [17, 90, 91].

CNF is amorphous and crystalline regions of nanocellulose. The most common method of manufacturing CNF is the physical grinding of cellulose fibers. They are ground by a grinder or high-pressure homogenizer, and to facilitate grinding, the surface is substituted through carboxymethylation and then ground [101-103]. Grinded fibers are classified into microfibrilled cellulose (MFC) and nanofibrilled cellulose (NFC) according to the degree of grinding. CNFs can also be prepared through chemical methods such as TEMPO oxidization. Isogai et al. treated the cellulose fibers with TEMPO to oxidize the fibers, and the oxidized fibers were nanosized [104]. The prepared CNFs have the form of flexible filaments and have over hundred nanometers in length and 3 to 100 nm in width.

CNC is crystalline nanocellulose from which the amorphous portion has been removed. CNCs are usually manufactured by hydrolysis with strong acids [18-23, 105]. When the CNC is treated with a strong acid, the hydronium ions enter the amorphous region of the cellulose and promote the hydrolysis of the glycosidic bonds between the cellulose chains. All amorphous regions of cellulose are hydrolyzed by strong acid within 1 hour, and crystalline regions with a relatively regular arrangement are not hydrolyzed. At this time, if water is added to complete the hydrolysis, CNC can be obtained. Various strong acids such as hydrochloric acid, sulfuric acid,

phosphoric acid, hydrobromic acid, and nitric acid were used for hydrolysis of cellulose. Depending on the type of acid used, the hydroxyl group of cellulose may be substituted. CNC can also be obtained through cellulose [106]. Cellulase is a cellulolytic enzyme that breaks down the amorphous region of cellulose. Manufacturing of CNC using cellulase does not corrode the crystalline region of CNC. Intact nanocrystals can be obtained in high yield. The manufactured CNC has a rod-like shape and has various lengths and widths depending on the extracted source. CNC has usually within a few hundred nanometers in length and 5 to 10 nm in width [94, 107].

2.3.2. Sulfuric acid hydrolysis of cellulose

Sulfuric acid hydrolysis is the most commonly used CNC manufacturing method (Figure 5C) [18-23]. When the cellulose fiber is treated with sulfuric acid, some of the hydroxyl groups on the surface of the cellulose undergo intramolecular esterification with the sulfate group of sulfuric acid to change to a negatively charged sulfonate group. The CNC with sulfate group is called sulfated CNC (S-CNC), and the negatively charged surface of CNC causes the CNC to be well dispersed in aqueous solution. Therefore, S-CNC produced by sulfuric acid has a higher relative colloidal stability than CNC made by other strong acids. The physical properties of CNC change according to acid concentration, temperature, and time. The most suitable concentration of sulfuric acid that does not corrode the crystalline structure of cellulose is 60-65%, and most of the reaction is carried out at a temperature of 45°C or less within 1 hour to obtain S-CNC.

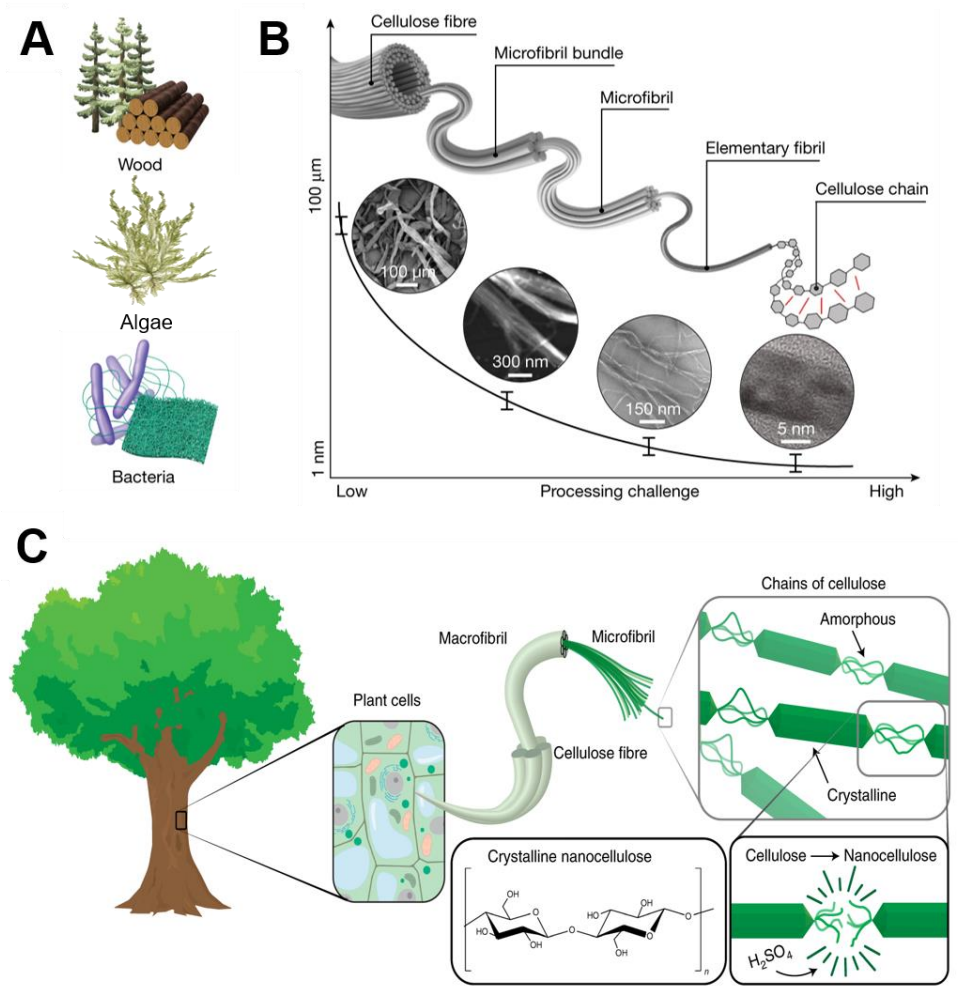

Figure 5. Cellulose and CNM. (A) Several common source materials of fibrillated cellulose [95, 98]. (B) Schematic description of the hierarchical structure and manufacturing challenge of fibrillated cellulose [95]. (C) Schematic illustration of the sulfuric hydrolysis of pulp cellulose [108]**.**

2.3.3. Crystalline structure of CNM

CNMs, bearing a large number of hydroxyl groups on their surface, have been considered to be hydrophilic materials. However, because of their unique crystalline structure, they have amphiphilic property. Lindman hypothesized that there would be a hydrophobic region on the surface of the CNM from the insolubility of CNM to water [109]. And he asserted that, like the amphiphilicity of polymers derived from polar/non-polar groups, the amphiphilicity of CNM may also be derived from the molecular structure. The crystalline structure of CNM consists of linearly linked glycopyranose rings. Since the linear structures are stacked each other with hydrogen bond, in the equatorial direction, three hydroxyl groups are exposed, and in the axial direction, C-H methane groups are exposed. The intrinsically structural anisotropy induced by inter- and intramolecular hydrogen bonding of the CNM molecule causes a polarity difference inside the CNM, and thus, the CNMs have amphiphilicity [110].

The amphiphilicity of CNM was studied by analysis of the crystalline region of CNM using X-ray and neutron diffraction and reproduction of the crystalline structure of CNM using molecular dynamics simulation [25, 109, 111-113]. The diffraction showed that the several characteristic crystal planes revealed at the cellulose [109]. The crystal plane of the CNM based on the diffraction technique was reconstructed through modeling work, and it has been proved that the plane of the CNM had various characteristics. With the reconstructed crystal planes, the researchers revealed that the CNM has two types of crystal planes where extensive hydrogen bonding could occur and less prone to deformation or attachment. Capron et al. suggested that the flat and hydrophobic (200) crystal plane was induced by the abundance of C-H

methane groups whereas the hydrophilic (1-10) and (110) crystal plane were induced by the abundance of hydroxyl group or substituted group (Figure 6A) [17]. Tsubasa et al. demonstrated the amphiphilicity of CNF using Calcofluor white dye, which stains the hydrophilic part of CNM, and Congo red dye, which dyes the hydrophobic part of CNM (Figure 6B) [23]. The different wettability derived from difference in molecular structures makes CNM adsorbed to the interface of two immiscible phases through slight buckled. Because the CNM has a relatively large hydrophilic area, the crystalline plane in contact with water expands a lot, so the CNM is located on the hydrophobic solution. In all direction, the buckling angle of CNM was showed above 60°, and (200) plane showed high buckling potential compared to (1-10) and (110) planes [114, 115]. The surface tension of CNC suspension is also decreased the more CNC particles added to the solution (Figure 6C) [17]. Lots of unmodified or modified CNCs were showed interfacial active effect when they were mixed with water [32, 116], and Pascal et al. obtained micelle-like microbubble images without any surfactant in AFM analysis (Figure 6D) [21].

In many studies, the crystallinity of CNCs was generally obtained in the range of 70-80% by X-ray diffraction [115]. CNC with high crystallinity does not easily deform its structures, but some expansion may occur due to heat or acid treatment. As heat is treated to the CNC, the 2θ value of each crystalline plane obtained from X-ray diffraction are shifted to the lower angles with no change of peak intensities and the widths. This shift derived only by thermal expansion of CNC's crystal structure. With thermal expansion, the d-spacing between the crystalline planes is gradually and linearly increase [114, 117]. The treated acid also shift the 2θ value of each crystalline plane to the lower side. The *d*-spacing expansion between crystal planes by acid is caused by the

breaking of inter-crystalline planes hydrogen bonds by hydronium ions. Expansion by strong acid deforms the cellulose structure from I to II and hydrolyzes the crystal structure when treated for a long time. Weak acids can also cause acid expansion and it is occurring more rapidly at higher processing temperatures [118]. In the previous study, desulfation reaction of S-CNC using low hydrochloric acid caused a slight change in crystal size due to expansion between crystal planes. Each of the expansion and *d*-spacing changes was observed through the shift of the XRD peak in the lower direction [119, 120].

2.3.4. Application of Pickering emulsions stabilized by CNMs

CNMs based Pickering emulsions are applicable in biological technology because of their biocompatibility and amphiphilicity (Figure 7). In recent, CNM-Pickering emulsion has been attracted in various areas. Liu et al used the strong amphiphilic Corncob CNM as a natural detergent [20]. For the reinforcement of the material, Pickering emulsion stabilized by CNM was also used. Researchers combined CNF-Pickering emulsion with poly(methyl methacrylate) (PMMA) for reinforcement the polymers [121, 122].

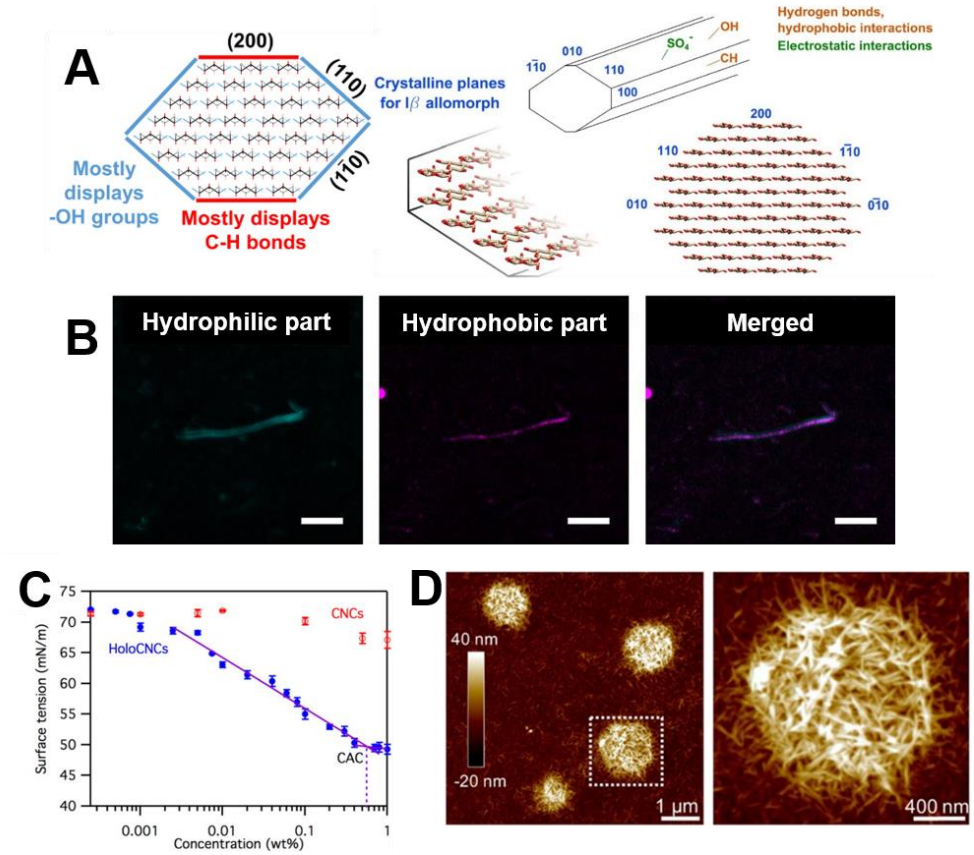

Figure 6. Amphiphilicity of CNM. (A) Schematic illustration of crystalline region of CNMs [112, 113]. (B) CLSM images of Calcofluor white and Congo red stained CNFs (Scale bar: 2 μm) [23]. (C) Surface tension of aqueous CNCs and holoCNCs suspensions [17]. (D) Microbubbles on displaced A/W interfacial layers formed at 0.1 wt% CNC and 20 mM NaCl with close-up as indicated by the frame [21].

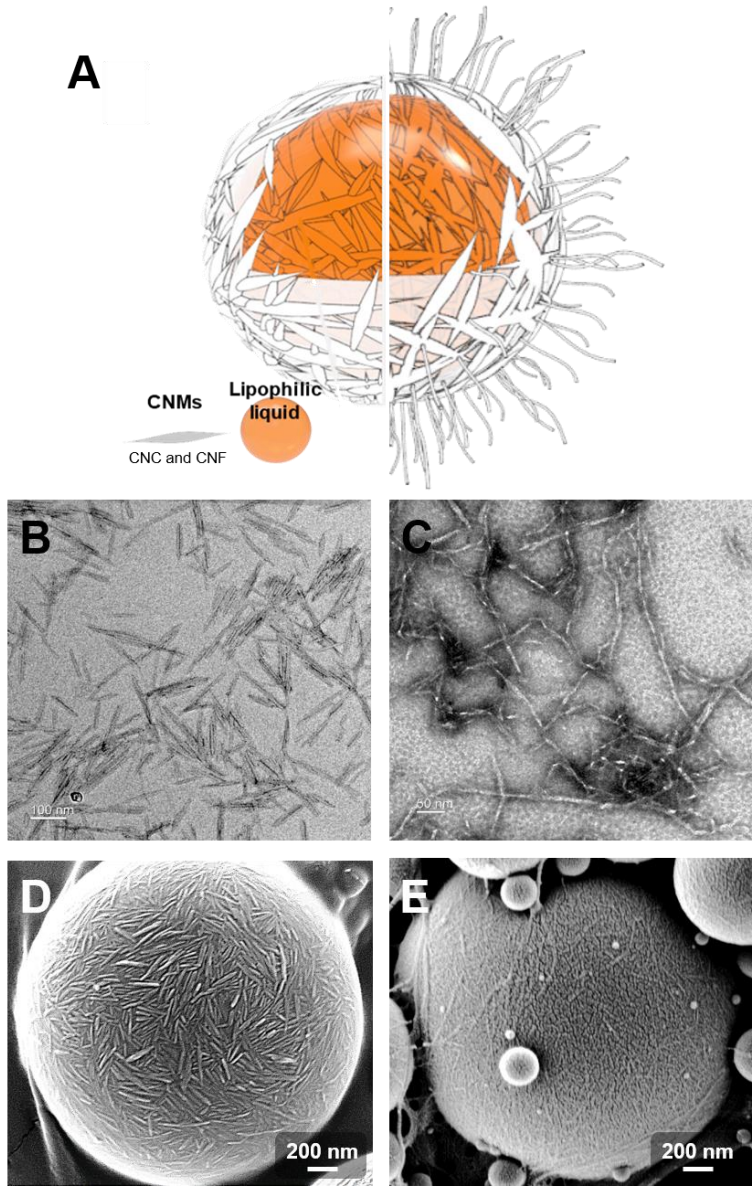

Figure 7. CNM stabilized Pickering emulsion. (A) Schematic illustration of suspended Pickering emulsion stabilized by CNMs (Left: CNC/Pickering emulsion, Right: CNF/Pickering emulsion). (B-E) TEM images of CNMs and SEM images of polystyrene-Pickering emulsion stabilized by CNMs. (A, C) CNC and (B, D) CNF.

2.4. Oil chemistry and properties

Oil is usually a liquid with low surface tension derived from plants, animals, or minerals. The unique characteristics of oil due to its various composition can be utilized in various fields, and in particular, various nutritional properties provide lots of benefits to mankind. However, since the low surface tension makes the oil immiscible with water, it requires pretreatment such as emulsification for use in aqueous solution. It is necessary to understand the composition and properties of oil in the emulsification process [123-125].

Most oils are composed of carbon and hydrogen. The basic structure of oil is called hydrocarbon. Oil may contain components such as oxygen, nitrogen, and sulfur, and various properties are given depending on the components included.

Primary alkanes consisting only of hydrogen and carbon called to the saturated oil. Alkanes linked by carbon-carbon single bonds are less reactive to external elements and have no biological activity. They are also colorless and odorless. The groups of primary alkane contain straight- and branched-chain alkanes and cycloalkanes. The alkanes containing 18 or more carbons are called waxes [125, 126].

Oils containing at least one benzene ring are called aromatic oils. The three carbon-carbon double bonds on the benzene ring make the oil stable and persistent for a long period. Aromatic oils include benzene, toluene, ethyl-benzene, and xylene, and most of them are toxic to organisms [125, 127].

Olefins are unsaturated hydrocarbons with at least one double bond between carbon-carbon. Unsaturated hydrocarbons can displace hydrogen with ionic molecules such as sulfur, nitrogen, and oxygen, and charged

molecules impart polarity to the oil. The oil becomes unstable with increasing polarity [125].

Heavy molecules without any polarity present in the oil increase the resistance to flow of the fluid by intermolecular interactions. Viscous oils require more driving force in the O/W emulsification process to form homogeneous droplets. When the same force is applied, the viscous oil forms larger emulsion droplets, and coalescence of the droplets due to viscosity occurs during the emulsification process. The prepared droplets also have poor permeability to the porous structure due to their resistance to flow. In order to successfully penetrate the porous structure, viscous oil emulsions are required higher pressures than pressure drop during emulsion injection.

The water solubility of the oil due to its high polarity increases the minimum area between the head groups of ionic surfactants located at the O/W interface. The emulsion droplet size increases as the water solubility of the oil increases, and the oil solubility too high prevents the droplet formation of the ionic surfactant. Oils with high water solubility can form droplets through emulsifiers with counter ions or nonionic emulsifiers, and can induce droplet formation through control of the surface charge [57].

2.4.1. Plant essential oil

Essential oils are the secondary metabolic compounds extracted from non-woody part of plants such as stems, leaves, flowers or roots [36-38]. Essential oils contain several bioactive ingredients including alcohols, aldehydes, ketones, esters, phenols, terpenes, lactones, monoterpenes, sesquiterpenes and so on [39, 40]. Because essential oil contains a large amount of antioxidant and preservative components, it is widely used in food, cosmetics and drugs. Essential oils usually extracted by steam distillation or

solvent extraction of non-woody organ of plants [128].

Steam distillation is the broadest separation technique for extraction of essential oil from plants [129]. Most of essential oil are made up of natural aromatic compounds and they have temperature sensitive volatile properties. The original boiling points of essential oils are up to 200°C, however, with steam or boiling water can volatilize the components of essential oils at the 100°C and atmospheric pressure. For extraction of these compounds, the dried plant organs, such as leaves, petals, and stems, are placed in a steam distilling chamber with connected line. After that, the generated steam of the other flask connected with plant debris chamber passes through the chamber and let the essential oils escaping in air form. The temperature of the boiling water maintained over 100°C for steam generation, but it has to control not so high to destroy or burn the plant debris [128]. The vaporized essential oils with the steam move to the cooling zone and the mixed vapor to form a double layer of liquid in the cooled flask. The immiscible solution can be isolated using by density difference between essential oils and water.

Non-volatile essential oil components are separated using solvent extraction method [130]. The oleic compounds of plant have high solubility to the solvent, and the selected solvent is play an important role to isolated the essential oil from plant debris. Ethanol and methanol are generally the most used for solvent extraction because of their solubility, safety and low cost [131]. The slightly ground plant organs are used for extraction, since extraction efficiency increases on the surface area of plant particles. The solvent extraction method of essential oil is usually carried out overnight at ambient temperature to prevent the destruction of the chemical component, and the extracted essential oil is isolated from the mixed solution through solvent evaporation.

2.4.2. Antimicrobial and larvicidal activity of essential oils

Essential oils have attracted attention for their potential medicinal applications, specifically their antibacterial and larvicidal activities [36-38]. Terpenes or phenylpropenes constituting essential oil are continuously accumulated in the lipid structure of the microbial cell membrane [132-134]. Essential oil components stocked on the surface of microorganisms paralyze the biological function of microorganisms and cause the failure of chemical osmosis control. The membranes of microorganisms with increased permeability due to disruption of chemical osmosis lead to loss of essential proteins, unexpected passive diffusion of ions, and inhibition of ATP production [135].

Similarly, essential oils also accumulate in the bodies of small insects, inhibiting the insect's respiratory system and interfering with normal metabolic activity. The Asian tiger mosquito, *Aedes albopictus* Skuse (*Ae. albopictus)*, is a vector insect of dengue virus (DENV) and chikungunya virus (CHIKV), and spread quickly to new locations from its native geographical origin [136]. *Ae. albopictus* management has mainly dependent on various synthetic pesticide around the world [137, 138]. However, the continued use of synthetic pesticide has caused several side effects such as environmental and human health concerns and undesirable effects on natural enemies, non-targeted organisms [139, 140]. Another problem is that the resistance of *Ae. albopictus* to synthetic pesticide has been reported in several countries [137, 138]. Recently, plant essential oils and their constituents are considered as good sources for mosquito-controlling agents. Larvicidal activities of many plant essential oils against *Ae. albopictus* have been reported [141-145]. Development of proper formulation is another research field for practical use

of plant essential oil based mosquito larvicides. Nanoemulsion based formulation have been reported to improve efficacy, stability and solubility of plant essential oils in water [61].

The most representative components of essential oil that induce antibacterial and larvicidal activity include eugenol, thymol, carvacrol, limonene, lactone, linalool, permethrin, citronellol, geraniol, and nerol. In particular, euganol, thymol, and carbacrol have excellent antibacterial and larvicidal activities and are effective even in small amounts. Some kinds of essential oil, extracted from irritating plants such as black pepper and red pepper, or pharmaceutical plants such as *Angelica tenuissima* and *Cnidium officinale*, can occur weak antibacterial and larvicidal activities without terpene or phenylpropenes [41-43].

III

Surface charge effect on Pickering encapsulation with ionic CNCs

3.1. Introduction

CNCs is the rod-like crystal particle obtainable by the acid hydrolysis of cellulose pulps [26, 27]. The sulfuric acid hydrolysis is a well-known process to prepare CNCs modified into anionic sulfate group (S-CNC) at the surface [28, 29]. Such a negative charge stabilizes the colloid or emulsion systems by the electrostatic repulsion between the particles [76, 146]. Besides, since the sulfonate group on S-CNC can be substituted to the hydroxyl group in the presence of hydroxide ion, a diverse functionality can be introduced to the CNC surface [30-32]. Researchers have controlled the surface charge of S-CNC using hydrochloric acid and trifluoroacetic acid [17, 33, 34]. The highly acidic reaction, however, also results in additional acidic hydrolysis of CNCs. To prevent the hydrolysis of CNCs, Tiffany et al. conducted modification of the S-CNC to dS-CNC under the low concentration of acid [35].

Pickering emulsions are based on the amphiphilic solid particles adsorbed at the interface of the different phase of liquids [2, 3]. The amphiphilic particles enhance the oil solubility and dispersibility to the aqueous solution and prevent loss of critical component of oil. In recent, Pickering emulsion has been attracted in cosmetic, food, and pharmaceutical areas for long term storage of phenolic antioxidant compounds and aromatic materials of functional oil [4-6], protection from microbial or food aging [7-9], and sustainable encapsulation of drug [10, 11].

The surface charge of surface active particles is one of the critical factors in Pickering emulsion [12, 13]. Especially, it is difficult for charged surfactant particles to form emulsion droplets due to the repulsive force comprising from Coulomb's law against oils with high polarity [14]. In order to form stable emulsion droplets and introduce thermodynamically stable colloidal

dispersion between the droplets, it is necessary to control charge of the surface-active materials.

CNCs are a potential candidate for Pickering particles applicable in biological technology because of their biocompatibility and amphiphilicity [18-23]. Moreover, the CNC particles can form various oil-encapsulated emulsion by controlling functional groups at the surface [24, 25]. In this study, S-CNC hydrolyzed with sulfuric acid and dS-CNCs desulfurized with HCl at the difference reaction times were used for the emulsification of nonpolar oils (*n*-decane, *n*-dodecane, *n*-tetradecane and *n*-hexadecane) and polar oils (chloroform and 1-octanol). Pickering emulsions prepared with the CNCs are evaluated by the emulsion fraction, emulsion droplet size and surface tension, which are parameters to evaluate the stability of the Pickering emulsion. It will provide a generic idea on the surface charge effect for CNC-based Pickering emulsions.

3.2. Materials and method

3.2.1. Preparation and characterization of CNCs

S-CNC was prepared with commercially available filter paper (Whatman, grade 2, Kent, UK) and sulfuric acid (Junsei Chemical Co. Ltd., 95.0%(w/w) purity, Tokyo, Japan) [26, 41]. 10 g filter paper was ground by a blender for 5 minutes and 100 mL of 60% (w/w) sulfuric acid was added. Then, acidic pulp slurry was hydrolyzed with stirring at 45°C for 60 minutes. The hydrolyzed solution was diluted 10 times with deionized (DI) water and centrifuged at 6000 rpm for 20 minutes using a high speed refrigerated centrifuge (VS-24SMTi, Vision Scientific Co., Ltd., Daejeon, Korea). The obtained suspending S-CNC solution was dialyzed with a cellulose dialysis

membrane (12-14 kDa, Spectra/Por, Breda, the Netherlands) for 7 days and subsequently concentrated using a rotary evaporator (N-1210BV-W, EYELA, Tokyo, Japan).

The concentrated S-CNC (1%) was desulfated with 0.025 M hydrochloric acid at 80°C with stirring at 100 rpm for 5, 10, 20 and 30 hours [35]. Then, dS-CNCs suspensions were concentrated using a rotary evaporator.

A transmission electron microscope (TEM, JEM1010, JEOL, Tokyo, Japan) was used to image the morphology of S-CNC and dS-CNC. 1% of the S-CNC and dS-CNC was diluted 500 times and loaded on a glow-discharged carbon copper grid. The loaded CNCs were negatively stained with uranyl acetate solution (1% w/v) and the obtained images were analyzed using the ImageJ program (1.52a, National Institutes of Health, Bethesda, MA, USA). The nanoparticle tracking analysis (NTA) was performed to obtain the length of S-CNC and dS-CNC using NanoSight (NanoSight LM10, Malvern Panalytical, Malvern, UK).

The surface topography of S-CNC and dS-CNC (30H) images were obtained using by atomic force microscopy (AFM, NX-10, Park Systems, Korea) in a non-contact mode (PPP-NCHR-10, NanoSensors, Switzerland) at room temperature. 0.01 wt% of S-CNC and dS-CNC (30H) solution was deposited onto mica film and air-dried overnight. The thickness of CNCs were calculated using the XEi software (Park Systems, Korea).

Zeta-potential of the CNCs was measured with 0.1% solutions of S-CNC and dS-CNC using Zetasizer (Zetasizer Nano ZS90, Malvern Panalytical, Malvern, UK).

The sulfate content of S-CNC and dS-CNC was measured by conductometric titration method. 40 mg of the S-CNC and dS-CNC was

suspended in 15 mL of 0.01 M HCl solution and stirred for 10 minutes. Then, the conductivity of the solution was measured using a conductometer (FiveGo Cond meter F3, Mettler Toledo, Zürich, Switzerland) during titration with 0.01 M NaOH solution. The degree of substitution was calculated by the Equation (1) [94, 147, 148]:

$$\text{Degree of substitution} = (V_{eq} \times C_{NaOH})/w \qquad \text{Eq. (1)}$$

Where V_{eq} is the amount of NaOH in liters at the equivalent point, C_{NaOH} is the concentration of NaOH (10 mmol/L), and w is the weight of titrated cellulose (kg).

Attenuated total reflection Fourier transform infrared spectra (ATR-FTIR) (Nicolet iS5, Thermo Scientific, Newington, NH, USA) were obtained in the range of 4000 to 650 cm^{-1} with 32 scan number and 4 cm^{-1} resolution.

The wide angle X-ray diffraction (WAXD) of S-CNC and dS-CNC was analyzed with a x-ray scattering system (D8 Discover with VANTEC500 detector, Bruker, Berlin, Germany) with 0.154 nm wavelength of Cu-kα radiation at 50 kV and 1000 μA. The WAXD patterns were recorded in the 2θ range of 4 to 39 degree at a scanning speed of 0.02 steps per 300 seconds. The each of WAXD peaks were fitted with Gaussian peak functions. The crystallinity of CNC was calculated using Equation (2) [115, 149] and the average dimension of the crystal size to the diffracting planes according to the *hkl* Miller indices, crystal size was calculated using Equation (3) [17]:

$$\text{Crystallinity} = (I_{TOTAL} - I_{AM})/I_{TOTAL} \qquad \text{Eq. (2)}$$

$$\text{Crystal size} = 0.94\lambda/\beta_{1/2} \times \cos\theta \qquad \text{Eq. (3)}$$

Where at the Equation (2), I_{TOTAL} is the total peak of CNC, I_{AM} is the total amorphous peak of CNC. At the Equation (3) θ is the diffraction angle, λ is the X-ray monochromatic wavelength, and $\beta_{1/2}$ is the peak width at half-maximum intensity.

The films of S-CNC and dS-CNCs were obtained by air-drying 1 wt% CNC solution on borosilicate slide glass. The water affinity of films was observed by droplet shape analyzer (EasyDrop FM40, KRÜSS, Hamburg, Germany) with 10 µl DI water in sessile drop mode. The 10 µl solutions of various S-CNC and dS-CNCs content were also observed by droplet shape analyzer in sessile drop mode. The surface tension of CNC films and suspended CNCs were calculated by the Equation (4) [150]

$$\cos\theta = -1 + 2\left(\gamma_S^d/\gamma_{LG}^d\right)^{1/2} \qquad \text{Eq. (4)}$$

Where θ is the contact angle of the CNC and Pickering emulsion droplet on the borosilicate glass, γ_S^d is the surface tension of the borosilicate glass (47.6 mNm^{-1}), and γ_{LG}^d is the surface tension of the CNC and Pickering emulsion.

3.2.2. Preparation and characterization of CNC stabilized Pickering emulsions

n-Decane (Sigma Aldrich, St. Louis, MI, USA), *n*-dodecane (Sigma Aldrich), *n*-tetradecane (Sigma Aldrich), *n*-hexadecane (Sigma Aldrich), chloroform (99.5%, Samchun chemical Co., Ltd., Seoul, Korea) and 1-octanol (Sigma Aldrich) were encapsulated with S-CNC or dS-CNC at the

different content of 90, 180 and 270 mg per 1 mL of oil. The oil concentration in the water and oil mixture solution was fixed at 10% (v/v) and the mixture was tip-sonicated with an ultrasonic processor (VCX 130, 435-09, Sonics & Materials Inc., Newtown, CT, USA) at 50% amplitudes for 30 seconds.

Prepared Pickering emulsion were stored at room temperature for 14 days, and the solution appearance was captured with a digital camera. The height of separated layer was divided by the height of the solution to determine the fraction of emulsion.

The shape and morphology of Pickering emulsion droplet were observed with a polarized light microscope (LV100, Nicon, Tokyo, Japan) or an inverted optical microscope (Eclipse Ts2, Nikon, Tokyo, Japan). S-CNC and dS-CNC stabilized-Pickering emulsion were diluted 100 times and the image of Pickering emulsion particles was captured at the dark-field mode with 40× inverted routine microscope (Eclipse Ts2, Nikon, Tokyo, Japan) and bright-field mode with a 60× oil immersion objective lens (CFI plan apochromat lambda, Nikon, Tokyo, Japan). The diameter of Pickering emulsions was measured using the ImageJ program.

The confocal fluorescence images of Pickering emulsion stabilized with dS-CNC was obtained by staining with 1 $\mu l/mg_{CNC}$ Calcofluor white (Sigma Aldrich) and 1.5 $\mu g/\mu l_{oil}$ Nile red (Sigma Aldrich) using a confocal laser scanning microscope (LSM710, Carl Zeiss, Overkochen, Germany) (CLSM SP8 X, Leica, Wetzlar, Germany).

The contact angle of S-CNC and dS-CNC stabilized-Pickering emulsion was measured using a droplet shape analyzer in sessile drop mode. 10 µL CNC and Pickering emulsion were dropped on the borosilicate glass and their droplet shape was captured for the analysis of angles. The films of S-CNC and dS-CNCs were obtained by air-drying 1 wt% CNC solution on

borosilicate slide glass. The water affinity of films was also observed by droplet shape analyzer with 10 μL DI water in sessile drop mode. The surface tension of CNC films, CNC suspension and Pickering emulsion was calculated by the Equation (4) [150].

3.3. Results and discussion

3.3.1. Properties of S-CNC and dS-CNCs

The prepared CNCs showed the same morphology and size distribution (Figure 8A-8E). dS-CNCs did not show significant difference in length from S-CNC regardless the treatment time with a hydrochloric acid solution (Figure 8F). Their average size was approximately 150 nm in length and the chemical treatment modified the surface chemistry of CNCs rather than the degradation of the CNC molecular chains because of their high crystallinity. In contrast, the width of dS-CNCs increased to 9.2 nm after the acid treatment (Figure 8G). The average thickness of S-CNC and dS-CNC (30H) also increased as the acid treatment approximately 7 nm to 9 nm (Figure 9). It resulted from the swelling of molecular chains by the penetration of acid solution through the CNC surface [94].

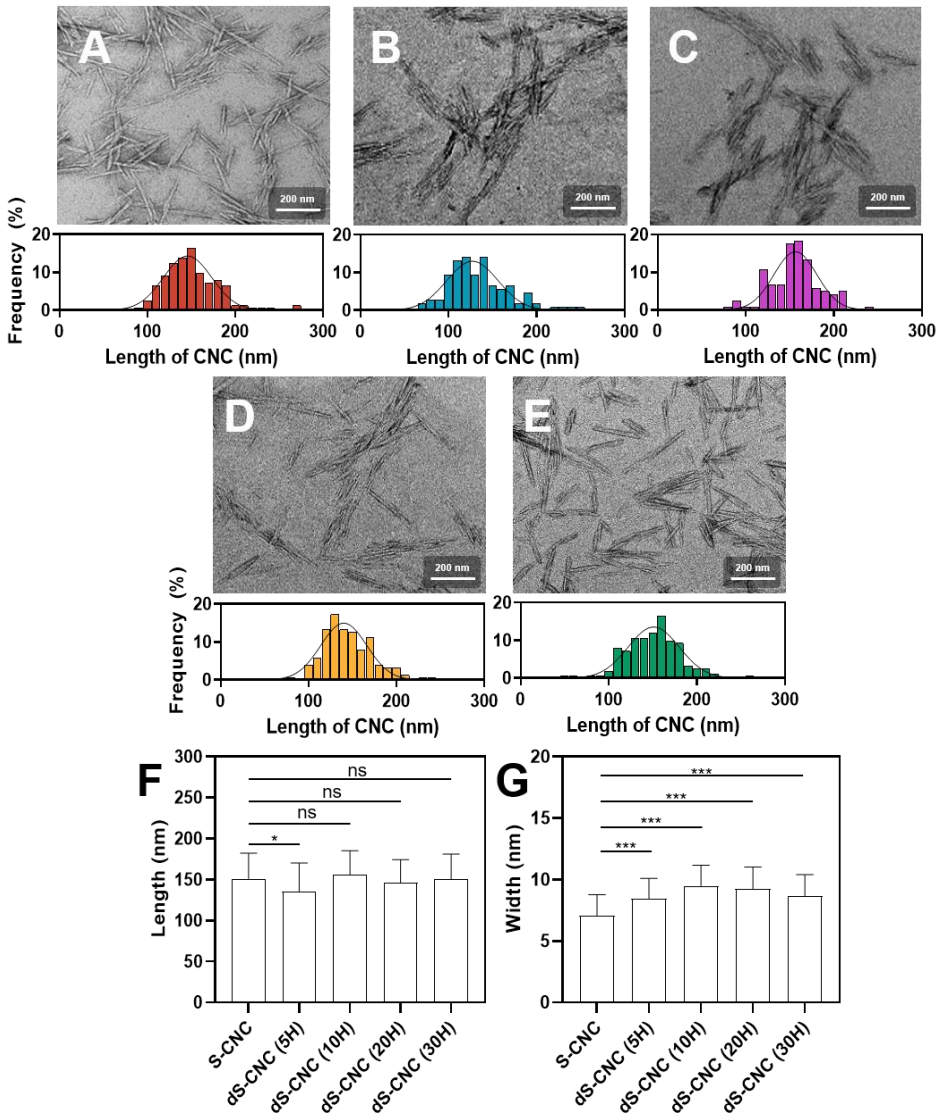

Figure 8. Transmission electron microscope images and size distribution of S-CNC and dS-CNCs. (A) S-CNC, (B) dS-CNC (5H), (C) dS-CNC (10H), (D) dS-CNC (20H) and (E) dS-CNC (30H). (F) Length and (G) width of CNCs. (N=200, error bar=SD).

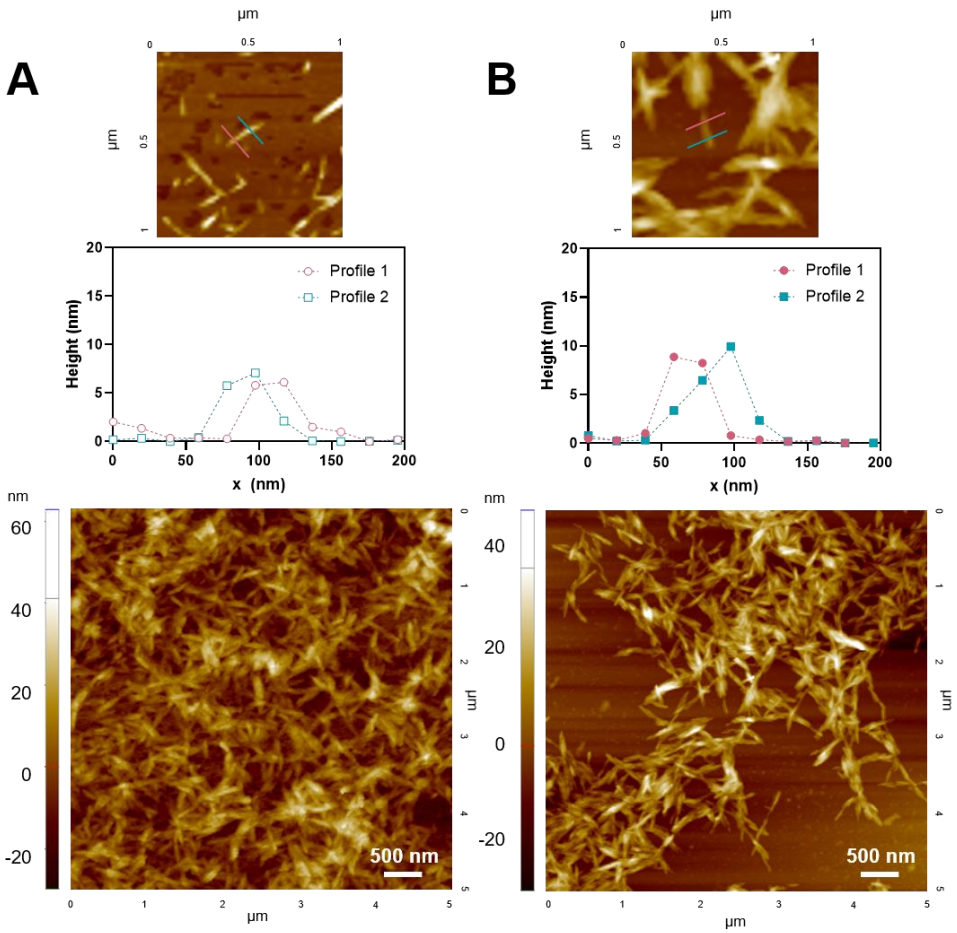

Figure 9. Surface topography and thickness profiles of (A) S-CNC and (B) dS-CNC (30H). The AFM image size is 1 × 1 µm and 5 × 5 µm.

The overall XRD peaks of CNCs were slightly shifted to the lower side as the reaction proceed. The 2D WAXD patterns of each CNCs were showed Figure 10. The WAXD patterns of each CNCs were obtained at 2θ 14.7, 16.2, 20.6, 22.5 and 34.4 degrees, respectively, and the each of patterns means that (1-10), (110), (120)/(021), (200) and (004) crystalline plane of CNCs. The crystallinity and sizes of crystal planes were calculated using by WAXD value of S-CNC and dS-CNCs (Figure 11). With multiple peak deconvolution, the full width at half maximum (FWHM) values, crystallinity and each of crystal size were calculated (Table 1 and 2). The added HCl molecules hydrolysis remaining the amorphous region of S-CNC. Since acid treatment reduced the amorphous fraction of S-CNC, the crystallinity of CNCs increased 77% to 79% (Table S1). According to the calculated miller indices, the average sizes of the (1-10) and (110) planes which related with the width and thickness of the crystalline structure of CNC were also around 4.7 nm in width, and from 4.85 nm in thickness, respectively. The FWHM and 2θ values of two crystalline edges had similar values as the reaction progressed. The (200) crystalline edge which have relatively hydrophobic property was also maintained their crystal size even though the reaction proceeded for 30 hours. The size change of all crystal planes had a slight size change according to thermal and acid expansion, but could be controlled without significant change.

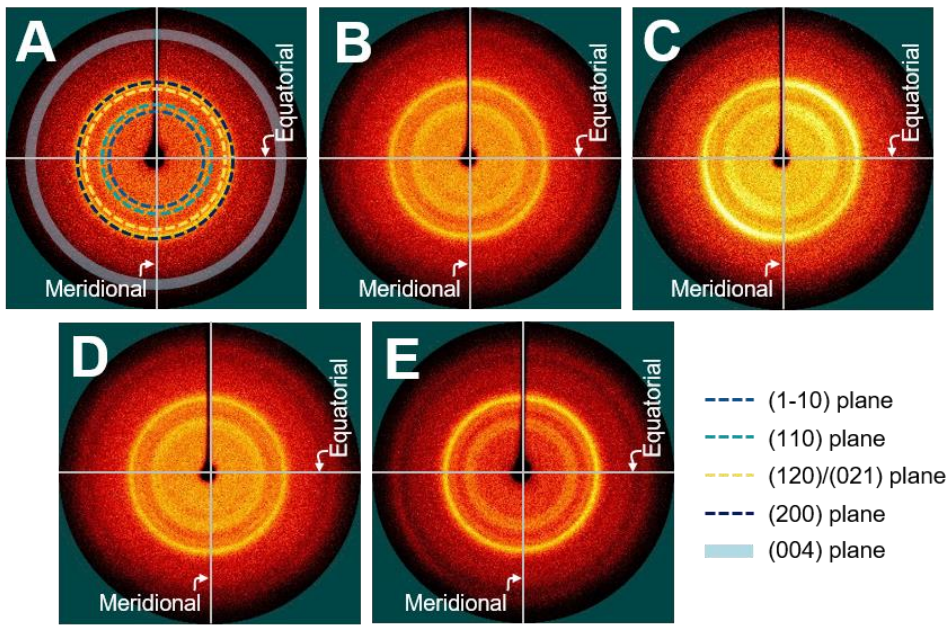

Figure 10. 2D WAXD patterns of CNCs. (A) S-CNC, (B) dS-CNC (5H), (C) dS-CNC (10H), (D) dS-CNC (20H), and (E) dS-CNC (30H).

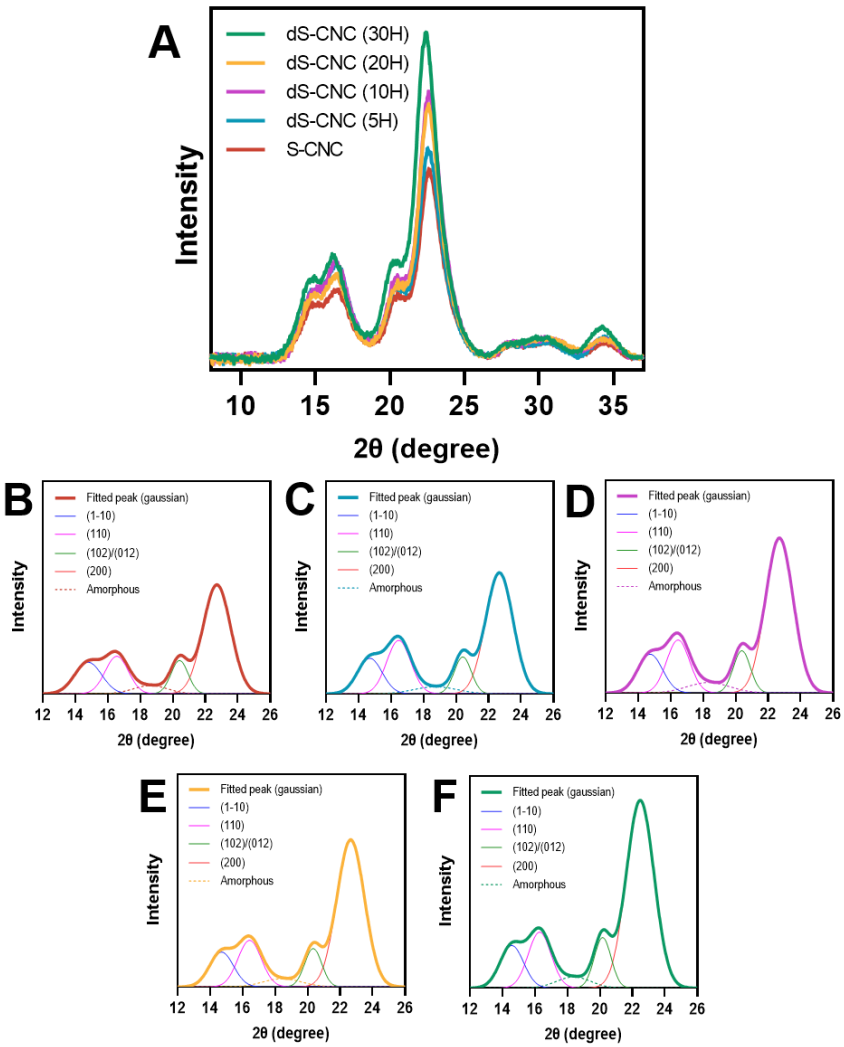

Figure 11. 1D XRD graph. (A) WAXD of 0.1 % S-CNC and dS-CNC films. (B-F) Deconvolution of the XRD graph. (B) S-CNC, (C) dS-CNC (5H), (D) dS-CNC (10H), (E) dS-CNC (20H) and (F) dS-CNC (30H).

Table 1. FWHM values from 1D XRD graph of CNCs.

Materials	FWHM (°)		
	(1-10)	(110)	(200)
S-CNC	1.81	1.73	2.00
dS-CNC (5H)	1.78	1.73	2.00
dS-CNC (10H)	1.77	1.73	2.00
dS-CNC (20H)	1.73	1.70	2.00
dS-CNC (30H)	1.71	1.70	2.00

Table 2. Crystal sizes at (1-10), (110), and (200) planes and crystallinity of S-CNC and dS-CNCs.

Materials	Miller indices			Crystallinity (%)
	(1-10) (nm)	(110) (nm)	(200) (nm)	
S-CNC	4.6	4.9	4.2	77
dS-CNC (5H)	4.7	4.8	4.2	77
dS-CNC (10H)	4.7	4.8	4.2	78
dS-CNC (20H)	4.8	4.9	4.2	79
dS-CNC (30H)	4.9	4.9	4.2	79

The decrease in the sulfate group and the increase in the OH group were observed by the FTIR spectra (Figure 12). The O-H stretching vibration was routinely observed between 3650 and 3000 cm^{-1} [26, 146, 151-153]. Especially, dS-CNCs showed the increase of the peak intensity at 3350 cm-1 compared with the peak of S-CNC. In contrast, the peak at 811 cm-1 assigned for C-O-S decreased as the desulfate reaction time increased inferring the chemical modification of the sulfoxide group to the hydroxyl group [26, 34, 146, 151, 154, 155]. The surface charge of CNCs were changed by the treatment with HCl solution (Figure 13). The zeta potential of CNCs showed the decease of the negativity from -44.3 ± 0.5 mV to -26.8 ± 0.7 mV. Similarly, the degree of sulfate substitution decreased significantly from 300.7 ± 9.3 mmol/kg to 74.3 ± 15.6 mmol/kg due to the desulfation supporting the decrease of the zeta potential as the treatment time increased.

Surface tension of S-CNC and dS-CNCs films was obtained by sessile drop methods (Figure 14). The surface tension decreased from about 34 mNm^{-1} to about 21 mNm^{-1} and contact angle increased from about 16 to about 25 as the desulfation reaction. A decrease in the ionic group of a substance means a decrease in water affinity. The change in CNC surface properties according to the desulfation reaction suggested that the ionic sulfate groups of S-CNC were successfully substituted with nonionic hydroxyl groups.

Although the size of the CNCs was not changed by the surface treatment with a weak acid solution, the surface charge of the CNC was changed by the control of the treatment time. The surface charge of particular emulsifiers is one of the critical factors to influence the emulsion formation with phase separating liquid systems such as water and oils. The effect of surface charge on emulsification was investigated with CNCs prepared at different surface modification time and six oils with a different surface tension.

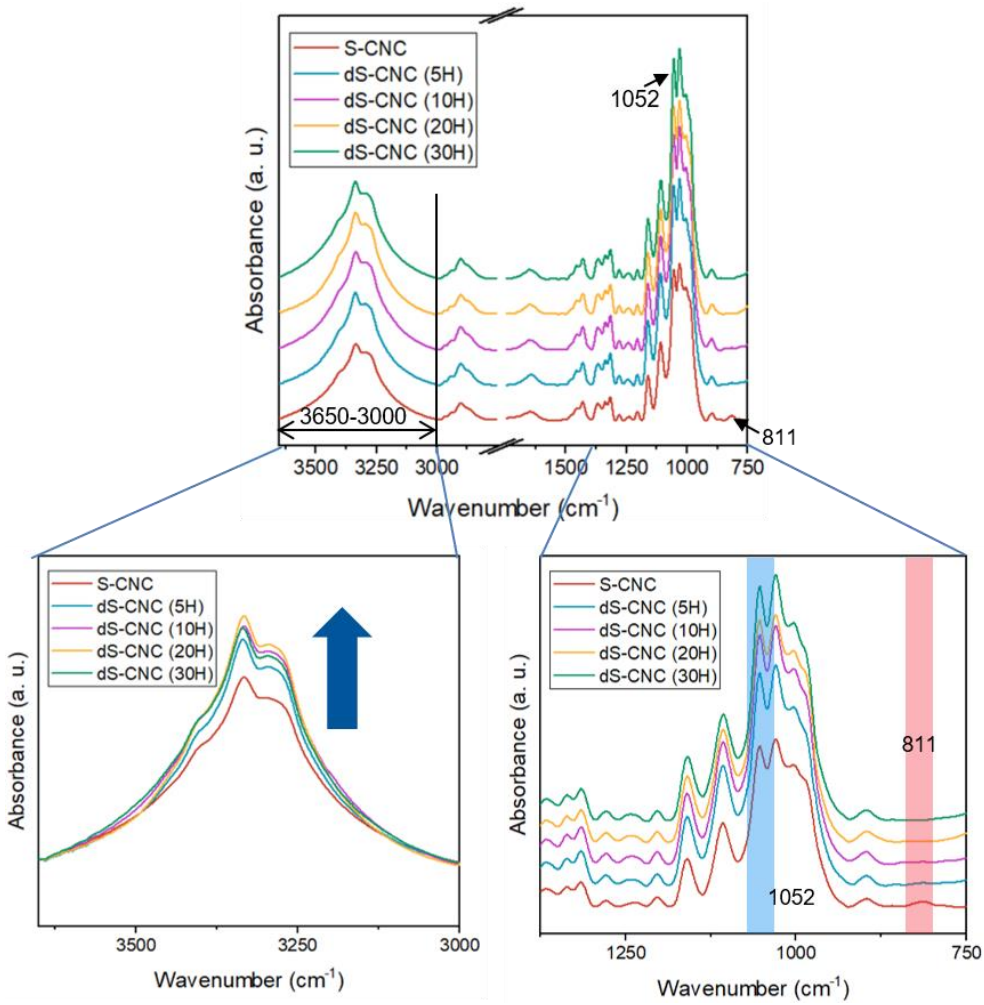

Figure 12. FTIR spectra of S-CNC and dS-CNCs films according to the different desulfation time. The peak changes are shown in detail from 3650 cm^{-1} to 3000 cm^{-1} and from 750 cm^{-1} to 1375 cm^{-1}.

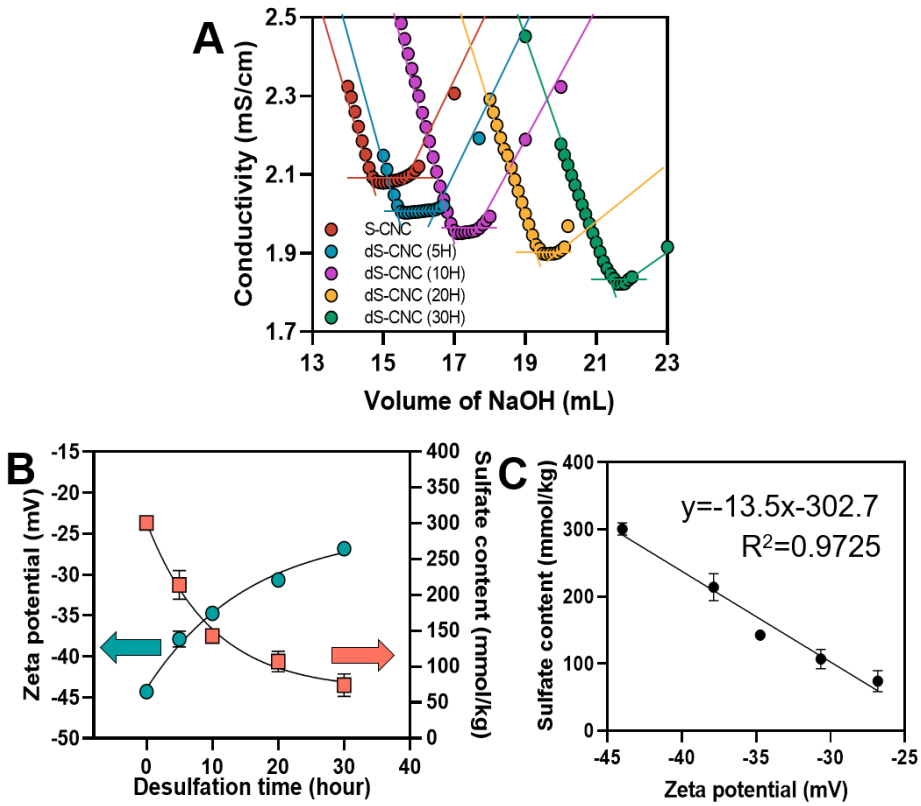

Figure 13. Measured sulfate content and zeta potential of S-CNC and dS-CNCs. (A) Conductivity titration of S-CNC and dS-CNCs. (B) Surface charge of S-CNC and dS-CNCs (Zeta potential: N=5, error bar=SD, Sulfate content: N=3, error bar=SD). (C) Correlation between zeta potential and sulfate content of CNCs according to the desulfation time.

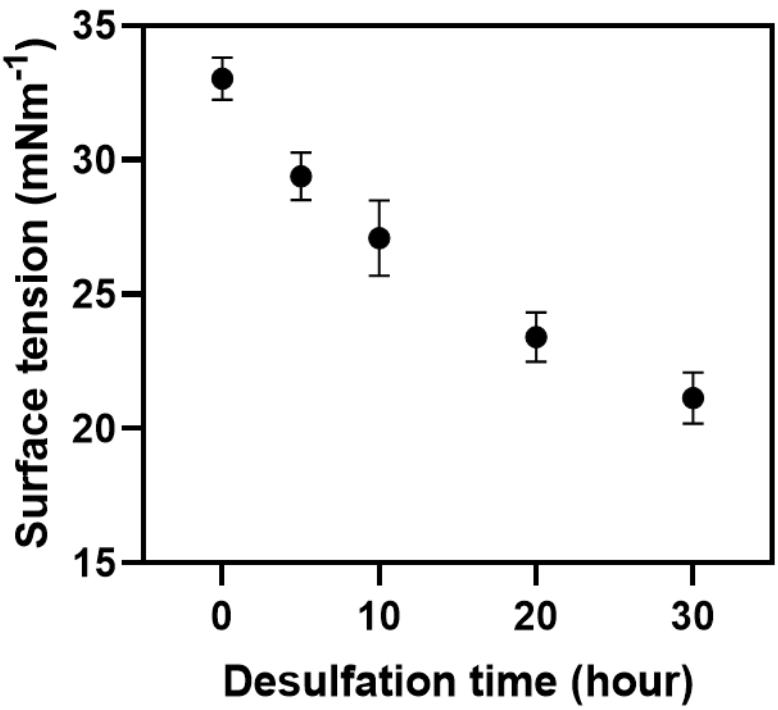

Figure 14. Surface tension of S-CNC and dS-CNCs films. The dry concentration of all the films was 1 wt% S-CNC and dS-CNCs and the surface tension was calculated by sessile drop mode contact angles (N=5, error bar=SD).

3.3.2. Surface tension of used lipophilic liquids

The surface tension of the six oils used are shown in Table 3 [156, 157]. The surface tension of normal organic liquids is determined by the dispersive and polar contributions. *n*-Decane, *n*-dodecane, *n*-tetradecane, and *n*-hexadecane have only dispersive contribution of 23.9, 25.4, 26.6, and 27.6 mNm^{-1}, respectively because they are a nonpolar liquid. The increase of the surface tension resulted from the length of the molecular chain inducing the increase of dispersion force between the molecules. Chloroform and 1-octanol have almost the same surface tension as n-hexadecane but different polar contributions of 1.6 and 6.3 mNm^{-1}. The use of three liquids including n-hexadecane, chloroform and 1-octanol would provide the idea of polar effect on encapsulation of liquids with the charged CNCs.

Table 3. Surface tension of oils and water.

Material	Molecular formula	Disperse contribution (mNm^{-1}, 20 °C)	Polar contribution (mNm^{-1}, 20 °C)	Surface tension (mNm^{-1}, 20 °C)
n-Decane	$C_{10}H_{22}$	23.9	0	23.9
n-Dodecane	$C_{12}H_{26}$	25.4	0	25.4
n-Tetradecane	$C_{14}H_{30}$	26.6	0	26.6
n-Hexadecane	$C_{16}H_{34}$	27.6	0	27.6
Chloroform	$CHCl_3$	25.9	1.6	27.5
1-Octanol	$C_8H_{18}O$	21.3	6.3	27.6
Water	H_2O	21.8	51	72.8

3.3.3. Colloidal stability of CNC based lipophilic liquids Pickering emulsions

The amount of CNCs is critical to encapsulate the oils completely because the micellar structure with a low packing density can be easily destroyed. Furthermore, electrical repulsion of negatively charged S-CNCs reduces the affinity between the emulsifying particles, which requires higher content of CNCs for the stable emulsion formation. Pickering emulsions stabilized with S-CNC were phase-separated for all six oils regardless of the CNC content in the range. In contrast, the oils emulsified with dS-CNCs was stable for a long period compared with emulsion of S-CNC (Figure 15-21). The emulsion stability increased as the dS-CNC content increased due to the sufficient encapsulation of oils.

Pickering emulsion formed with CNC 90 mg/mL$_{oil}$ showed the phase separation in a short storage time showing a low emulsion fraction for the oils. Meanwhile, the addition more than CNC 180 mg/mL$_{oil}$ increased the stability of the emulsion with non-polar oils (Figure 15-18 and 21A-21D). Since the surface chemistry of S-CNC was modified from sulfate to hydroxyl groups by the desulfation reaction, the relative hydrophobicity of dS-CNC increased. dS-CNC (30H) formed the emulsions with non-polar oils in water system, and the fraction of emulsions was near 100% at CNC 180 mg/mL$_{oil}$ due to high colloidal stability. Meanwhile, the other dS-CNCs showed a stable emulsion fraction at CNC 270 mg/mL$_{oil}$ in encapsulation of non-polar oils. For a polar chloroform and 1-octanol encapsulation, only dS-CNC (30H) at 270 mg/mL$_{oil}$ showed a stable emulsion for the long term storage (Figure 19, 20, 21E and 21F).

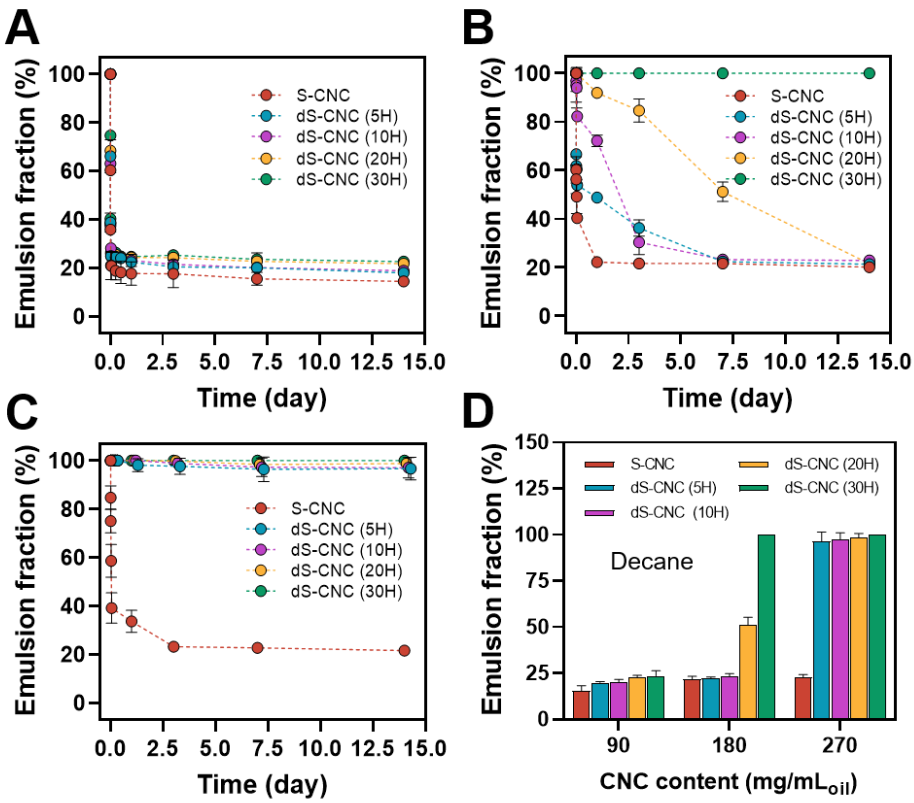

Figure 15. Phase behavior of CNC/*n*-decane Pickering emulsions at the different CNC content for 14 days. (A) CNC 90 mg/mL$_{oil}$, (B) CNC 180 mg/mL$_{oil}$, and (C) CNC 270 mg/mL$_{oil}$. (D) Emulsion fraction of CNC/*n*-decane Pickering emulsions in Day 7. (N=3, error bar=SD).

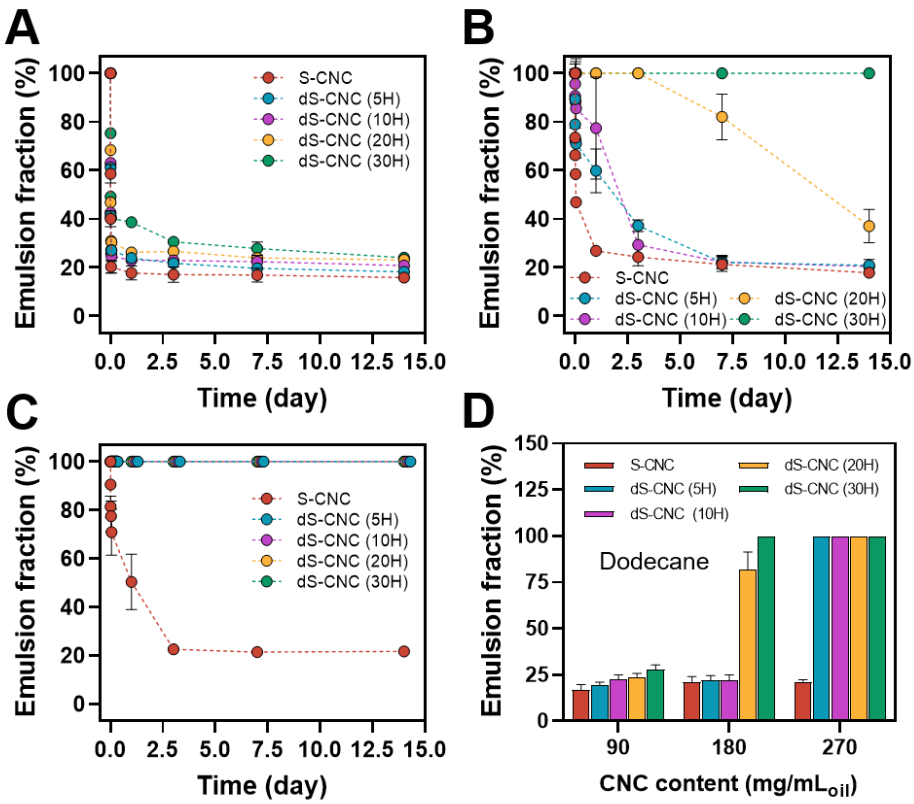

Figure 16. Phase behavior of CNC/*n*-dodecane Pickering emulsions at the different CNC content for 14 days. (A) CNC 90 mg/mL$_{oil}$, (B) CNC 180 mg/mL$_{oil}$, and (C) CNC 270 mg/mL$_{oil}$. (D) Emulsion fraction of CNC/*n*-dodecane Pickering emulsions in Day 7. (N=3, error bar=SD).

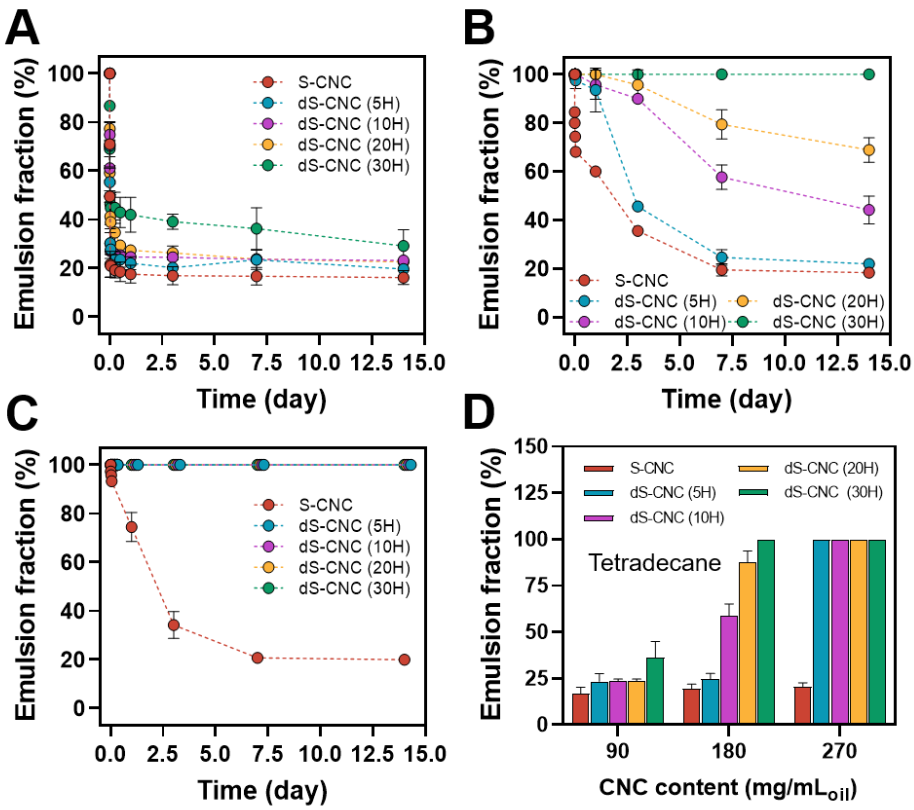

Figure 17. Phase behavior of CNC/*n*-tetradecane Pickering emulsions at the different CNC content for 14 days. (A) CNC 90 mg/mL$_{oil}$, (B) CNC 180 mg/mL$_{oil}$, and (C) CNC 270 mg/mL$_{oil}$. (D) Emulsion fraction of CNC/*n*-tetradecane Pickering emulsions in Day 7. (N=3, error bar=SD).

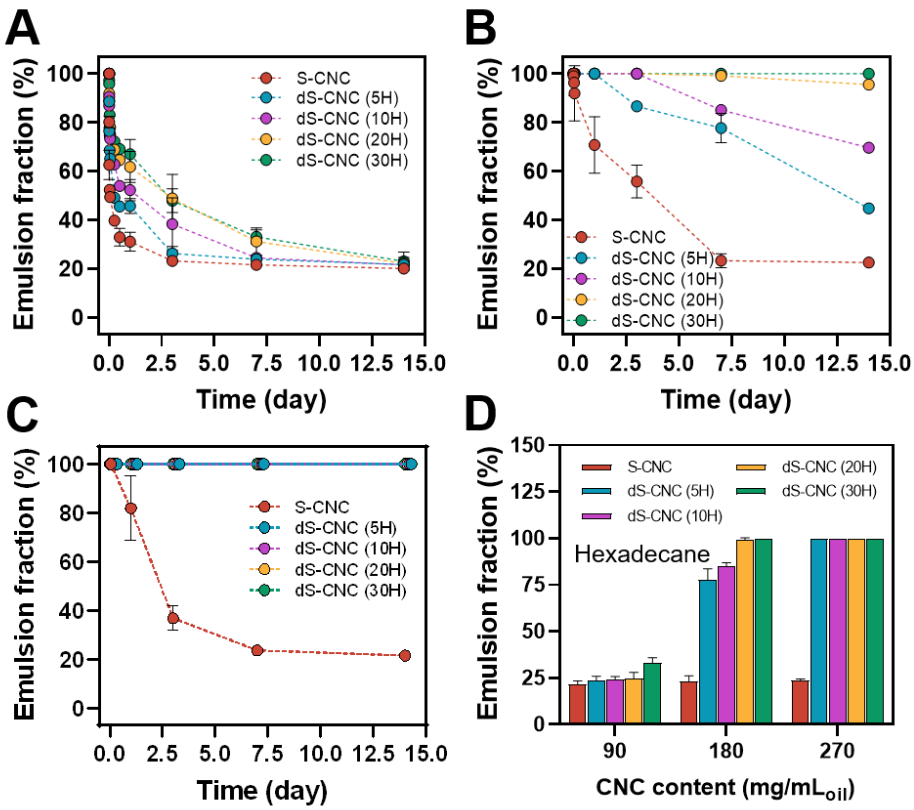

Figure 18. Phase behavior of CNC/*n*-hexadecane Pickering emulsions at the different CNC content for 14 days. (A) CNC 90 mg/mL$_{oil}$, (B) CNC 180 mg/mL$_{oil}$, and (C) CNC 270 mg/mL$_{oil}$. (D) Emulsion fraction of CNC/*n*-hexadecane Pickering emulsions in Day 7. (N=3, error bar=SD).

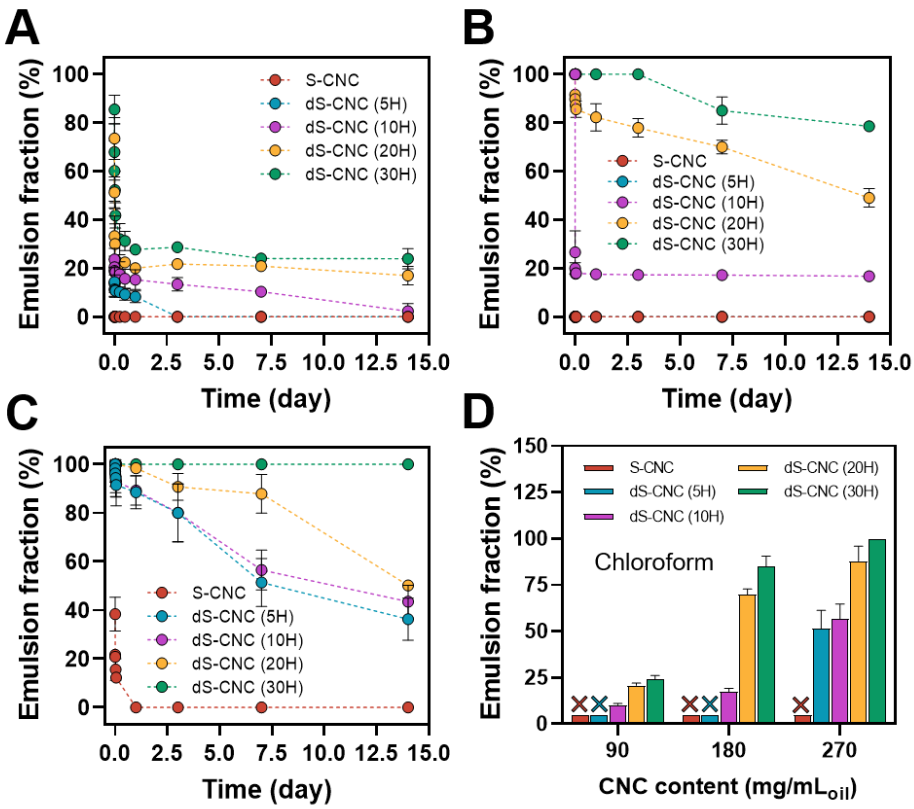

Figure 19. Phase behavior of CNC/chloroform Pickering emulsions at the different CNC content for 14 days. (A) CNC 90 mg/mL$_{oil}$, (B) CNC 180 mg/mL$_{oil}$, and (C) CNC 270 mg/mL$_{oil}$. (D) Emulsion fraction of CNC/chloroform Pickering emulsions in Day 7. (N=3, error bar=SD).

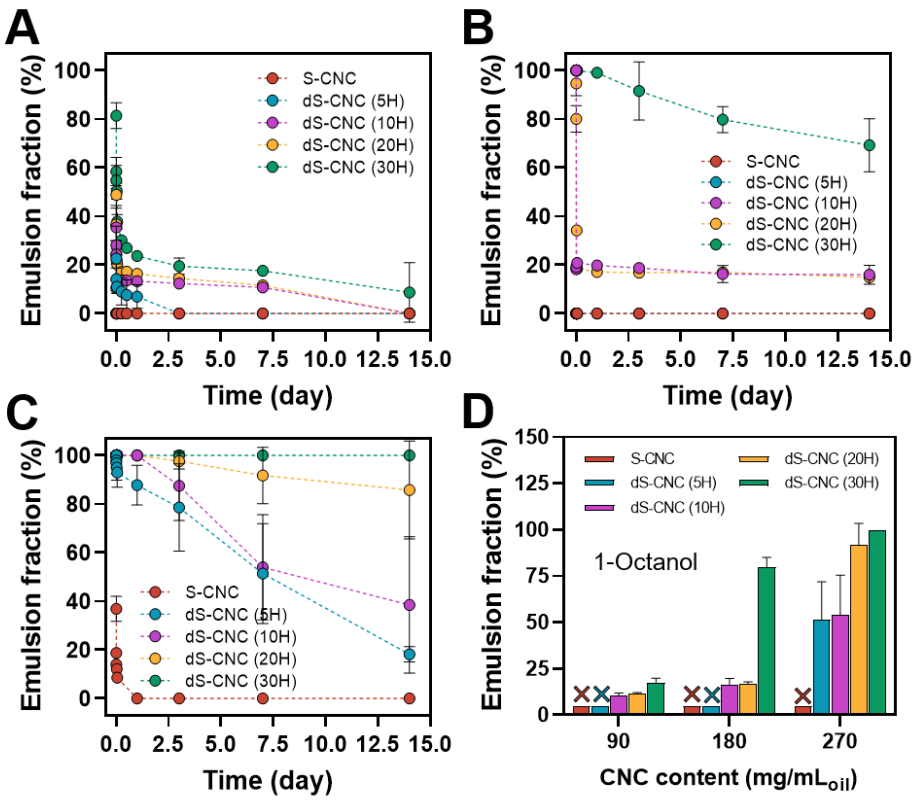

Figure 20. Phase behavior of CNC/1-octanol Pickering emulsions at the different CNC content for 14 days. (A) CNC 90 mg/mL$_{oil}$, (B) CNC 180 mg/mL$_{oil}$, and (C) CNC 270 mg/mL$_{oil}$. (D) Emulsion fraction of CNC/1-octanol Pickering emulsions in Day 7. (N=3, error bar=SD).

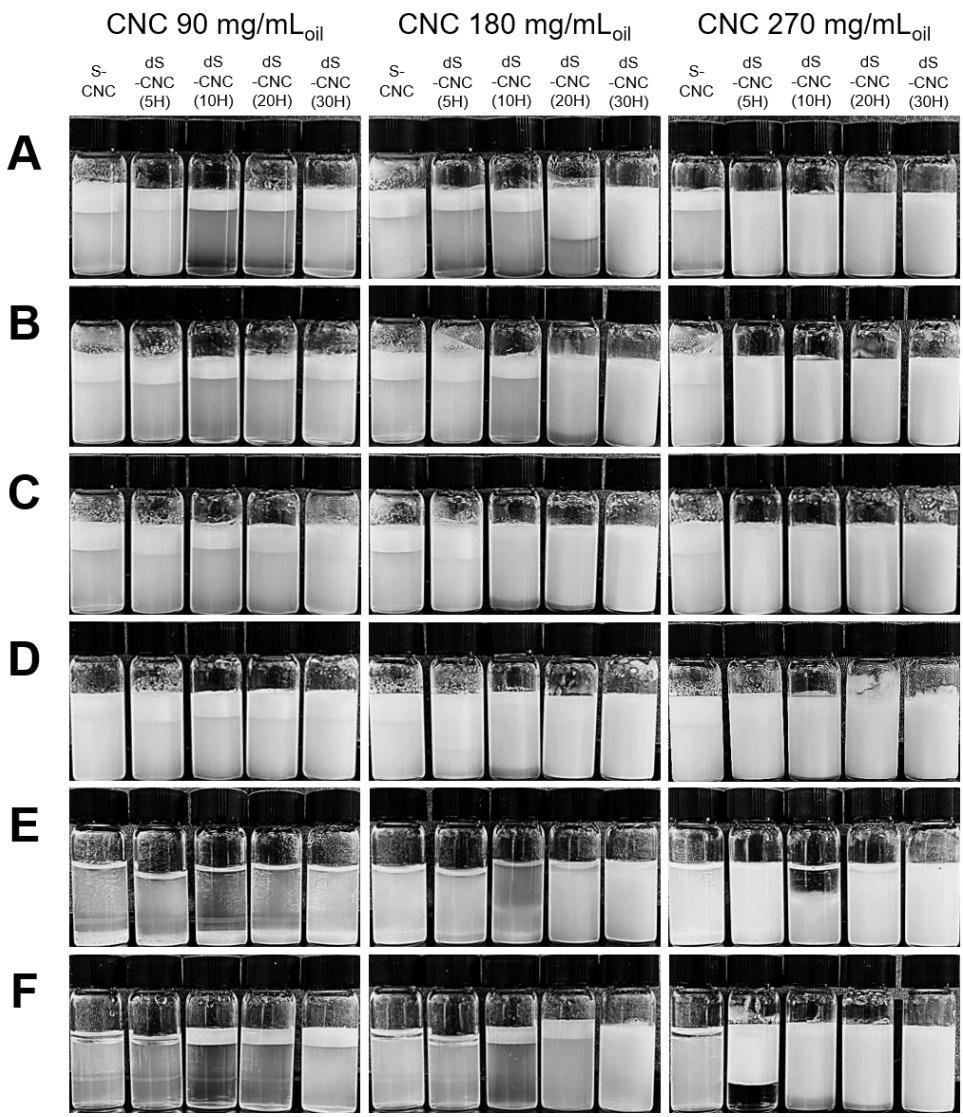

Figure 21. Visual appearances of CNC/oil Pickering emulsion at different CNC content stored for 7 days. (A) *n*-Decane, (B) *n*-dodecane, (C) *n*-tetradecane, (D) *n*-hexadecane, (E) chloroform and (F) 1-octanol.

The average size of emulsion droplet is other method to describe how much CNC are needed to stable the emulsion. For the oils in water solution, the amphiphilic CNC is located at the oil-water interface to remain thermodynamically stable. The CNC encloses the oil in a spherical shape to achieve high thermodynamic stability. Since it is impossible to cover all the oil with insufficient CNCs, the size distribution of the droplet becomes wide due to weak micellar structure and coacervate formation. As the number of CNCs increases, the CNC can form strongly bound micelles with a narrow size distribution.

S-CNC encapsulated 4 non-polar oils but the average droplet size was larger than droplets with dS-CNCs (Figure 22A-22D). Especially, the average droplet size was relatively small with n-hexadecane whose surface tension was high (Figure 22D). Meanwhile it was not possible to encapsulate polar oils such as chloroform and 1-octanol with S-CNC. It resulted from the high hydrophilicity by sulfate group on the S-CNC (Figure 22E and 22F).

dS-CNC enabled the formation of encapsulated structures with the six oils. The droplet size decreased consistently as the dS-CNC content increased (Figure 21). The longer desulfation time of dS-CNCs formed a smaller size of droplet with high uniformity to compare the size deviation. The increased surface hydrophobicity enhanced the adsorption of CNCs at the interface between nonpolar liquid and polar water inducing more stable emulsion structure. Short desulfation time of dS-CNC (5H) could not form the stable droplets with 1-octanol while it formed the large size of droplets with chloroform (Figure 22F). In normal, most of the droplets were unstable with dS-CNC (5H) and dS-CNC (10H) compared with dS-CNC (20H) or dS-CNC (30H) (Figure 21). Especially, dS-CNC (30H) showed the smallest average droplet size and high stability. The desulfurization of CNC emulsifying

particles reduced the electrical repulsion between the particles and enhanced the stability of oil emulsions.

The oil emulsions formed with dS-CNC (30H) were observed by confocal microscopy (Figure 23). All of the oils were successfully emulsified at 270 mg/mL of dS-CNC (30H) content maintaining a stable emulsion. The dS-CNCs (blue-labeled) were tightly packed and enclosed the oils (red-labeled) and the dimensional structure of the emulsion was stable without coacervate formation for a long term storage. In the case of nonpolar oils, the smaller droplets were formed due to their high affinity to dS-CNCs, which formed a micellar structure with a high density of dS-CNCs. In contrast, the emulsions of chloroform and 1-octanol were not stable due to the high miscibility with water despite the presence of dS-CNCs as a surface active particles. Furthermore, the low affinity between the polar liquid and dS-CNC allowed the growth of emulsion droplets through coacervate formation. It resulted in the broad range of emulsion droplet size in storage.

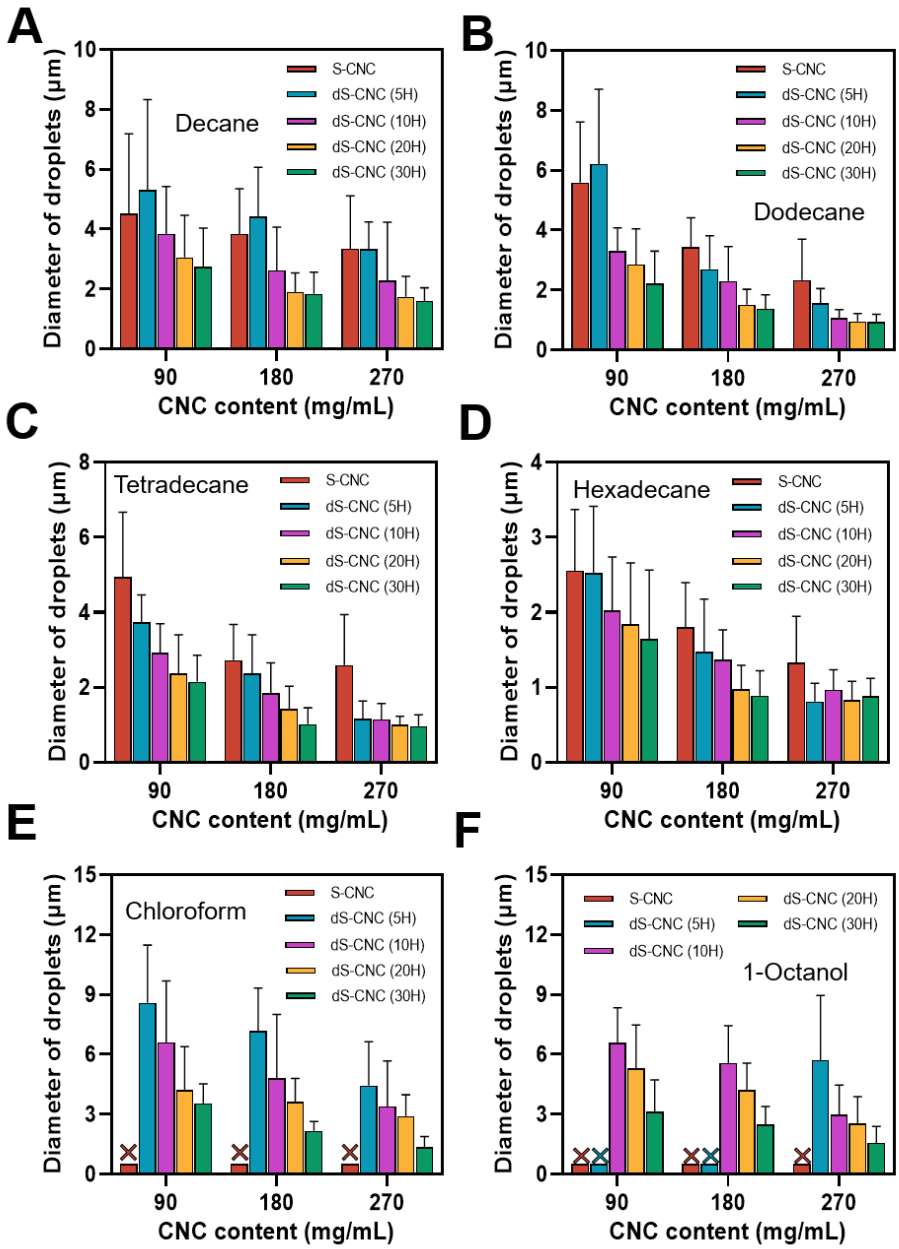

Figure 22. CNC/oil Pickering emulsions diameter of droplets at different CNC content. (A) *n*-Decane, (B) *n*-dodecane, (C) *n*-tetradecane, (D) *n*-hexadecane, (E) chloroform, and (F) 1-octanol. (N=150, error bar=SD).

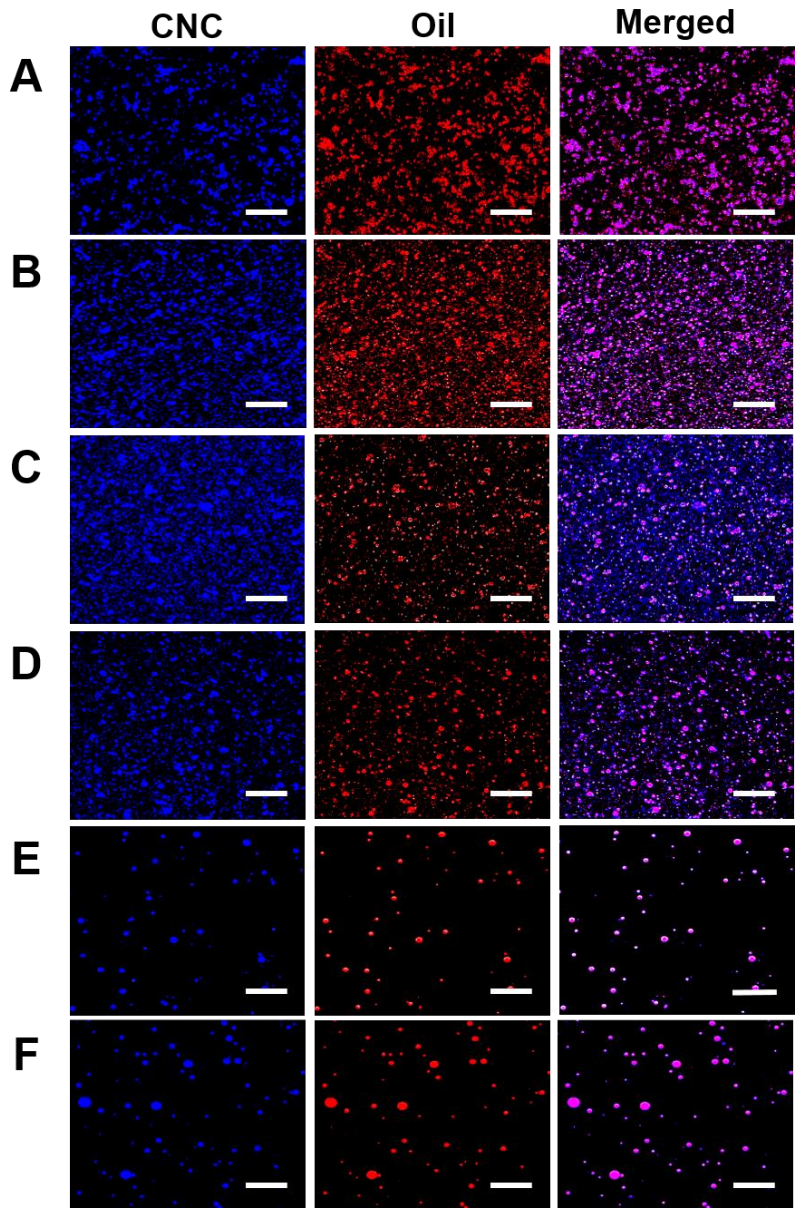

Figure 23. Emulsion CLSM images or microscope images. (A) *n*-Decane, (B) *n*-dodecane, (C) *n*-tetradecane, (D) *n*-hexadecane, (E) chloroform and (F) 1-octanol. Each of CNCs labeled with Calcofluor white fluorescent dye and 6 oils labeled with Nile red fluorescence dye. (Scale bar: 10 μm) (dS-CNC (30H) 270 mg/mL$_{oil}$).

The effect of charged CNCs on the change of water surface tension was investigated at the different CNC content and the different surface treatment time of CNCs (Figure 24A). As the amount of CNC increased, the surface tension of water decreased from 72 mNm^{-1} to 55 mNm^{-1} for S-CNC and 60 mNm^{-1} for dS-CNC (30H) due to the amphiphilicity of CNCs. The higher hydrophilicity of S-CNCs enabled the mixing with water and filled the water surface rapidly. It resulted in the rapid decrease of the surface tension at the low S-CNC content in water. The addition of S-CNC above 50 mg/mL stabilized the water surface tension and showed the steady contact angle inferring the structuring of S-CNCs (Figure 24B). Meanwhile, dS-CNC (30H) showed a slower decrease of surface tension at below 50 mg/mL and contact angles due to the lower miscibility with water than S-CNC (Figure 24C). Higher content of dS-CNCs induced the rapid decrease of surface tension as S-CNC showed but the ultimate surface tension was higher than S-CNC because the dS-CNCs preferred the interaction between particles rather than with water molecules. It reduced the effective content of dS-CNC in water and the polar contribution of water molecules in surface tension was not dramatically reduced as S-CNC showed at a low content.

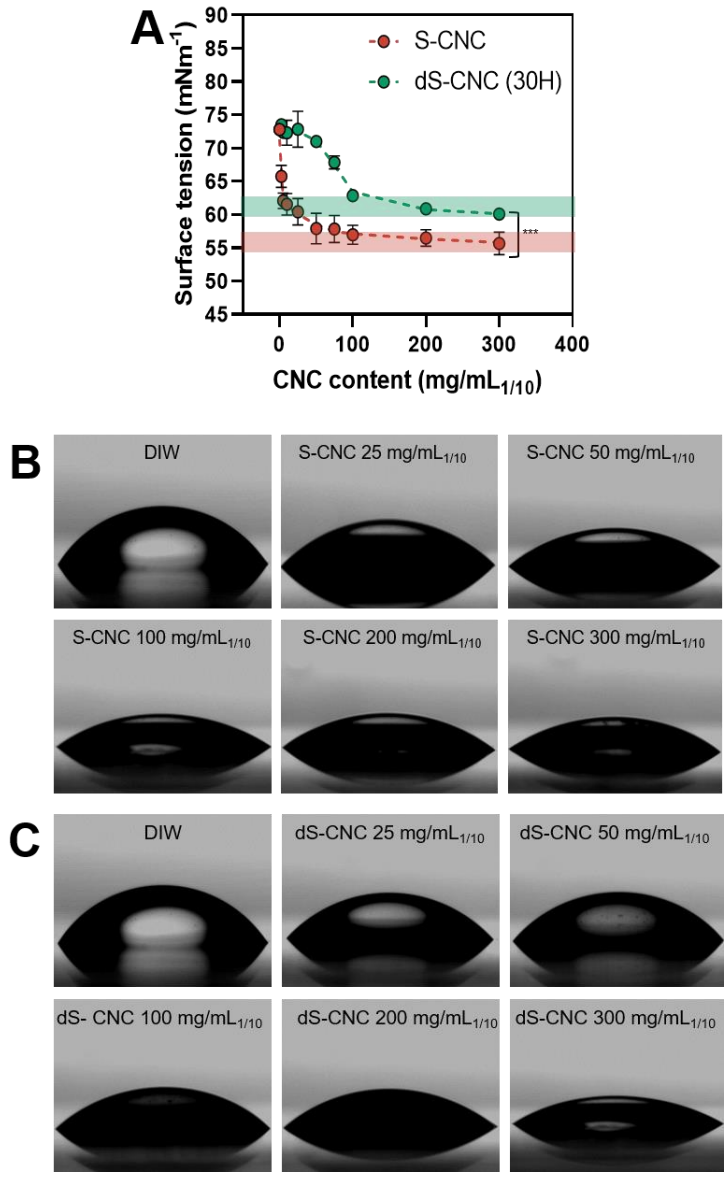

Figure 24. Surface tension and contact angle images. (A) Surface tension of the S-CNC and dS-CNC (30H). (N=4, error bar=SD). Contact angle images of CNC suspended solution. (B) S-CNC and (C) dS-CNC (30H).

The decrease of surface tension was similarly observed with emulsions formed by mixing oils in water and CNCs. In forming emulsions, CNCs moved to adsorb at the oil surface due to their amphiphilic property until all the oil was completely encapsulated by CNCs. The emulsion droplet size was determined by the mechanical stress applied to the liquid mixture and the amount of surface active CNCs. After the complete formation of emulsion, the remaining CNCs were dispersed in water, which reduced the surface tension of water by decreasing the attractive interaction between the water molecules. It could be confirmed by the nonpolar liquids at the high CNC content showing the decrease of surface tension to near 60 mNm^{-1} which was the surface tension of dS-CNC (Figure 25A-D). In contrast, the polar liquids such as chloroform and 1-octanol showed relatively high surface tension with dS-CNC (5H), dS-CNC (10H) and dS-CNC (20H) compared with dS-CNC (30H) (Figure 25E and 25F). It resulted from the low emulsion stability because the hydrophilicity of dS-CNC (5-20H) surface was still high so that water and polar liquids were miscible. Meanwhile, S-CNCs did not form stable emulsions due to the high miscibility with polar liquids and incompatibility with nonpolar liquids. It resulted in the high content of S-CNCs dispersed freely in water and the rapid decrease of the water surface tension.

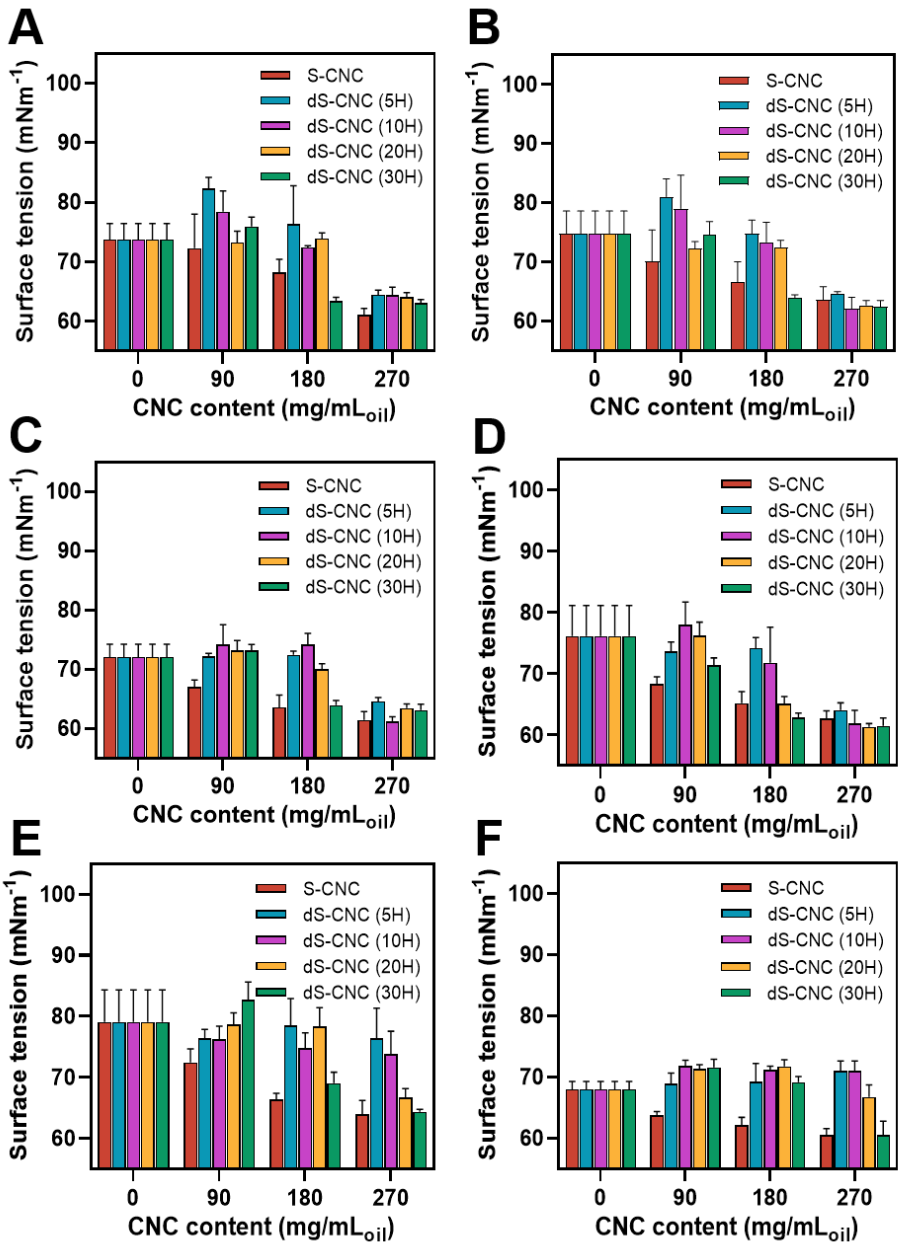

Figure 25. Surface tension of the CNC/oil Pickering emulsion at different CNC content. (A) *n*-Decane, (B) *n*-dodecane, (C) *n*-tetradecane, (D) *n*-hexadecane, (E) chloroform, and (F) 1-octanol. (N=4, error bar=SD).

3.4. Summary

CNCs are promising for an emulsifying agent in food and compositing processes. Their functionality could be modified by the control of the surface chemistry including surface charge and polarity. The surface charge of CNCs was controlled by the desulfurization of sulfonated CNCs which were negatively charged. The dS-CNCs with a different negativity showed the surface charge effect on encapsulation of four nonpolar liquids and two polar liquids. The emulsion stability verified that highly charged S-CNC was insufficient as an emulsifying agent and the reduction of surface charge was required. dS-CNC desulfated for 30 hours formed a small size of emulsion droplets with high stability for a long term storage. The desulfation could be one of the top-down protocols to modulate the CNC surface properties.

IV

Larvicidal and antimicrobial activities of essential oil stabilized by S-CNC

4.1. Introduction

Plant essential oils are natural substances that have been actively studied in the fields of pharmaceuticals, packaging and cosmetics for reducing microbial contamination [158-161]. Essential oils contain several bioactive ingredients including alcohols, phenols, terpenes, esters and other [39, 40] and show strong antimicrobial activities. Essential oil is a well-known substance showing antimicrobial activity against gram (-) and gram (+) bacteria [132, 133]. They also present larvicidal activity against insects and could be a potential matter for mosquito-controlling agent.

However, essential oils have a low surface energy and high volatility, which makes it difficult to use essential oils in an aqueous phase [161]. The low surface tension of essential oils causes phase separation with aqueous solutions, and the high volatility of essential oils reduces the sustainability and stability of antimicrobial and larvicidal activities. For this reason, volatile essential oils need to be encapsulated in the form of an emulsion that is dispersible in water.

The Asian tiger mosquito, *Ae. albopictus*, is a vector insect of DENV and CHIKV, and spread quickly to new locations from its native geographical origin [136]. *Ae. albopictus* management has mainly dependent on various synthetic pesticides around the world [137, 138]. However, the continued use of synthetic pesticides has caused several side effects such as environmental and human health concerns and undesirable effects on natural enemies, non-targeted organisms [139, 140]. Another problem is that the resistance of *Ae. albopictus* to synthetic Pesticide has been reported in several countries [137, 138]. Recently, plant essential oils and their constituents are considered as good sources for mosquito-controlling agents. Larvicidal activities of many

plant essential oils against *Ae. albopictus* have been reported [141-145]. Development of proper formulation is another research field for practical use of plant essential oils based mosquito larvicides. Nanoemulsion based formulation have been reported to improve efficacy, stability and solubility of plant essential oils in water [61].

Pickering emulsions are one method for encapsulating a phase separating liquid phase with surface active particles [1-3]. Pickering emulsion stabilizes biphases with different surface energies using amphiphilic particles instead of a low molecular weight linear surfactant. S-CNCs are appropriate particles for Pickering emulsions because they have a high aspect ratio of crystalline rods, as well as amphiphilicity [17, 162].

The stability and morphology of Pickering emulsions are closely related with the properties of emulsifying particles. A high aspect ratio S-CNC provides high structural stability to the emulsion and colloidal dispersion in the aqueous solution. Recently, emulsions stabilized with cellulose-based particles were demonstrated using MFC, NFC and CNCs [94, 163-166]. Such a cellulose-based stabilizer for Pickering emulsions is advantageous over synthetic or inorganic nanoparticles due to biocompatibility, degradability and cost issues [167].

In particular, CNCs are attractive as stabilizers compared with other types of cellulose particles such as sphere and nanofibers due to the better control in morphology and reproducibility of emulsion formation [79, 168, 169]. The rod-like CNCs tend to pack orderly because of the strong capillary forces, and space steric hindrance is structured at the interface inducing the resistance to coalescence of emulsions. On the contrary, a low aspect ratio of CNCs arrange disorderly on the emulsion droplet and desorb easily from the interface.

Here, volatile essential oils are encapsulated in Pickering emulsions using nature-derived CNC particles, and the essential oil solubility can be improved by dispersion in water. The amount of CNC and emulsifying agent in the process affects the size distribution of Pickering emulsion particles as well as the emulsion stability. Since sustained biological activity is one of the critical issues in ensuring reliable quality and reduced cost in industry, a long term evaluation of biocidal effects using S-CNC stabilized Pickering emulsion of essential oil is required.

4.2. Materials and method

4.2.1. Preparation of S-CNC

S-CNC was prepared with commercially available filter paper (Whatman, grade 2, Kent, UK) and sulfuric acid (Junsei Chemical Co. Ltd., 95.0%(w/w) purity, Tokyo, Japan) [26, 41]. 10 g filter paper was ground by a blender for 5 minutes and 100 mL of 60% (w/w) sulfuric acid was added. Then, acidic pulp slurry was hydrolyzed with stirring at 45°C for 60 minutes. The hydrolyzed solution was diluted 10 times with deionized (DI) water and centrifuged at 6000 rpm for 20 minutes using a high speed refrigerated centrifuge (VS-24SMTi, Vision Scientific Co., Ltd., Daejeon, Korea). The obtained suspending S-CNC solution was dialyzed with a cellulose dialysis membrane (12-14 kDa, Spectra/Por, Breda, the Netherlands) for 7 days and subsequently concentrated using a rotary evaporator (N-1210BV-W, EYELA, Tokyo, Japan).

4.2.2. Preparation and characterization of S-CNC stabilized Pickering emulsion

Nutmeg (*Myristica fragrans*, Jin Aromatics, Anyang, Korea) thyme white (*Thymus vulgaris*, Korea Similac, Pochun, Korea), and *Cnidium officinale* root extract (*C. officinale* RE) were mixed with various content of S-CNC at a 1:10 ratio. The mixed solutions were tip-sonicated at 50% amplitude for 30 seconds using the ultrasonic processor (VCX 130, 435-09, Sonics & Materials Inc., Newtown, CT, USA). The S-CNC contents were fixed at 45, 90, 135, 180 and 225 mg per 1 mL of nutmeg essential oil. The S-CNC contents were fixed at 45, 90, 135 and 180 mg per 1 mL of thyme white. The S-CNC contents were fixed at 9, 22.5, 45, 67.5 and 90 mg per 1

mL of *C. officinale* RE.

Massoia (*Massoia aromatica*, Oshadhi Ltd., Cambridge, UK) and *Piper kadsura* stem extract (*P. kadsura* SE) were mixed with various S-CNC content solution at a 1:10 ratio. The mixed solutions were tip-sonicated at a 60% amplitude for 1 minute using the ultrasonic processor (VCX 130, 435-09). The S-CNC contents were fixed at 135, 180, 270, 360 and 450 mg per 1 mL of massoia essential oil. The S-CNC contents were fixed at 22.5, 45, 90, 135 and 180 mg per 1 g of *P. kadsura* SE.

All of Pickering emulsions consist of that S-CNC suspension (90 mL) was mixed with 10 mL or 10 g of essential oil.

Prepared Pickering emulsions were stored at room temperature for 25 days, and the solution appearance was captured with a digital camera. The height of separated layer was divided by the height of the solution to determine the emulsion fraction.

Pickering emulsions were placed in a Turbiscan (Turbiscan Lab Expert, Formulaction, Toulouse, France), and the dispersion stability of the Pickering emulsion was observed for 24 hours at room temperature. The turbiscan stability index (TSI) was calculated using the Turbiscan Easy Soft program installed in the equipment.

The shape and morphology of Pickering emulsion droplets were observed with a polarized light microscope (LV100, Nicon, Tokyo, Japan) or an inverted optical microscope (Eclipse Ts2, Nikon, Tokyo, Japan). S-CNC stabilized Pickering emulsions were diluted 100 times and the images of Pickering emulsion droplets were captured at the dark-field mode with 40× inverted routine microscope (Eclipse Ts2, Nikon, Tokyo, Japan) and bright-field mode with a 60× oil immersion objective lens (CFI plan apochromat lambda, Nikon, Tokyo, Japan). The diameter of Pickering emulsions was

measured using the ImageJ program.

The confocal fluorescence images of Pickering emulsion stabilized with dS-CNC was obtained by staining with 1 µl/mg$_{CNC}$ Calcoflour white (Sigma Aldrich) and 1.5 µg/µl$_{oil}$ Nile red (Sigma Aldrich) using a confocal laser scanning microscope (LSM710, Carl Zeiss, Overkochen, Germany) (CLSM SP8 X, Leica, Wetzlar, Germany).

The contact angle of S-CNC stabilized Pickering emulsions was measured using a droplet shape analyzer (EasyDrop FM40, KRÜSS, Hamburg, Germany) in sessile drop mode. 10 µL of Pickering emulsions were dropped on the borosilicate glass and their droplet shape was captured for the analysis of angles. The surface tension of Pickering emulsions was calculated by the Equation (4) [150].

$$\cos\theta = -1 + 2\left(\gamma_S^d/\gamma_{LG}^d\right)^{1/2} \qquad \text{Eq. (4)}$$

Where θ is the contact angle of the CNC and Pickering emulsion droplet on the borosilicate glass, γ_S^d is the surface tension of the borosilicate glass (47.6 mNm^{-1}), and γ_{LG}^d is the surface tension of the CNC and emulsion.

Rheological measurements were carried out using a digital rheometer (MARS III, Thermo Scientific, Newington, NH, USA) equipped with a 35 mm plate-plate geometry and a temperature controller [170]. Specifically, 50 µl of the Pickering emulsion was dropped on the plate for dynamic viscoelastic measurements. The gap size of the plate-plate was then adjusted to 0.1 mm, and mineral oil was dropped around the plate. The frequency sweep was performed at 0.5% strain in the range of 0.1 to 10 Hz [79, 171]. The value of tan δ was calculated at the 10 Hz frequency.

4.2.3. Antimicrobial activity test

All antimicrobial tests were carried out using Mueller Hinton (MH) broth (BD Difco, Bergen, NJ, USA) and Biochemie micro agar (Duchefa Biochemie, Amsterdam, The Netherlands) following the protocol of Wiegand et al. [172] Briefly, a liquid medium was prepared by addition of 15 g/L micro agar to a 21 g/L MH broth solution. After sterilization of a medium solution at 121°C for 20 minutes, the medium solution was added to a 15 mL petri dish (15 mm×100 mm) and solidified at room temperature. Prior to the experiment, the solid medium was incubated at 37°C for 30 minutes to identify the contamination. The antimicrobial activity of essential oil was evaluated using *E. coli* and *S. aureus*.

The S-CNC/essential oil Pickering emulsion and crude essential oil were added at 0.25, 0.5, 1, 2 and 4 μl/mL to the liquid medium containing 1 OD_{600}/mL of microbial solution, and it was incubated at 37°C while shaking. To measure the MIC and MBC of S-CNC/essential oil Pickering emulsion and crude essential oil, 1 mL of each solution was sampled. The absorbance of sampled solutions was measured at 600 nm with a microplate reader (Synergy HT, Bio Tek Instruments, Winooski, VT, USA). Then, the sampled solution was diluted 1000 times, spread on a solid medium, and incubated at 37°C for 3 days, subsequently. The same concentration of Penicillin-Streptomycin solution (Life technologies, Carlsbad, CA, USA) was added to the liquid medium as a positive control sample.

4.2.4. Larvicidal activity test

Ae. albopictus was incubated without exposure to pesticide at a temperature of 26±1°C and a relative humidity of 60%. Larvae were incubated for 16 hours in light and 8 hours in dark and were supplied the larva with a sterilized diet (Super TetraMin®, Sewha Pet Food Co. Seoul, Korea) composed of 40-mesh chick chow powder and yeast (4:1). To supply blood to *Ae. albopictus*, live mice in a steel cage were supplied using a method approved by the Institutional Animal Care and Use Committee (KCDC-020-11-2A). The larvae obtained from the adult *Ae. albopictus* were incubated in plastic pans (24×35×5 cm^3) with sterilized food and water at the same temperature and relative humidity.

All of essential oils dissolved in ethanol and CNC based Pickering emulsions dissolved in water at treated concentration was prepared, and 1 mL of essential oils was applied in 200 mL of water in 270 mL paper cups. 10 early third instar *Ae. albopictus* larvae were used in each treatment. A separate set of cups that received 1 mL of ethanol or S-CNC only served as the controls. Treated and control larvae were kept at 26±1°C, with a relative humidity of 60±5%, under a 16:8 hours light:dark cycle, and larval mortality was investigated 48 hours after treatment. All treatments were replicated 4 times.

4.3. Results and discussion

4.3.1. Colloidal stability of S-CNC/nutmeg Pickering emulsions

Nutmeg Pickering emulsions were stable at S-CNC 180 and 225 mg/mL_{Nutmeg} after the storage for 10 days while the emulsion fraction was decreased to about 20% after the storage for 1 day due to the phase separation of emulsion at S-CNC 45, 90 and 135 mg/mL_{Nutmeg} (Figure 26).

Microscopic images showed S-CNC shell structures at the surface of Pickering emulsions (Figure 27A). The size of Pickering emulsions was in the range between 4 and 10 μm and the size was decreased the S-CNC content increased (Figure 27B-27D).

The nutmeg encapsulated in Pickering emulsions was imaged by confocal microscopy (Figure 28). Blue fluorescence represented S-CNCs stained with Calcofluor white, and red fluorescence represented nutmeg stained with Nile red. Nutmeg were encapsulated in the S-CNC Pickering emulsions. The S-CNCs formed a shell structure at the surface of the Pickering emulsions and the nutmeg were contained inside the shells. The densely packed S-CNC shells formed a rigid structure, reducing the aggregation of particles and maintaining colloidal stability for an extended period.

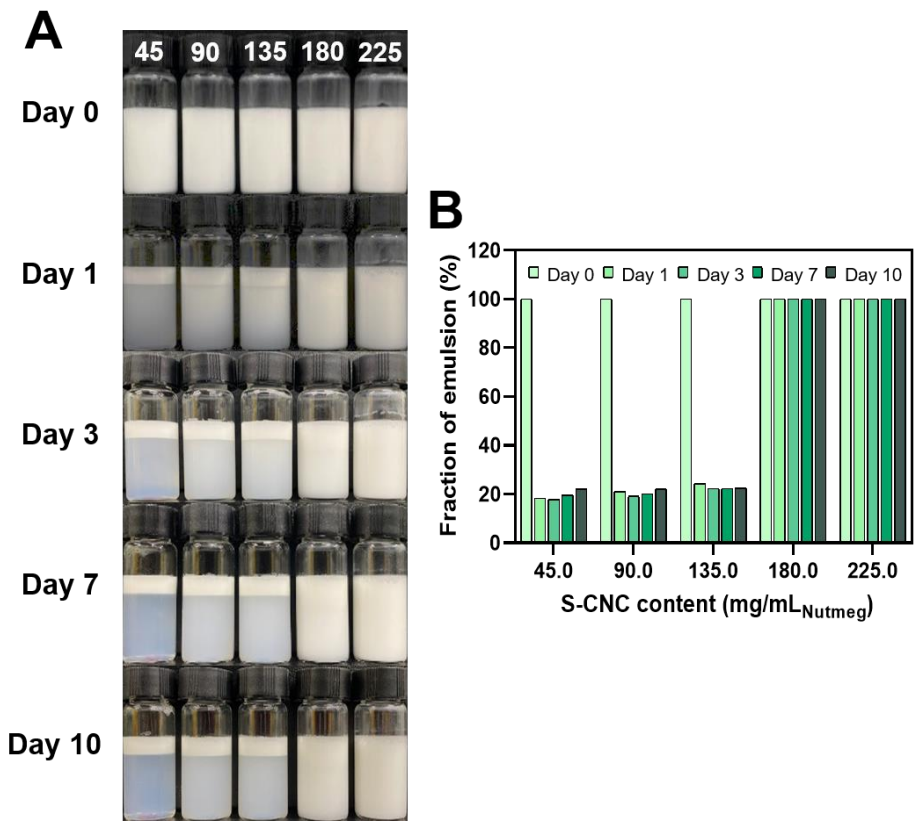

Figure 26. Phase separation of S-CNC/nutmeg Pickering emulsion at different S-CNC content and storage time. (A) Digital images of Pickering emulsion (Unit: S-CNC mg/mL$_{Nutmeg}$) and (B) the emulsion fraction stored for 10 days.

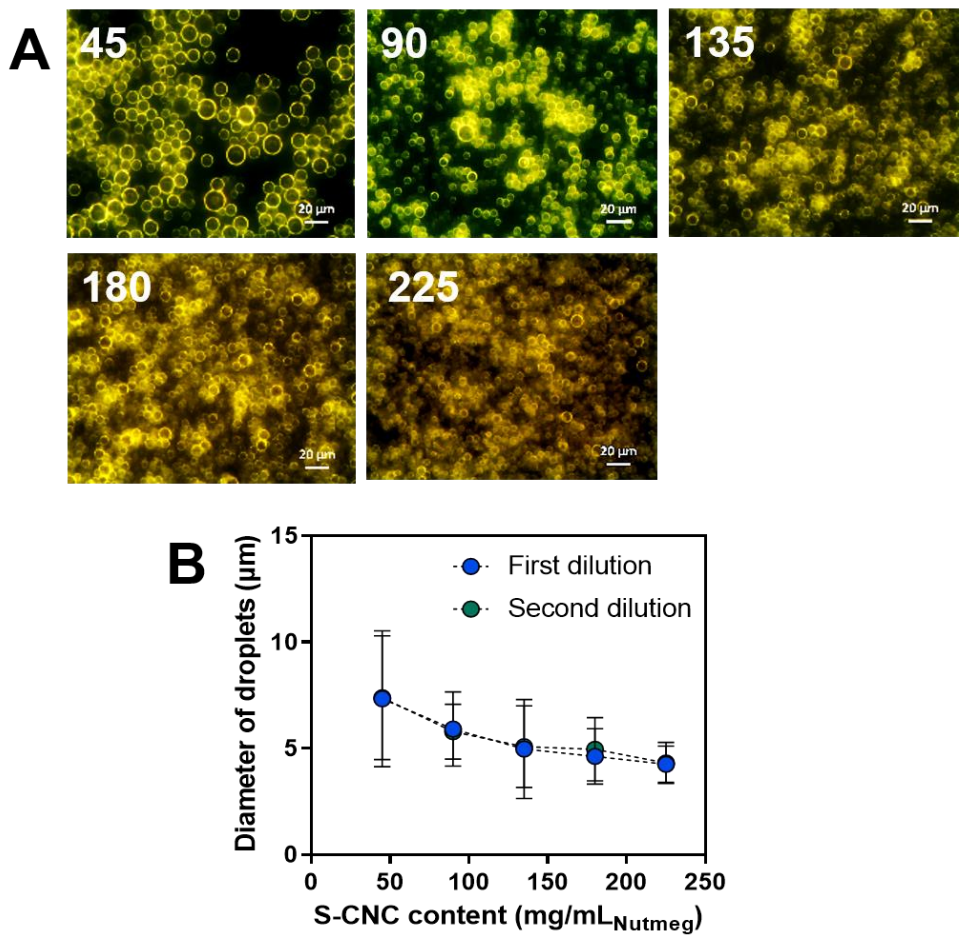

Figure 27. S-CNC/nutmeg Pickering emulsions at different S-CNC content. (A) Dark-field microscopic images of Pickering emulsion (Unit: S-CNC mg/mL$_{Nutmeg}$), (B) size of emulsion droplets and, (C, D) size distribution of emulsion droplets. (C) First dilution and (D) second dilution. (N = 300, error bar = SD).

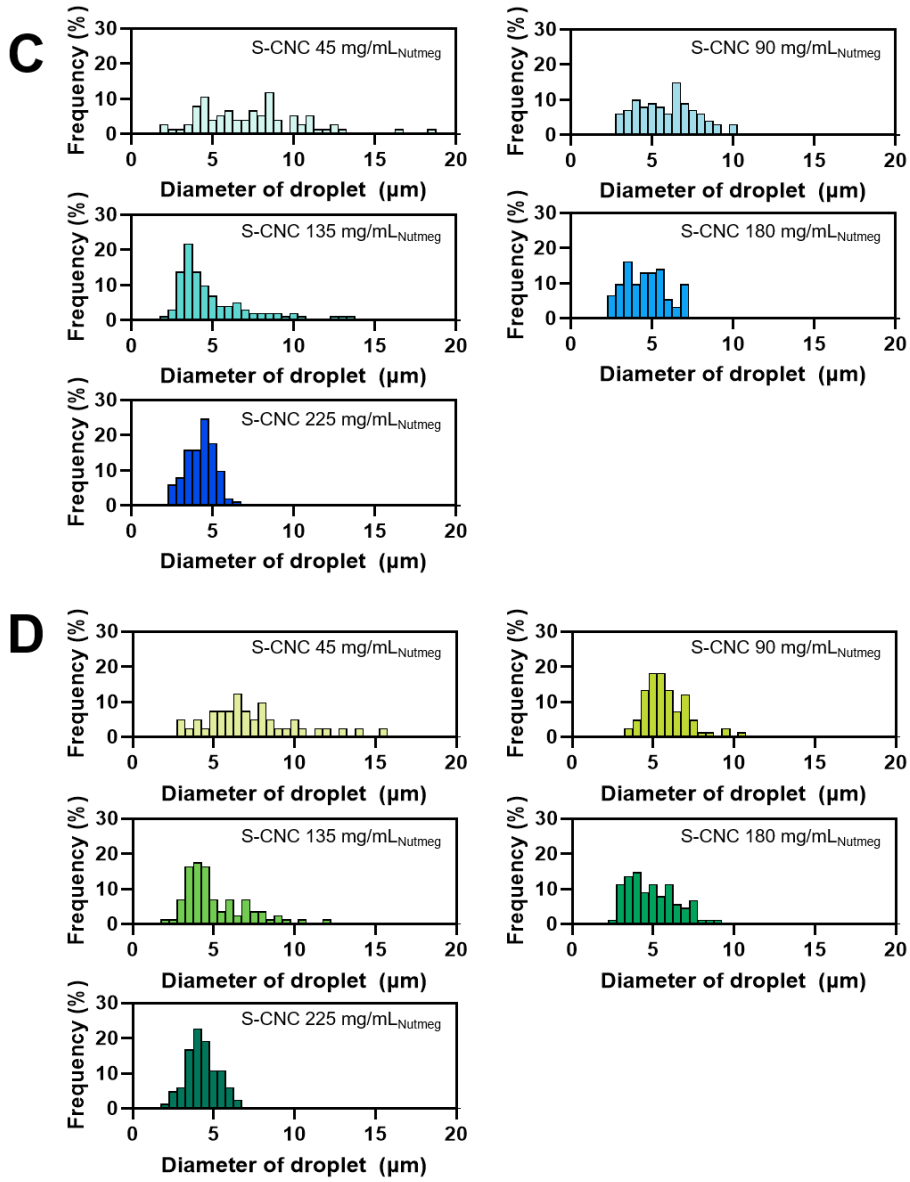

Figure 27. (Continued)

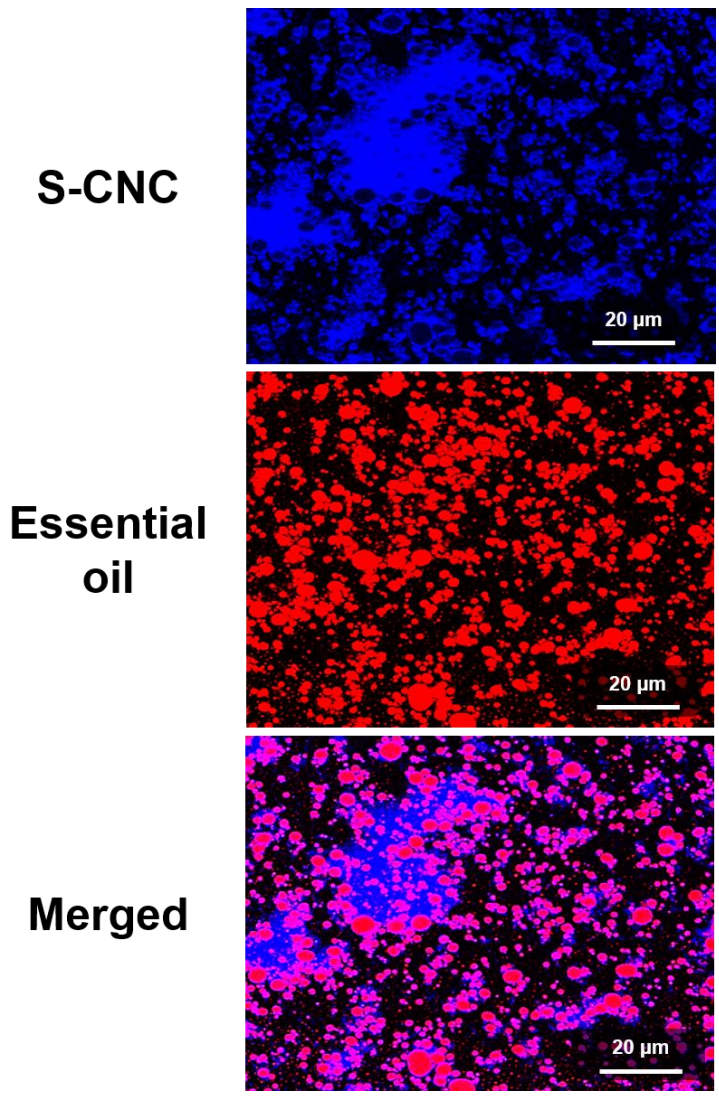

Figure 28. Confocal microscopic images of S-CNC/nutmeg Pickering emulsions (S-CNC 180 mg/mL$_{Nutmeg}$). S-CNCs labeled with Calcofluor white fluorescent dye and nutmeg labeled with Nile red fluorescence dye.

4.3.2. Larvicidal activity of S-CNC/nutmeg Pickering emulsions

The larvicidal effect of S-CNC/nutmeg Pickering emulsions against *Ae. albopictus* are shown in Table 4. The LC_{50} values of S-CNC/nutmeg Pickering emulsion and crude nutmeg were 18.30 and 39.62 μg/mL, respectively. S-CNC/nutmeg Pickering emulsion was 2.1-fold more active than crude nutmeg. The larvicidal activities of S-CNC/nutmeg Pickering emulsions were stronger than those of crude nutmeg. This may be a function of the high solubility of nutmeg essential oils in water. Another reason for the strong activity of S-CNC-based Pickering emulsions may be controlled release of nutmeg, as nutmeg and their constituents easily evaporate when treated in water.

Larvicidal effect of nutmeg constituents against *Ae. albopictus* have been documented in previous studies [141, 142, 173-176]. Lee et al. [177] reported that the LC_{50} values of (+)-*α*-pinene, (-)-*α*-pinene, myrcene, and (+)-terpinen-4-ol against *Ae. albopictus* were 55.65, 28.61, and 35.98 mg/L, respectively. However, the values for (+)-*α*-pinene, (-)-*α*-pinene, myrcene, and (+)-terpinen-4-ol were > 100 μg/mL in this study. The larvicidal activities of (+)-limonene, *α*-terpinene, *α*-phellendrene, and *γ*-terpinene reported in previous study [174] were slightly stronger than those in this study, but the larvicidal activity of terpinolene was slightly weaker than that of this study. A previous research effort [141] and this study discovered different larvicidal activities associated with eugenol and methyleugenol. Larvicidal activity of eugenol was stronger than that of methyleugenol in a previous study [141] but the relationship was reversed in this study. In a report by Seo et al. [175] the insecticidal activities of myristicin and elemicin were similar to those of this study. The differences in larvicidal activities of essential oils constituents

against *Ae. albopictus* may be attributable to the use of a different strain of test insect. Larvicidal activities of eugenol and its derivatives, such as methyleugenol, isoeugenol, and methylisoeugenol, showed that the methoxy group and a double-bond position affected activity. Larvicidal activities of eugenol and methyl eugenol with an allyl group were stronger than those of isoeugenol and methylisoeugenol with a propenyl group, and larvicidal activities of methyl eugenol and methylisoeugenol with two methoxy groups at a benzene ring were stronger than those of eugenol and isoeugenol with one methoxy group. Bhardwaj et al. [177] reported that larvicidal activity of methyl eugenol was stronger than that of eugenol against the tobacco armyworm, *Spodopter litura*. Methyleugenol exhibited strong contact toxicity against the cigarette beetle, *Lasioderma serricorne* compared with methylisoeugenol [181].

Table 4. Larvicidal activity of S-CNC stabilized Pickering emulsions of nutmeg against *Ae. albopictus*.

Test materials	Larvicidal activity (%, mean ± S.E., N=4)			
	100[1]	**50**	**25**	**12.5**
Crude nutmeg	90.0 ± 4.1b[2]	85.0 ± 9.6a	12.5 ± 2.5cd	0b
S-CNC/nutmeg Pickering emulsion	100a	100a	82.5 ± 8.5a	12.5 ± 4.8a
Conctrol (S-CNC only)	0c	0b	0d	0b
	$p < 0.0001$	$p < 0.0001$	$p < 0.0001$	$p < 0.024$

[1] μg/mL
[2] Means within a column followed by the same letters are not significantly different (Scheffe's test)

4.3.3. Colloidal stability of S-CNC/massoia Pickering emulsions

The stability of Pickering emulsions could be evaluated by observing the phase separation of the emulsion and the change of emulsion fraction for a long term storage at different S-CNC content (Figure 29). The phase separation of the emulsion was observed at S-CNC 135 and 180 mg/$mL_{Massoia}$ Pickering emulsions. It resulted from the insufficient S-CNC content for emulsifying the massoia. In contrast, S-CNC 270 mg/$mL_{Massoia}$ and more content formed a stable emulsion state without phase separation for 10 days (Figure 29A). The fraction of emulsion was decreased to about 20% for S-CNC 135 and 180 mg/$mL_{Massoia}$ Pickering emulsions, but no significant change was shown for S-CNC 270 mg/$mL_{Massoia}$ and more (Figure 29B).

Microscopic images showed a shell structure of Pickering emulsions due to the densely packed S-CNCs at the surface (Figure 30A). The size of Pickering emulsions was in the range between 3 and 8 μm and the size distribution of Pickering emulsions prepared at S-CNC 135 and 180 mg/ $mL_{Massoia}$ was relatively wider than the other Pickering emulsions (Figure 30B-30D). Typically, the Pickering emulsion size was decreased as the S-CNC content increased.

The droplets encapsulated in Pickering emulsions were imaged by confocal microscopy (Figure 31). It was confirmed that massoia were encapsulated in the S-CNC Pickering emulsions. S-CNCs formed a shell structure at the surface of Pickering emulsions and massoia were contained inside the shells. The packed S-CNC shells formed a rigid structure reducing the aggregation of particles and keeping the colloidal stability for a long-term.

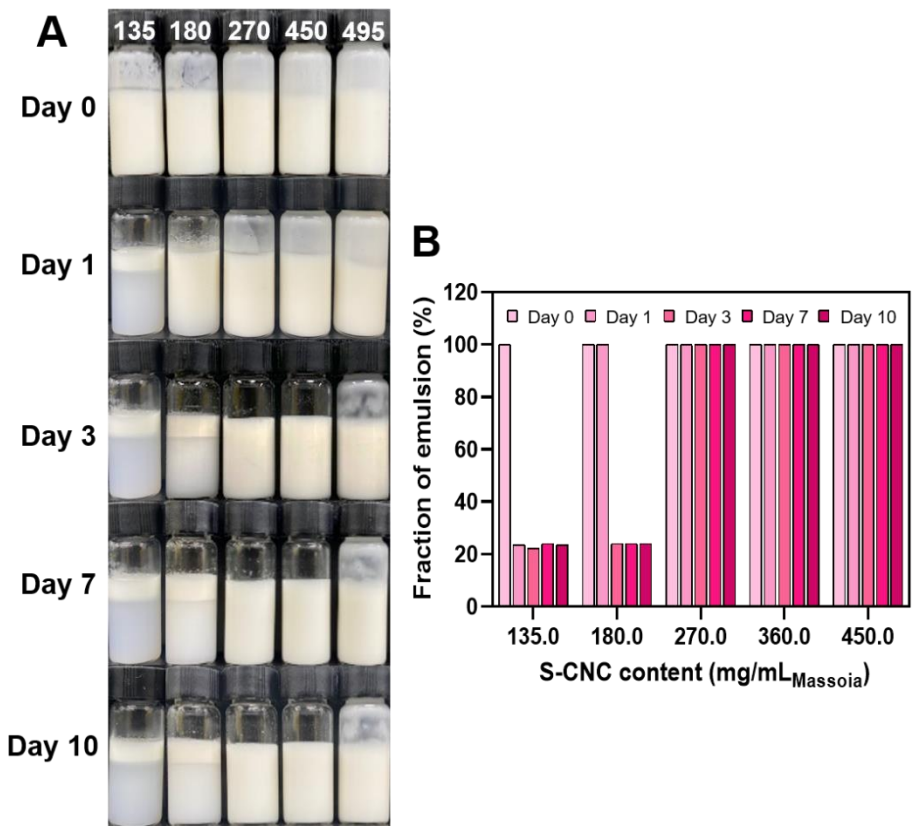

Figure 29. Phase separation of S-CNC/massoia Pickering emulsions at different S-CNC content and storage time. (A) Digital images of Pickering emulsion (Unit: S-CNC mg/mL$_{Massoia}$) and (B) the emulsion fraction stored for 10 days.

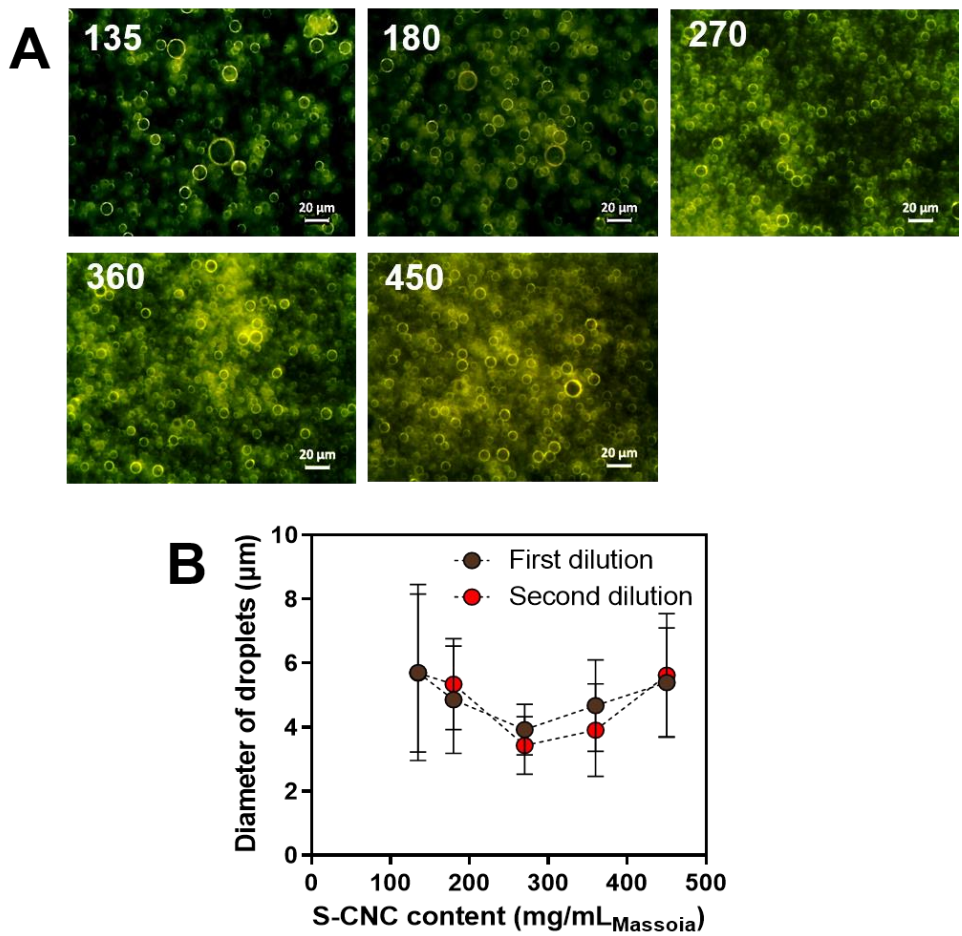

Figure 30. S-CNC/massoia Pickering emulsions at different S-CNC content. (A) Dark-field microscopic images of Pickering emulsions (Unit: S-CNC mg/mL$_{Massoia}$), (B) size of emulsion droplets and, (C, D) size distribution of emulsion droplets. (C) First dilution and (D) second dilution. (N = 300, error bar = SD).

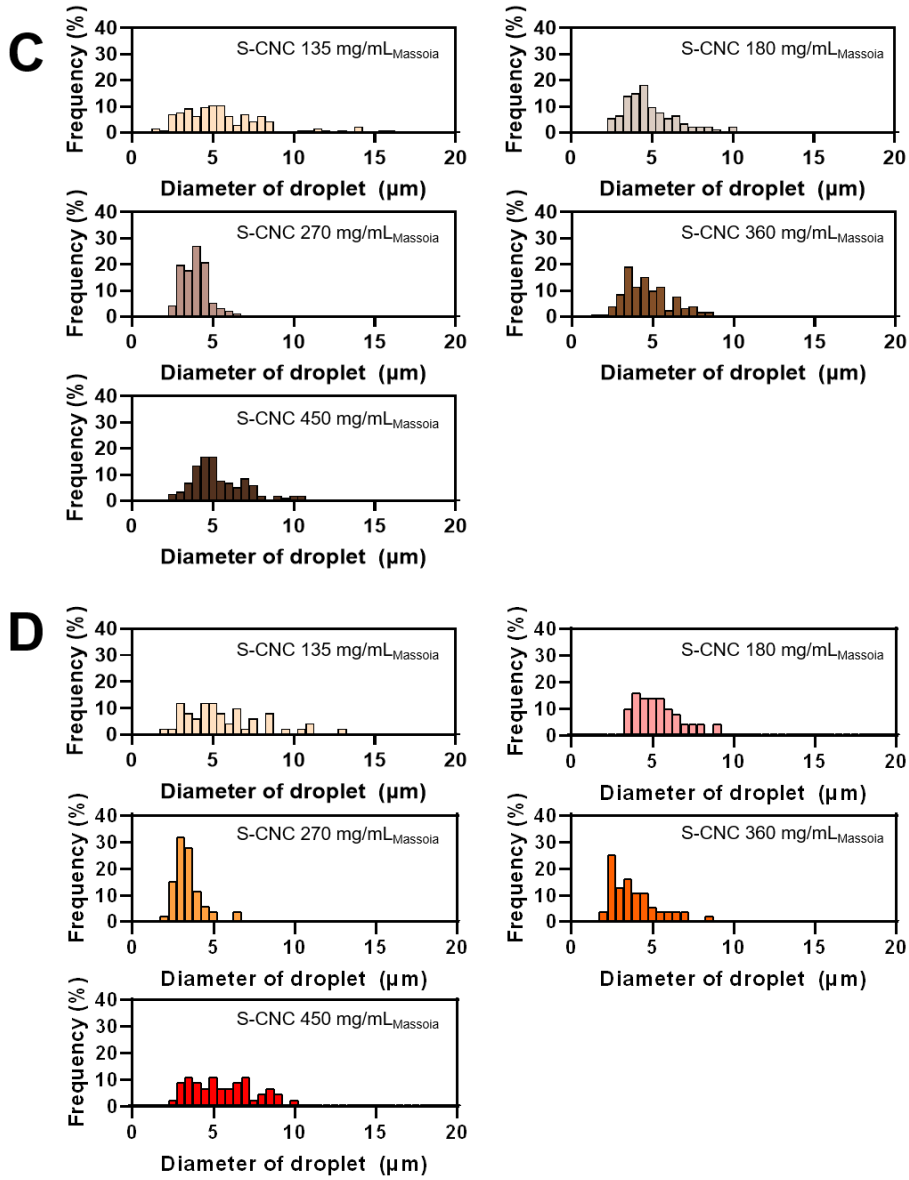

Figure 30. (Continued)

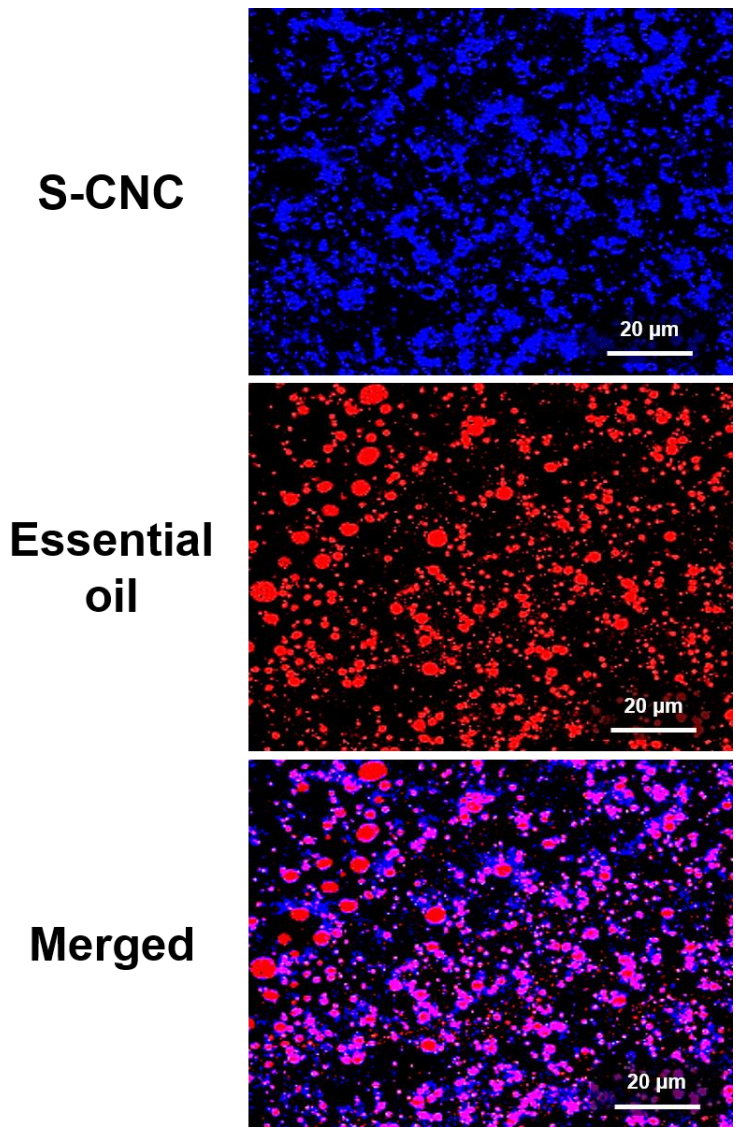

Figure 31. Confocal microscopic images of S-CNC/massoia Pickering emulsions (S-CNC 270 mg/mL$_{Massoia}$). S-CNCs labeled with Calcofluor white fluorescent dye and massoia labeled with Nile red fluorescence dye.

4.3.4. Larvicidal activity of S-CNC/massoia Pickering emulsions

The larvicidal effect of S-CNC/massoia Pickering emulsions against *Ae. albopictus* are shown in Table 5. Larvicidal activity of S-CNC/massoia Pickering emulsions was higher than that of crude massoia. Larvicidal activities of S-CNC/massoia Pickering emulsion and crude massoia were 100% and 97.5% at 50 μg/mL, respectively. Mortality of *Ae. albopictus* treated with S-CNC only was 0%.

Bin Jantan et al. [141] reported that the LC_{50} values of benzayl salicylate, benzyl benzoate, and safrole were 5.5, 6.5, and 28.0 μg/mL, respectively. Larvicidal activity of benzyl salicylate was weaker than that of this study, but larvicidal activities of benzyl benzoate and safrole were slightly stronger.

Differences in the chemical structure of C10 and C12 massoia lactones include the aliphatic chain length at the C6 position, and this may be responsible for the difference in larvicidal activity against *Ae. albopictus*. Previous studies indicated that the chain length of compounds with similar chemical structures can play an important role in insecticidal and nematicidal activity [179, 180]. Hammond and Kubo [179] evaluated the larvicidal activity of alkanols with C1-C20 chain lengths against the mosquito *Culiseta incidens*. They found that larvicidal activities of dodecanol, tridecanol, and undecanol, with chain lengths of 12, 13, and 11, respectively, were stronger than those of alkanols with other chain lengths. Seo et al. [180] also reported that an optimal chain length of aliphatic compounds was necessary for nematicidal activity against the pine wood nematode *Bursaphelenchus xylophilu*. Nematicidal activities of aliphatic compounds with a C9-C11 chain length were stronger than other aliphatic compounds with other chain lengths.

Table 5. Larvicidal activity of S-CNC stabilized Pickering emulsions of massoia against *Ae. albopictus*.

Test materials	**Larvicidal activity (%, mean ± S.E., N=4)**			
	100[1]	**50**	**25**	**12.5**
Crude massoia	100a[2]	97.5 ± 2.5b	37.5 ± 4.8bc	-
S-CNC/massoia Pickering emulsion	100a	100a	65.0 ± 8.7ab	12.5 ± 4.8a
Conctrol (S-CNC only)	0c	0b	0d	0b
	$p < 0.0001$	$p < 0.0001$	$p < 0.0001$	$p < 0.024$

[1] μg/mL
[2] Means within a column followed by the same letters are not significantly different (Scheffe's test)

4.3.5. Colloidal stability of S-CNC/*P. kadsura* SE Pickering emulsions

The colloidal stability of Pickering emulsions was investigated by storing Pickering emulsions up to 10 days (Figure 32A). The S-CNCs adhered to the surface of the *P. kadsura* SE oleic compound solution and increased the solubility in the aqueous solution by the ionic hydrophilic groups. The destruction of emulsion occurred due to the aggregation of insoluble particle components and incomplete formation of Pickering emulsions, which deteriorated the colloidal stability of Pickering emulsion. The oleic compound in the incomplete Pickering emulsions was released rapidly and formed a clear region at the upper part as the storage time increased. The stability of S-CNC/*P. kadsura* SE Pickering emulsions was dependent on the S-CNC content in the formulation process and it needed at least S-CNC 135 mg/$g_{P. kadsura\ SE}$ to maintain the emulsion stability for the long term storage up to 10 days. Pickering emulsions formed at less than S-CNC 135 mg/$g_{P. kadsura\ SE}$ showed the phase separation of the emulsion structure.

The emulsion stability of S-CNC/*P. kadsura* SE Pickering emulsions was evaluated by the comparison of the emulsion fraction remaining after the storage (Figure 32B). The Pickering emulsion fraction with S-CNC 22.5 mg/$g_{P. kadsura\ SE}$ decreased below 60% after the storage for 7 days. The phase separation was inhibited by the increase of the S-CNC content in the emulsion formulation process but approximately 20% of Pickering emulsions were phase-separated at S-CNC 90 mg/$g_{P. kadsura\ SE}$ after the storage for 10 days. The phase separation apparently decreased with the S-CNC content of 135 mg/$g_{P. kadsura\ SE}$ and more. It resulted from the complete formation of emulsion structure by the sufficient coverage of *P. kadsura* SE with emulsifying S-

CNCs. The spherical shape of Pickering emulsions was observed with dark filed microscopic images (Figure 33A). The average diameter of Pickering emulsions formed at S-CNC 22.5 mg/g*P. kadsura* SE was 6 μm and the size distribution was relatively broad (Figure 33B and 33C). It resulted from the high viscosity of *P. kadsura* SE which tended to coagulate to form large spherical droplets. The size of droplets decreased by the use of large amount of emulsifying agent such as S-CNCs. The droplet size decreased to 3 μm at S-CNC 135 mg/g*P. kadsura* SE with a narrow size distribution.

The encapsulation of *P. kadsura* SE oleic compounds in Pickering emulsions at S-CNC 135 mg/g*P. kadsura* SE was visualized by confocal microscopy (Figure 34). *P. kadsura* SE oleic compounds were stably encapsulated with S-CNCs showing separate and combined colors. The Pickering emulsions were well distributed without aggregation due to the electrostatic repulsion between the ionic S-CNCs and stable in the storage up to 10 days.

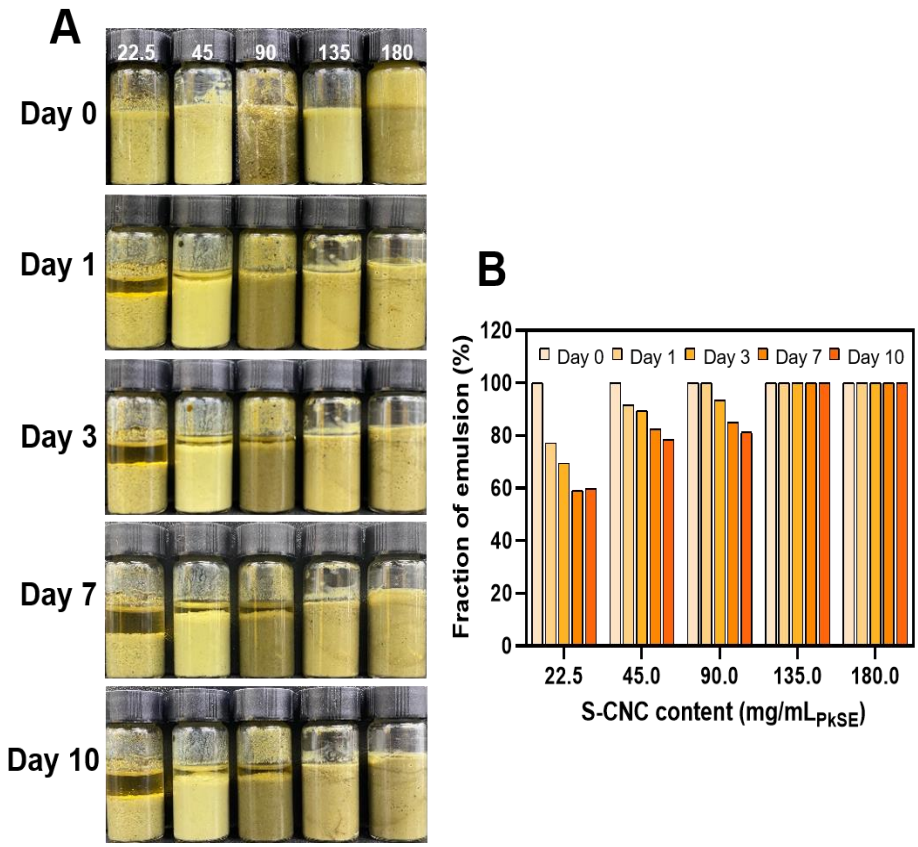

Figure 32. Evaluation of emulsion stability of S-CNC/*P. kadsura* SE Pickering emulsions at different S-CNC content and the storage time. (A) Visual appearance of stored Pickering emulsions (Unit: S-CNC mg/g$_{P. kadsura\ SE}$) and (B) fraction of remaining emulsions.

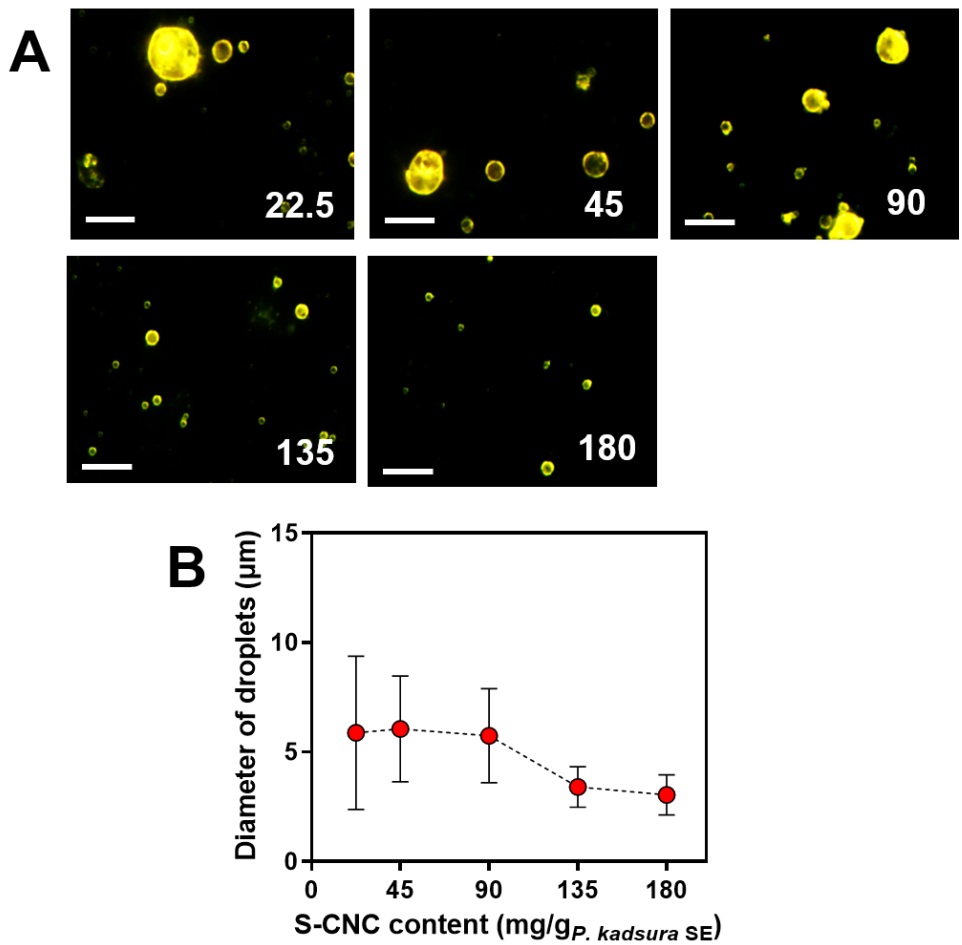

Figure 33. Size distribution of S-CNC/*P. kadsura* SE Pickering emulsions. (A) Dark-field microscopic images of Pickering emulsion (Unit: S-CNC mg/g*P. kadsura* SE), (B) size distribution and (C) average diameter of droplets prepared at different S-CNC concentrations. N= 150, error bar = SD. (Scale bar : 20 μm).

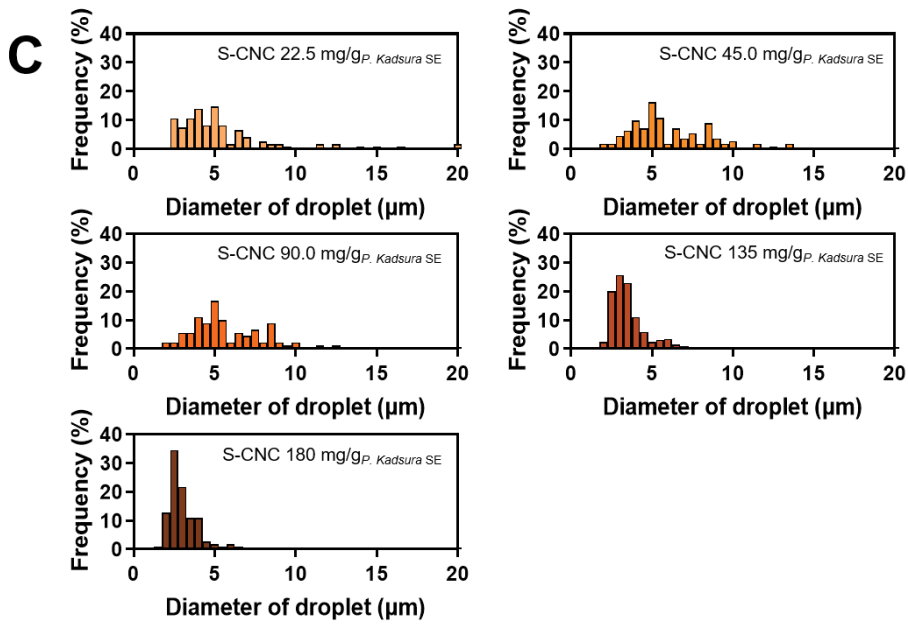

Figure 33. (Continued)

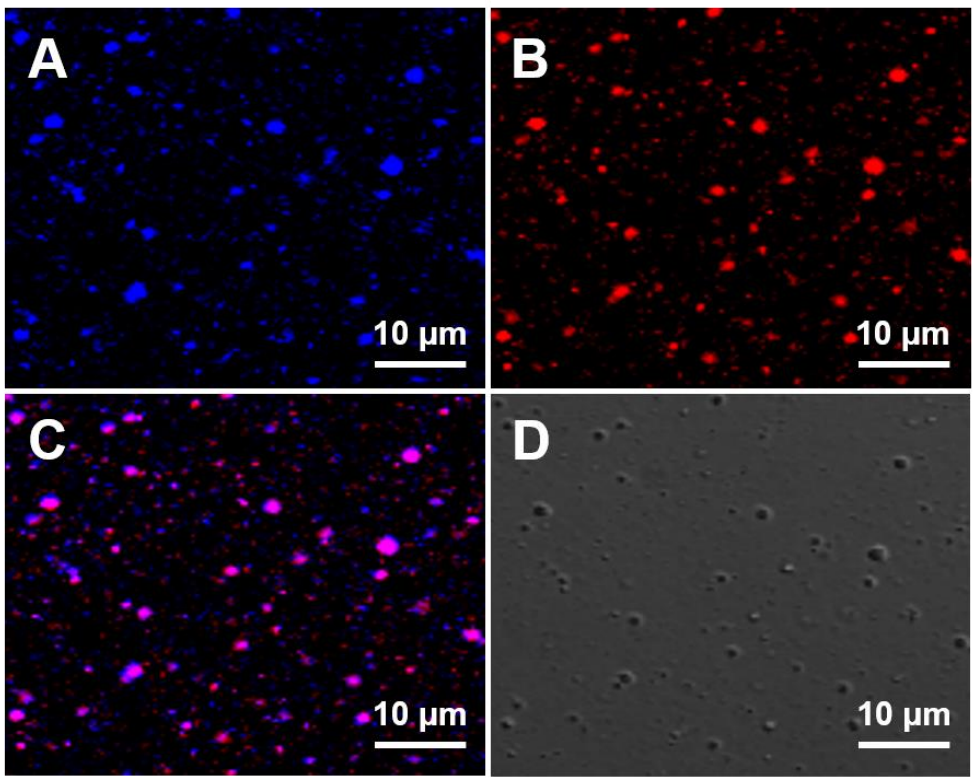

Figure 34. Confocal microscopic images of S-CNC 135 mg/mL*P. kadsura* SE Pickering emulsions. (A) S-CNCs labeled with Calcofluor white fluorescent dye, (B) *P. kadsura* SE labeled with Nile red fluorescence dye, (C) combined confocal image of A and B and (D) bright field optical image.

4.3.6. Larvicidal activity of S-CNC/*P. kadsura* SE Pickering emulsions

Larvicidal activity of pure *P. kadsura* SE and S-CNC/*P. kadsura* SE Pickering emulsions is shown in Table 6. Larvicidal activity of S-CNC/*P. kadsura* SE Pickering emulsions was slightly higher than that of pure *P. kadsura* SE. Larvicidal activities of *P. kadsura* SE and S-CNC/*P. kadsura* SE Pickering emulsions were 80.0 and 97.5% at 50 μg/mL concentration, and 25.0 and 30.0% at 25 μg/mL concentrations, respectively. In this article, the results showed that S-CNC stabilized Pickering emulsions of *P. kadsura* SE was stable and well diffused in water. In addition, larvicidal activity of S-CNC stabilized Pickering emulsion of *P. kadsura* SE was slightly higher than that of pure *P. kadsura* SE. This indicates that S-CNC stabilized Pickering emulsion is a suitable formulation for the practical use of botanical pesticide in field.

Insecticidal activities of piperamides have been documented in many previous studies [181-184]. Park et al. [181] reported the larvicidal activity of four piperamides such as pellitorine, guineensine, pipercide and retrofractamide A against three mosquito species. Although isobutylamine moiety of piperamides was found to be essential for toxicity against mosquito larvae, there was a difference in larvicidal activity between piperamides with and without methylendioxyphenyl moiety. Larvicidal activity of guineensine, pipercide and retrofractamide A with methylendioxyphenyl moiety was stronger than that of pellitorine without methylendioxyphenyl moiety against three mosquito species. This study showed the same result. Larvicidal activity of chingchengenamide A with methylendioxyphenyl moiety was stronger than that of pellitorine without methylendioxyphenyl moiety against *Ae.*

albopictus. Pellitorine with a conjugated dienamide chromophore (-C=C-C=C-CONH-) was quite unstable owing to unsaturation, and this might cause low activity of pellitorine compared to other piperamides. The methylenedioxyphenyl moiety is thought to stabilize the chemical structure of piperamides [181]. Although insecticidal activity of many piperamides have been documented [181-184], this is the first report on the larvicidal activity of chingchengenamide A against *Ae. albopictus*.

Neolignans are another important natural compounds found in almost every vegetative parts of *Piper* spp., and many biological activities of neolignans such as anti-inflammatory, antimicrobial, antioxidant, and antitumoral activity have been reported [185]. Insecticidal activity of neolignans has been also documented [186, 187]. Specifically, benzofuran-type neolignans such as eupomatenoid-5, eupomatenoid-6, concarpan, and burchellin showed strong insecticidal activity against mosquito, and piperenone belongs to benzofuran-type neolignans. Although antifeeding activity of piperenone against *S. litura* was reported in previous study [188], this is the first report on insecticidal activity of piperenone.

Table 6. Larvicidal activity of *P. kadsura* SE and S-CNC/*P. kadsura* SE Pickering emulsion against *Ae. albopictus*.

Test materials	**Larvicidal activity (%, mean ± S.E., N=4)**		
	100[1]	**50**	**25**
Crude *P. kadsura* SE	100a[2]	80.0 ± 14.14b	25.0 ± 5.77a
S-CNC/*P. kadsura* SE Pickering emulsion	100a	97.5 ± 5.00a	30.0 ± 8.16a
Conctrol (EtOH)	2.5 ± 5.0b	0c	0b
Conctrol (S-CNC only)	2.5 ± 5.0b	2.5 ± 5.0c	2.5 ± 5.0b
	$p < 0.0001$	$p < 0.0001$	$p < 0.0001$

[1] μg/mL
[2] Means within a column followed by the same letters are not significantly different (Tukey's HSD test)

4.3.7. Colloidal stability of S-CNC/*C. officinale* RE Pickering emulsions

The visual appearance of S-CNC/*C. officinale* RE Pickering emulsions for 14 days was depicted at the Figure 35. *C. officinale* RE is composed of not only hydrophobic oleic compounds but also hydrophilic polar compounds. Therefore, the side appearance of S-CNC/*C. officinale* RE Pickering emulsions seem to be well-dispersed in the aqueous solution without phase separation and the emulsion fraction of S-CNC/*C. officinale* RE Pickering emulsion maintained 100% without phase separation even after 14 days. However, in facts, since the encapsulated inner part by S-CNC was the hydrophobic oleic compounds, aggregation of the oleic compounds caused by insufficient S-CNC in the solution, so, after 14 days, S-CNC 9 and 22.5 mg/mL$_{C.\ officinale\ \mathrm{RE}}$ Pickering emulsion formed a dark brown sedimentation. The Pickering emulsions stabilized by S-CNC content at 45 mg/mL$_{C.\ officinale\ \mathrm{RE}}$ and more showed mild brown color like color of side appearance without sedimentation.

The surface tension of water and *C. officinale* RE mixture was governed by addition of S-CNC (Figure 36A). As the S-CNCs added to the mixed solution, the S-CNCs are absorbed to the interface between water and oleic compounds and, at the same time, absorbed to the interface between air and water. The S-CNC located surface of S-CNC/*C. officinale* RE Pickering emulsions gradually decreased interfacial energy gap between A/W by change S-CNC content from 0 mg/mL$_{C.\ officinale\ \mathrm{RE}}$ to 22.5 mg/mL$_{C.\ officinale\ \mathrm{RE}}$. As increase of the S-CNC content above 45 mg/mL$_{C.\ officinale\ \mathrm{RE}}$, the Pickering emulsions was finally reached equilibrium surface tension to near 55 mNm^{-1} which was the equilibrium surface tension of S-CNC (Figure 36B).

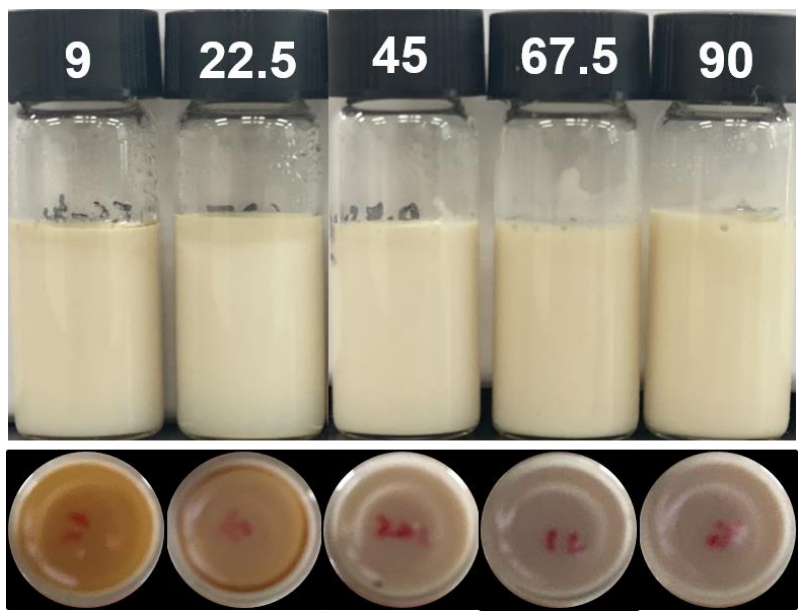

Figure 35. Side and bottom visual appearances of S-CNC/*C. officinale* RE Pickering emulsions stored at the room temperature for 14 days. The S-CNC contents was 9, 22.5, 45, 67.5 and 90 mg/mL*C. officinale* RE.

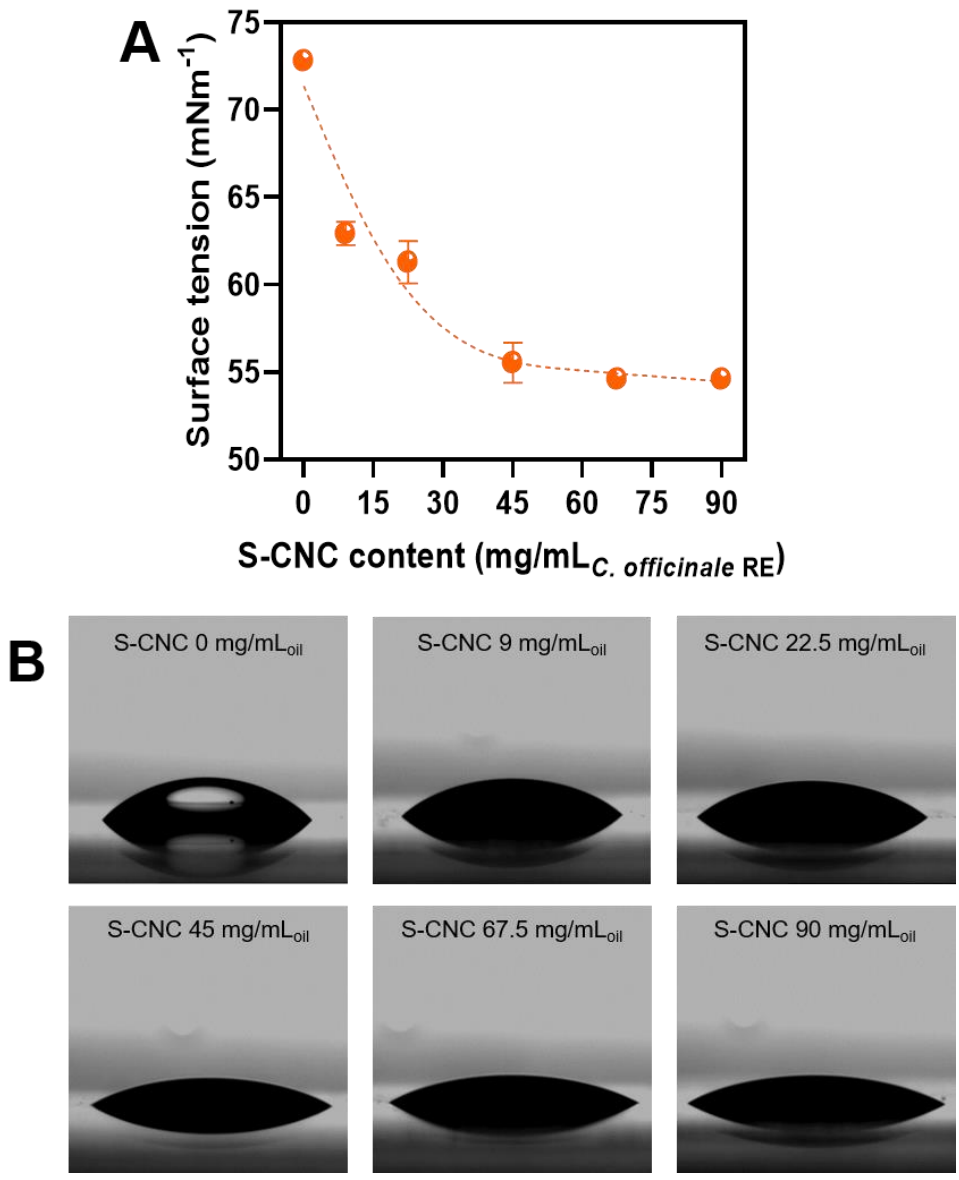

Figure 36. Surface properties of S-CNC/*C. officinale* RE Pickering emulsions at the different S-CNC content. (A) Surface tension and (B) contact angle images of *C. officinale* RE-Pickering emulsions on the glass.

The rheological properties of the S-CNC/*C. officinale* RE Pickering emulsion were investigated as a function of the S-CNC content (Figure 37). The SAOS flow of the stable S-CNC/*C. officinale* RE Pickering emulsions showed that the elastic storage modulus (G') was higher than the viscous storage modulus (G") in the frequency range of 0.1 to 10 Hz. When the shear occurred to the Pickering emulsion, the irreversibly adsorbed S-CNCs on the oleic compound formed network of droplets. The flocculation droplet network which occurred by shear force increased the G' value, as the increase of S-CNC content above 45 mg/mL*C. officinale* RE, the G' showed high value compared to G" (Figure 37C-37E). On the other hands, at the incompletely encapsulated S-CNC/*C. officinale* RE Pickering emulsions of S-CNC content below 22.5 mg/mL*C. officinale* RE, the small droplets aggregated each other and form one large droplet by coalescence. The decrease of solid areas induced sol-like property to the whole system of solution. Therefore, the G" increased more than G' at the high frequency range (Figure 37A and 37B). The value of loss factor (tan δ) at the high frequency showed more than 1 of S-CNC content below 22.5 mg/mL*C. officinale* RE and less than 1 of S-CNC content above 45 mg/mL*C. officinale* RE (Figure 37F).

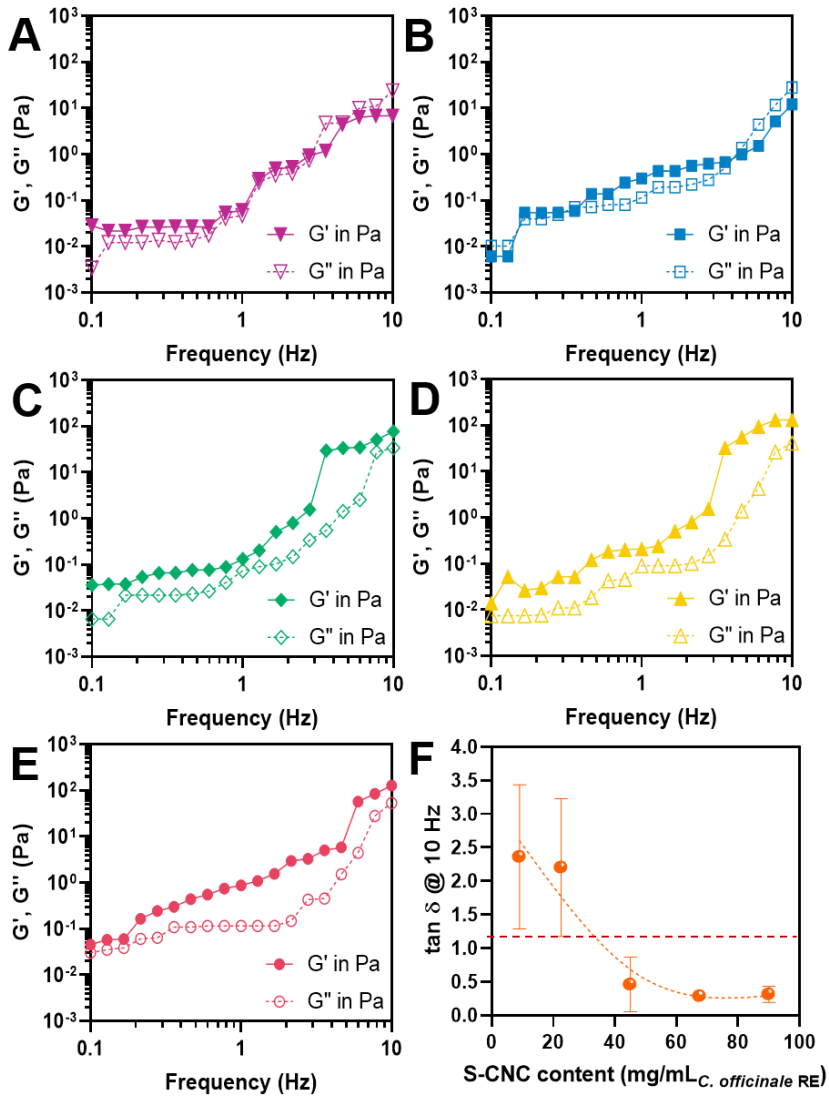

Figure 37. Rheological properties of S-CNC/*C. officinale* RE Pickering emulsions. (A) S-CNC 9.0 mg/mL*C. officinale* RE, (B) S-CNC 22.5 mg/mL*C. officinale* RE, (C) S-CNC 45.0 mg/mL*C. officinale* RE, (D) S-CNC 67.5 mg/mL*C. officinale* RE, and (E) S-CNC 90.0 mg/mL*C. officinale* RE. (F) Loss factor at the 10 Hz of S-CNC/*C. officinale* RE Pickering emulsions at different of S-CNC content.

The *C. officinale* RE Pickering emulsions stabilized by various S-CNC content were obtained by confocal microscopy (Figure 38). The S-CNC/*C. officinale* RE Pickering emulsions stabilized by S-CNC content below 22.5 mg/mL$_{C.\ officinale\ RE}$ formed solely dispersed large droplets (Figure 38A and 38B). As the S-CNC content increased above 45 mg/mL$_{C.\ officinale\ RE}$, lots of small droplets were formed by amphiphilic S-CNC. The S-CNC content of 45 mg/mL$_{C.\ officinale\ RE}$ and 67.5 mg/mL$_{C.\ officinale\ RE}$ showed relatively homogeneous range of droplet size distribution (Figure 38C and 38D). However, the S-CNC content of 67.5 mg/mL$_{C.\ officinale\ RE}$ manufactured too small droplets and the increased surface area rather deteriorates the thermodynamic stability of Pickering emulsion (Figure 38E). The droplets attached each other and formed several large droplet clusters. The each of droplet did not collapse for 14 days even though they formed clusters because of irreversibly absorbed S-CNC on the surface of oleic compounds.

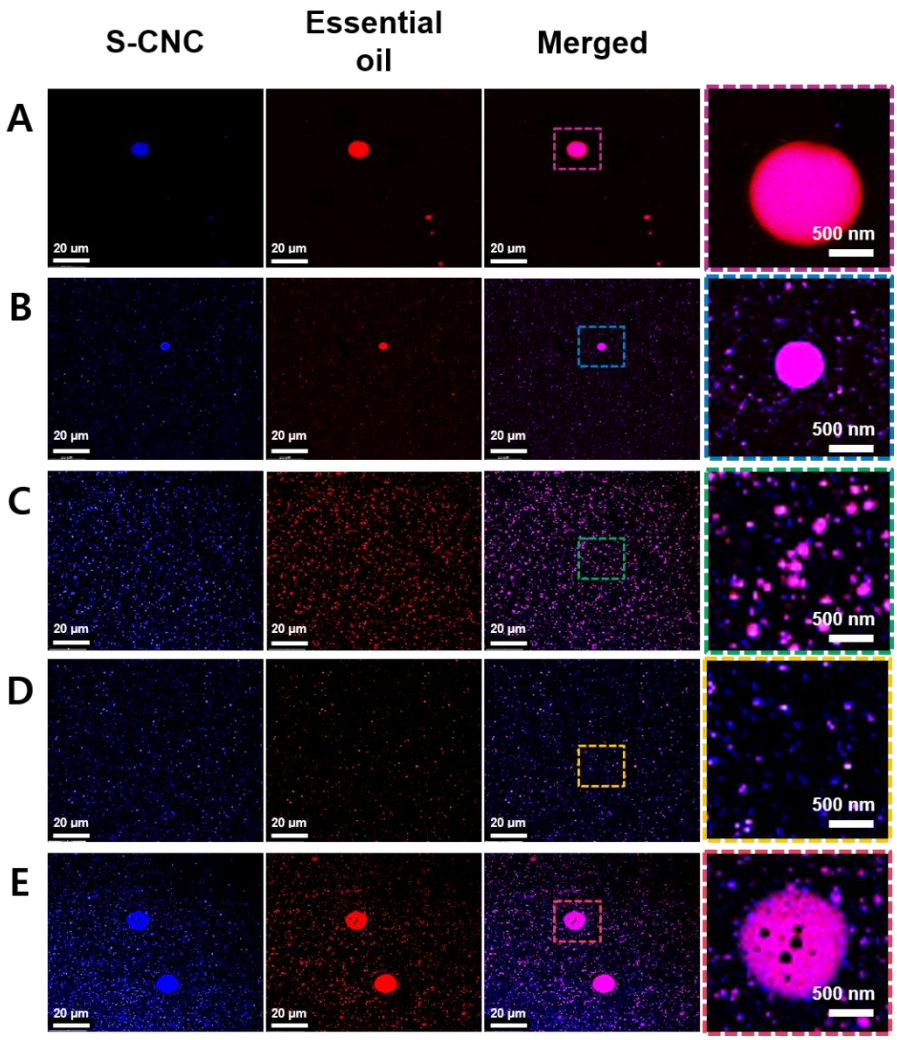

Figure 38. Confocal microscopic images of S-CNC/*C. officinale* RE Pickering emulsions. (A) S-CNC 9.0 mg/mL*C. officinale* RE, (B) S-CNC 22.5 mg/mL*C. officinale* RE, (C) S-CNC 45.0 mg/mL*C. officinale* RE, (D) S-CNC 67.5 mg/mL*C. officinale* RE, and (D) S-CNC 90.0 mg/mL*C. officinale* RE. S-CNCs labeled with Calcofluor white fluorescent dye and *C. officinale* RE labeled with Nile red fluorescence dye.

4.3.8. Larvicidal activity of S-CNC/*C. officinale* RE Pickering emulsions

Larvicidal activity of crude *C. officinale* RE and S-CNC/*C. officinale* RE Pickering emulsions is shown in Table 7. The LC_{50} of S-CNC/*C. officinale* RE Pickering emulsions was slightly higher than that of crude *C. officinale* RE at all of S-CNC content except 90 mg/mL$_{C.\ officinale\ RE}$. The S-CNC 90 mg/mL$_{C.\ officinale\ RE}$ Pickering emulsions exhibited weak larvicidal activity than the others. The decrease of larvicidal activity of the S-CNC 90 mg/mL$_{C.\ officinale\ RE}$ Pickering emulsions was caused from forming cluster of small droplets and essential oil release areas reduced.

Table 7. Larvicidal activities of *C. officinale* RE and its S-CNC 45 mg/mL*C. officinale* RE Pickering emulsions against *Ae. albopictus*.

Test materials	LC_{50} (µg/mL)	95% CL[1] (µg/mL)	Slope±SE[2]	df[3]	Chi-square	*p*-value
Crude *C. officinale* RE	60.01	53.67 – 67.23	3.28±0.57	4	0.646	0.958
S-CNC/*C. officinale* RE Pickering emulsion	59.66	53.06 – 67.33	2.87±0.44	4	1.583	0.812

[1] CL denotes confidence limit
[2] SE denotes standard error
[3] df denotes degree of freedom.

4.3.9. Colloidal stability of S-CNC/thyme white Pickering emulsions

A Pickering emulsion of S-CNC/thyme white was prepared by sonicating the mixture solution of thyme white and S-CNC suspension in water. The color of the solution changed to white, and the stability of the Pickering emulsion was determined by TSI values for 24 hours (Figure 39A). Typically, TSI values varied from 0 to 100, and emulsions with a lower TSI value are more stable. The TSI values decreased as the content of S-CNC increased. The TSI values of S-CNC 135 and 180 $mg/mL_{Thyme\ white}$ Pickering emulsions were less than 12 while the TSI values of S-CNC 45 and 90 $mg/mL_{Thyme\ white}$ Pickering emulsions were above 50. The visual appearance of the emulsions showed significant differences depending on the S-CNC contents after storage for 24 hours (Figure 39B). Usually, the light scattering of stabilized emulsions is high, and the transmission rate is very low through all the regions in the solution. However, transmission of light increased with the lower content of S-CNC emulsions because the emulsion particles were destroyed, and subsequent phase separation between thyme white essential oil and water occurred. This resulted from the insufficient content of emulsifying S-CNCs. The less covered thyme white essential oil was exposed to oil parts and the exposed parts were coalesced. The exposed oil flocculation moved to the aqueous surface and formed a floating creamy layer [94, 163, 189].

The backscattering of light through each emulsion is shown in Figure 38C-38F. The stability of emulsions was sustained without any significant phase separation with S-CNC 135 and 180 $mg/mL_{Thyme\ white}$ Pickering emulsions during storage for 24 hours (Figure 39C and 39D). In contrast,

phase separation was observed in 6 hours for emulsions prepared with S-CNC 45 and 90 $mg/mL_{Thyme\ white}$ compositions (Figure 39E and 39F). This demonstrated that there is a critical concentration of S-CNCs required for completely covering thyme white and ensuring the long-term stabilization of S-CNC based Pickering emulsions. These results suggest that S-CNC 135 mg/mL thyme white could be close to the critical concentration of S-CNC/thyme white emulsions.

Spherically shaped emulsion droplets were observed with a microscope as shown in Figure 40A-40D. The dark-field microscopic image clearly showed the contours of solid particles, as well as the size distribution. The shell structure implies that the liquid phase was enclosed in the solid phase. The shell consisted of S-CNC particles because light scattering occurred at the edge of the solid particles. Thicknesses of the shell were similar regardless of the S-CNC/thyme white compositions, meaning that the assembly of S-CNCs was regular and uniform. The size of the Pickering emulsion decreased as the S-CNC content increased. The average shell size of the S-CNC 45 $mg/mL_{Thyme\ white}$ Pickering emulsion was about 14 μm, and a broad size distribution was observed. It decreased to about 5 μm for S-CNC 135 and 180 $mg/mL_{Thyme\ white}$ Pickering emulsions with comparatively narrower size distributions (Figure 40E and 40F).

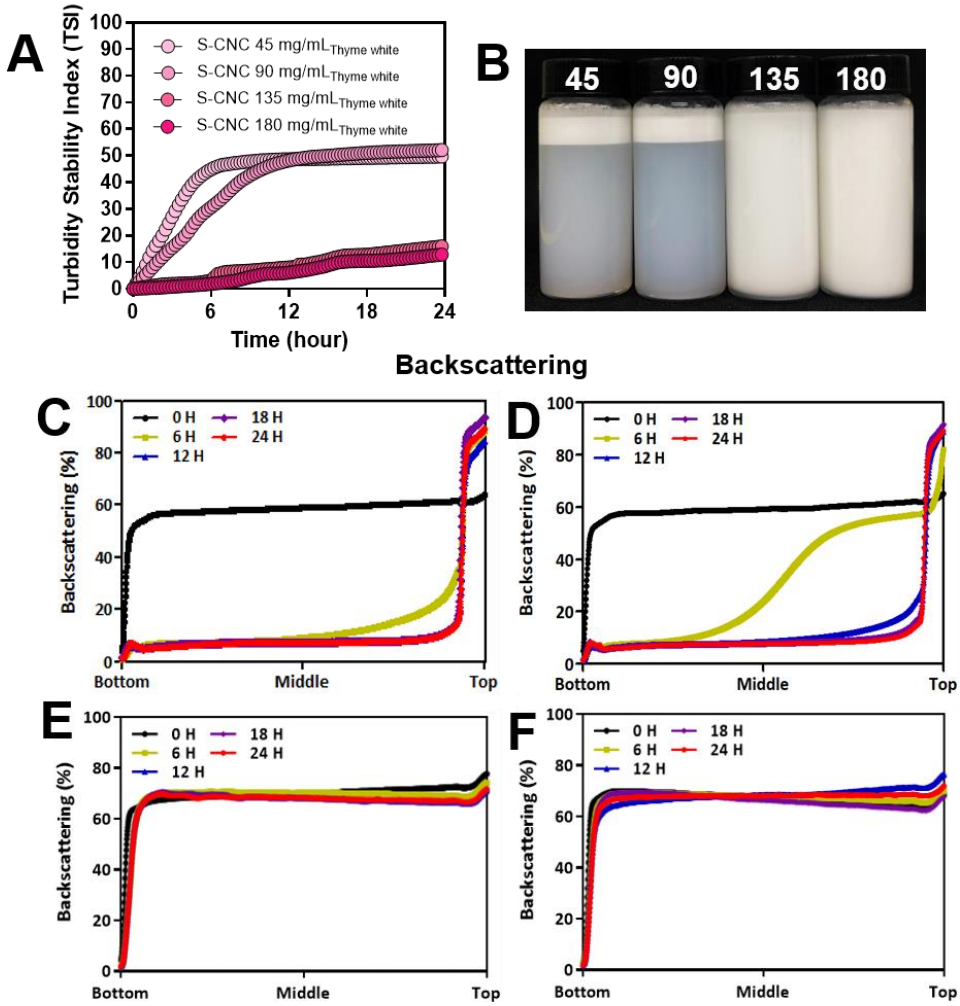

Figure 39. Colloidal stability of Pickering emulsion of S-CNC/thyme white prepared at different content of S-CNCs. (A) TSI change for Pickering emulsions for 24 hours. (B) Photograph of the vials containing Pickering emulsions after storage for 24 hours. The numbers mean the S-CNC content for 1 mL of thyme white, unit: S-CNC mg/mL$_{\text{Thyme white}}$. (C-F) Backscattering at the different vertical regions of the vial containing Pickering emulsion prepared with different content of S-CNCs. (C) S-CNC 45 mg/mL$_{\text{Thyme white}}$, (D) S-CNC 90 mg/mL$_{\text{Thyme white}}$, (E) S-CNC 135 mg/mL$_{\text{Thyme white}}$, and (F) S-CNC 180 mg/mL$_{\text{Thyme white}}$.

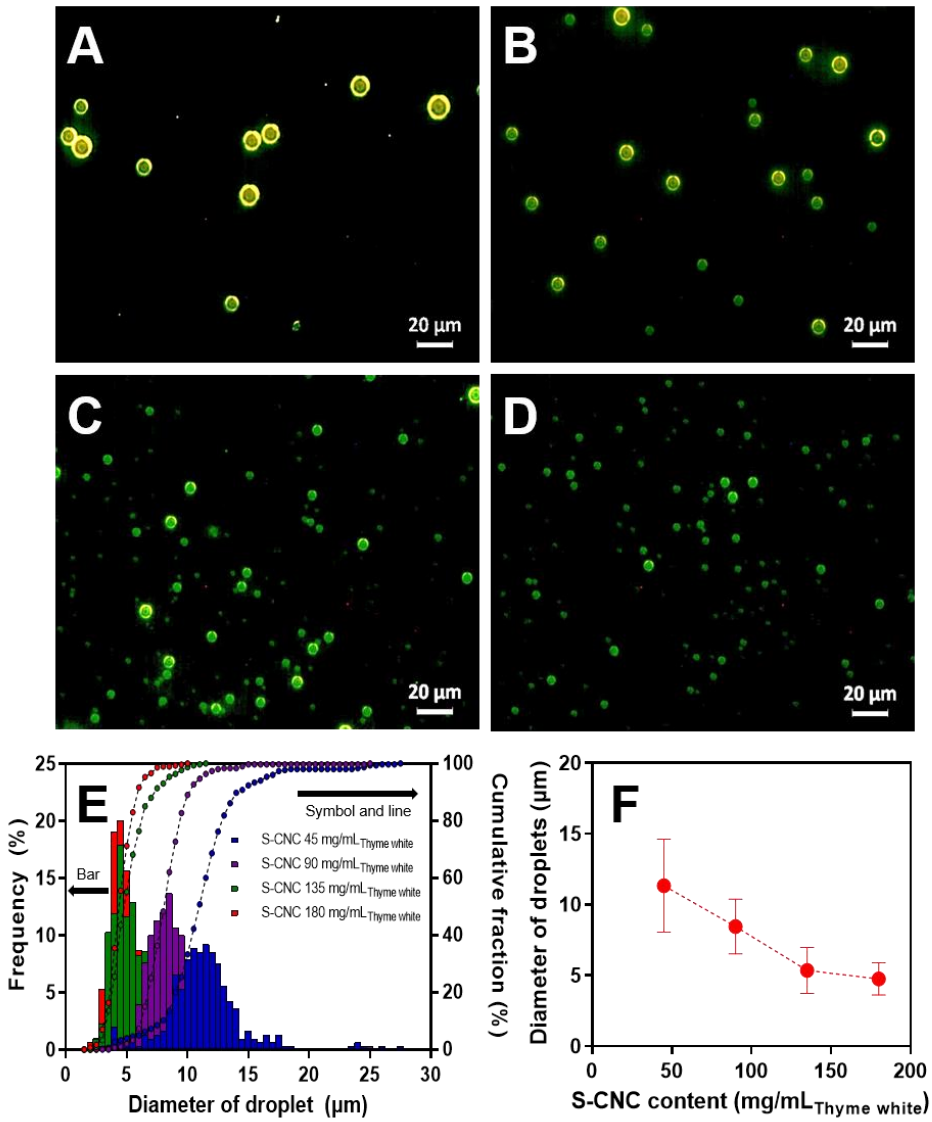

Figure 40. Size distribution of S-CNC/thyme white Pickering emulsions prepared at the different content of S-CNCs. Dark-field microscopic images of Pickering emulsion prepared at (A) S-CNC 45 mg/mL$_{\text{Thyme white}}$, (B) S-CNC 90 mg/mL$_{\text{Thyme white}}$, (C) S-CNC 135 mg/mL$_{\text{Thyme white}}$, and (D) S-CNC 180 mg/mL$_{\text{Thyme white}}$. (E) Distribution of the sizes of emulsions at different content of S-CNCs. (F) Average diameter of droplets as a function of the content of S-CNCs. (N=300, error bar=SD).

The enclosure of liquid thyme white in the S-CNC shell was confirmed with confocal microscope images (Figure 41). S-CNCs were labeled with blue fluorescent dye and were observed only at the boundary of the emulsion particles. Meanwhile, the thyme white labelled with red fluorescent dye was observed at the inner region of the emulsion. Smaller sized thyme white droplets were contained in the S-CNC Pickering emulsion with a higher content of S-CNCs in the emulsion. The emulsion particles were spherical and were well dispersed in the aqueous phase without aggregation.

The rheological properties of the S-CNC/thyme white Pickering emulsion were investigated as a function of the S-CNC content (Figure 42). The dynamic mechanical properties of the emulsions showed that the elastic storage modulus (G') was higher than the viscous storage modulus (G") in the frequency range of 0.1 to 10 Hz, and the Pickering emulsions appeared to be a gel in this range. As the shear occurs, the network structure of the Pickering emulsion collapses, and the emulsions combine to increase the size. As the size of the Pickering emulsion increases due to the coalescence of Pickering emulsions, the area of the entire interface decreases, resulting in a decrease in the storage modulus (G') [3]. This phenomenon was also observed in the S-CNC/thyme white essential oil Pickering emulsions. The stability of the Pickering emulsion was evaluated by increasing the S-CNC content from 45 $mg/mL_{Thyme\ white}$ to 180 $mg/mL_{Thyme\ white}$ by performing frequency sweeps. Pickering emulsions with less than S-CNC 90 $mg/mL_{Thyme\ white}$ showed a large particle size and wide distribution of particle sizes (Figure 42A and 42B). As the size of the Pickering emulsion increased, the interactions between Pickering emulsions decreased, leading to a decrease in G'. Increased Pickering emulsion size also reduced the regularity of the emulsion arrangement in the system, inducing the lower G' value. The Pickering

emulsions prepared with more than S-CNC 135 mg/mL$_{\text{Thyme white}}$ had a smaller emulsion size and narrower distribution than the other Pickering emulsions, implying a more regular arrangement of emulsion particles (Figure 42C and 42D). Especially, the Pickering emulsions with S-CNC 180 mg/mL$_{\text{Thyme white}}$ showed a constant strain value of 0.5% and a G' value of about 5.5 Pa over the entire frequency range. The value of loss factor (tan δ) at the high frequency showed equallibrium value of S-CNC content above 135 mg/mL$_{\text{Thyme white}}$ (Figure 42E).

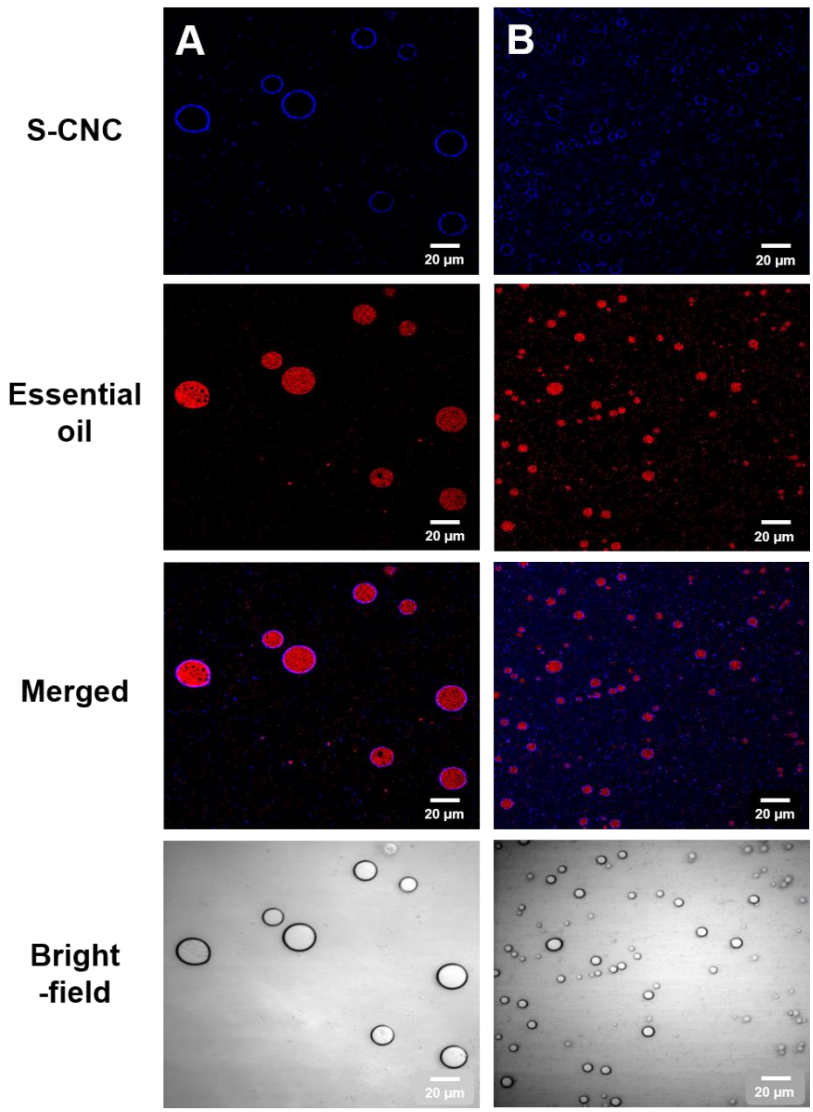

Figure 41. Confocal microscopic images of S-CNC/thyme white Pickering emulsions. (A) S-CNC 90 mg/mL$_{\text{Thyme white}}$ and (B) S-CNC 180 mg/mL$_{\text{Thyme white}}$. S-CNCs labeled with Calcofluor white fluorescent dye and thyme white labeled with Nile red fluorescence dye.

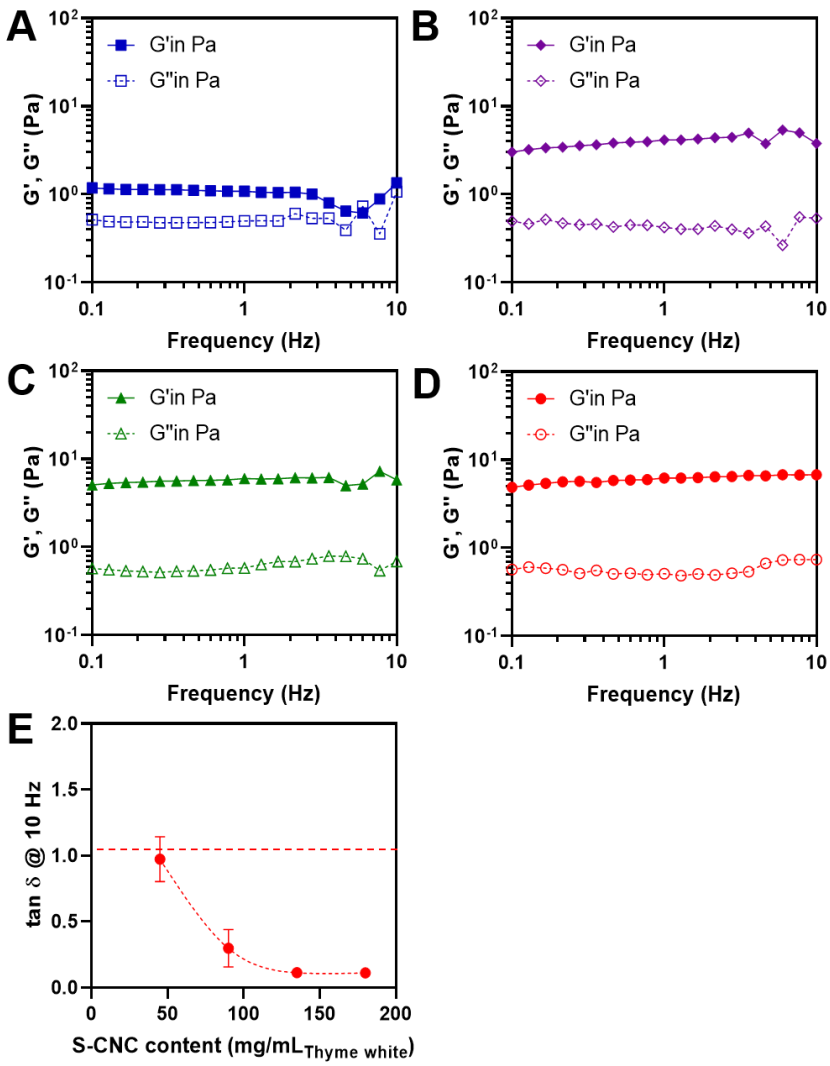

Figure 42. Rheological properties of S-CNC/thyme white Pickering emulsions. (A) S-CNC 45 mg/mL$_{\text{Thyme white}}$, (B) S-CNC 90 mg/mL$_{\text{Thyme white}}$, (C) S-CNC 135 mg/mL$_{\text{Thyme white}}$, and (D) S-CNC 180 mg/mL$_{\text{Thyme white}}$. (E) Loss factor at the 10 Hz of S-CNC/thyme white Pickering emulsions at different of S-CNC content.

4.3.10. Antimicrobial activity of S-CNC/thyme white Pickering emulsions

Essential oils are available from the natural resources and become continuously popular in biological and medical applications due to their antimicrobial effect. Thyme white in the research is known to cause the microbial cytoplasm to crack, and the thymol and carvacrol in it destroy microbial metabolic organelles or cause leakage of internal organs [134, 161, 190].

Pickering emulsion for the investigation of biological activity was prepared with S-CNC 135 $mg/mL_{thyme\ white}$ by tip sonication considering the uniformity of the emulsion droplets and narrow size distribution. The antimicrobial activity of crude thyme white and Pickering emulsions containing thyme white was determined by MIC and MBC against *E. coli* and *S. aureus* using streptomycin as a positive control (Table 8-11).

Crude thyme white showed weak antimicrobial activity against *E.coli* and no microbial growth or turbidity was observed over 0.625 μl/mL indicating the MIC value. On the other hand, S-CNC/thyme white Pickering emulsions showed strong activity against *E. coli* at 0.312 μl/mL which was lower MIC value than crude thyme white demonstrating the efficiency of antimicrobial activity. For *S. aureus*, the microbial growth was also inhibited by crude thyme white essential oil at MIC 0.625 μl/mL and S-CNC/thyme white Pickering emulsions at MIC 0.250 μl/mL (Table 8 and 9).

The lowest concentration of an antimicrobial agent for microbial death was demonstrated as a complementary to the MBC. For *E. coli*, MBC was 1.00 with crude thyme white essential oil and 0.750 with S-CNC/thyme white Pickering emulsions. For *S. aureus*, MBC was 1.00 with crude thyme white

essential oil and 0.650 with S-CNC/thyme white Pickering emulsions (Table 10 and 11). Streptomycin showed no microbial growth at the concentrations used in the investigation.

For the investigation of long term antimicrobial activity, the different contents of Pickering emulsion and crude thyme white were added to the medium containing microbes, and the mixture was incubated up to 25 days. The antibacterial activity of Pickering emulsion and crude thyme white was evaluated by counting the number of colonies at the gel surface after incubation for 3 days (Figure 43 and 44). Pickering emulsion showed antimicrobial activity with 1.0 μl/mL thyme white against *E. coli* (Figure 43A-43C). The microbes were bioactive immediately after the addition of Pickering emulsion, but no colony was observed with the extractions incubated for 10 days and 25 days. However, crude thyme white showed microbial activity with the extractions incubated for 10 days and 25 days at the same concentration. The bioactivity of *S. aureus* was also restricted by the addition of Pickering emulsion with 1.0 μl/mL thyme white or more (Figure 44A-44C). The dense S-CNC shell reduced the volatility of thyme white essential oil and prevented the rapid release of thyme white into the solution. As a result, the S-CNC enabled longer and sustained antimicrobial activity in the bulk environment.

Table 8. MIC of Pickering emulsions, crude thyem white essential oil and streptomycin against *E. coli*. [1]

Dilution of antimicrobial compounds for same No. of bacteria (µl/mL)	**Antimicrobial Activity (MIC, *Escherichia coli*)**							
	0.125[2]	**0.150**	**0.250**	**0.312**	**0.500**	**0.625**	**1.000**	**1.250**
Crude thyme white	+	+	+	+	+	-	-	-
S-CNC/thyme white Pickering emulsion	+	+	+	-	-	-	-	-
Control (S-CNC only)	+	+	+	+	+	+	+	+
Streptomycin	-	-	-	-	-	-	-	-

Positive (+) = Turbidity indicating growth; Negative (-) = No turbidity indicating absence of growth
[1] Results are means of three replicates
[2] µl/mL

Table 9. MIC of Pickering emulsions, crude thyem white essential oil and streptomycin against *S. aureus*. [1]

Dilution of antimicrobial compounds for same No. of bacteria (µl/mL)	**Antimicrobial Activity (MIC, *Staphylococcus aureus*)**							
	0.125[2]	**0.150**	**0.250**	**0.312**	**0.500**	**0.625**	**1.000**	**1.250**
Crude thyme white	+	+	+	+	+	-	-	-
S-CNC/thyme white Pickering emulsion	+	+	-	-	-	-	-	-
Control (S-CNC only)	+	+	+	+	+	+	+	+
Streptomycin	-	-	-	-	-	-	-	-

Positive (+) = Turbidity indicating growth; Negative (-) = No turbidity indicating absence of growth
[1] Results are means of three replicates
[2] µl/mL

Table 10. MBC of Pickering emulsions, crude thyem white essential oil and streptomycin against *E. coli*. [1]

Dilution of antimicrobial compounds for same No. of bacteria (µl/mL)	**Antimicrobial Activity (MIC, *Staphylococcus aureus*)**							
	0.125[2]	**0.150**	**0.250**	**0.312**	**0.500**	**0.625**	**1.000**	**1.250**
Crude thyme white	+	+	+	+	+	-	-	-
S-CNC/thyme white Pickering emulsion	+	+	-	-	-	-	-	-
Control (S-CNC only)	+	+	+	+	+	+	+	+
Streptomycin	-	-	-	-	-	-	-	-

Positive (+) = Turbidity indicating growth; Negative (-) = No turbidity indicating absence of growth
[1] Results are means of three replicates
[2] µl/mL

Table 11. MBC of Pickering emulsions, crude thyem white essential oil and streptomycin against *S. aureus*. [1]

Dilution of antimicrobial compounds for same No. of bacteria (µl/mL)	**Antimicrobial Activity (MBC, *Staphylococcus aureus*)**								
	0.600[2]	**0.650**	**0.700**	**0.750**	**0.800**	**0.850**	**0.900**	**0.950**	**1.000**
Crude thyme white	+	+	+	+	+	+	+	+	-
S-CNC/thyme white Pickering emulsion	+	-	-	-	-	-	-	-	-
Control (S-CNC only)	+	+	+	+	+	+	+	+	+
Streptomycin	-	-	-	-	-	-	-	-	-

Positive (+) = Indicating growth; Negative (-) = Indicating absence of growth
[1] Results are means of three replicates
[2] µl/mL

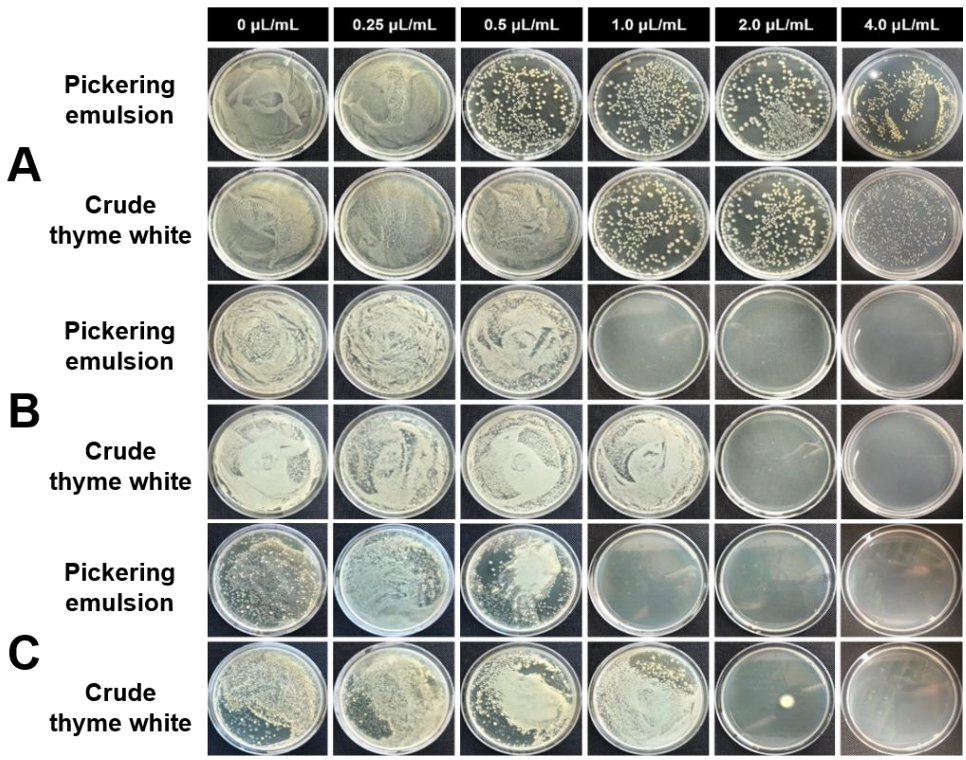

Figure 43. Antimicrobial activity of S-CNC/thyme white Pickering emulsions and crude thyme white against *E. coli* at different concentrations of thyme white. The extracts were diluted 1000 times and spread on an agar plate after the storage for (A) Day 0, (B) Day 10, and (C) Day 25.

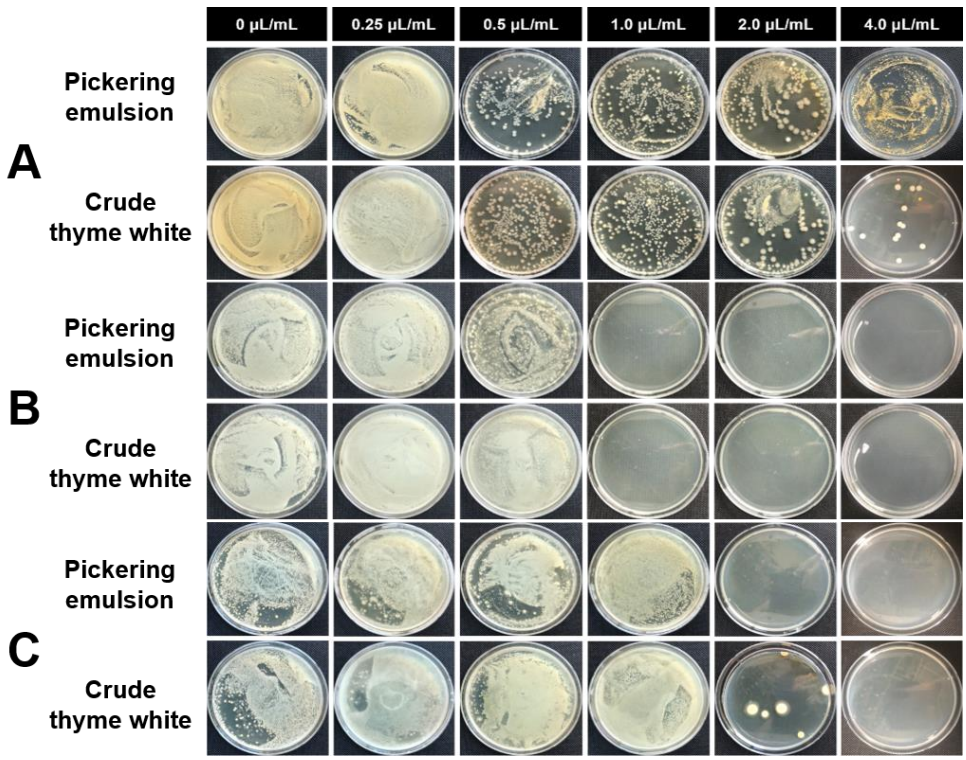

Figure 44. Antimicrobial activity of S-CNC/thyme white Pickering emulsions and crude thyme white against *S. aureus* at different concentrations of thyme white. The extracts were diluted 1000 times and spread on an agar plate after the storage for (A) Day 0, (B) Day 10, and (C) Day 25.

4.3.11. Larvicidal activity of S-CNC/thyme white Pickering emulsions

When essential oils are encountered by the small insects, the small insects trigger relatively unambiguous responses that, in addition to the added cellular components, have non-specific effects on a wide range of molecular targets such as proteins, nucleic acids, and biological membranes. As a result, the essential oil compounds, especially, thymol and carvacrol cause physiological disruption to the mosquito larvae to affect several crucial physiological function such as inhibition of chloride channel, interruption of Na-K ion exchange, and constriction of cellular respiration [191, 192].

The larvicidal activity of the thyme white essential oil and two types of formulation is shown in Table 12. Crude thyme white and S-CNC based formulation of thyme white showed 100% larvicidal activity against *Ae. albopictus* at 100 μg/mL concentration. S-CNC based formulation of thyme white exhibited 100% larvicidal activity at 50 μg/mL concentration, but no mortality was observed in crude thyme white. However, larvicidal activity of S-CNC based formulation of thyme white was weaker than that of temephos.

This result indicated that the thyme white was successfully liberated from the thyme white-loaded formulations. Larvicidal activity of thyme white-loaded formulations was stronger than that of thyme white. This might be attributed to high solubility in water of thyme white essential oil-loaded formulations. Plant essential oil is highly hydrophobic, and this is one obstacle for the development of plant-based mosquito larvicides. The result showed that S-CNC based formulation could solve the insolubility problem of plant essential oil in water. Another reason of high activity of S-CNC based formulation might be attributed to the controlled release of thyme white. Plant

essential oil easily evaporated when applied in water [175]. High mortality of S-CNC based thyme white formulation might be achieved by the controlled release of thyme white over the desired period. Development of proper formulation for practical use of plant essential oil in field has been conducted [61, 175]. Osanloo et al. [61] found that nonoemulsions of plant essential oil enhanced the larvicidal activity, stability and solubility of plant essential oils. Seo et al. [175] also reported that parsley oil-loaded PVA microemulsion showed strong larvicidal activity against *Ae. albopictus* and could solve the insolubility problem of plant essential oil in water.

Table 12. Larvicidal activities of crude thyme white and S-CNC/thyme white Pickering emulsions against *Ae. albopictus.*

Test materials	Larvicidal activity (%, mean ± S.E., N=4)		
	100[1]	**50**	**25**
Crude thyme white	100	0	-[2]
S-CNC/thyme white Pickering emulsion	100	100	38.0 ± 8.0
Conctrol (EtOH)	0	0	0
Conctrol (S-CNC only)	0	0	0
Temephos	100	100	100

[1] μg/mL
[2] Not tested

4.4. Summary

S-CNCs with a needle-like morphology were produced by sulfuric acid hydrolysis. These S-CNCs showed surface active ability for the formation of Pickering emulsion with various essential oils. A critical concentration of the S-CNC based Pickering emulsions was determined to be S-CNC 180 mg/mL_{Nutmeg}, 270 $mg/mL_{Massoia}$, 135 $mg/mL_{P.\ kadsura\ SE}$, 45 $mg/mL_{C.\ officinale\ RE}$ and 135 $mg/mL_{Thyme\ white}$. Smaller emulsion particles resulted in a higher G' value, implying a more regular arrangement of emulsion particles and dimensional stability. The size of S-CNC/essential oil Pickering emulsion varied according to the S-CNC content in the emulsifying process. The size of Pickering emulsion droplets decreased as the S-CNC content increased. The surface tension of Pickering emulsion decreased as the S-CNC content increased and the equilibrium surface tension showed at the stable Pickering emulsion. Encapsulation of essential oil in S-CNC shell was visualized by distinct fluorescent labelling. The size of each stable Pickering emulsion showed narrower size distributions. The antimicrobial ability of S-CNC/essential oil Pickering emulsion was confirmed by the determination of minimum bactericidal concentration with long-term storage up to 25 days. The larvicidal activity of S-CNC/essential oil Pickering emulsion was stronger than that of crude essential oil due to high solubility and sustainability of essential oil in water. The thyme white Pickering emulsion enhanced their larvicidal activity 2.6-fold more than crude thyme white. In addition nutmeg Pickering emulsion showed 2.1-fold, *P. kadsura* SE Pickering emulsion showed 1.7-fold, Massoia Pickering emulsion showed 1.3-fold, and *C. officinale* RE Pickering emulsion showed 1.1-fold more active than crude essential oils.

V

Larvicidal composite alginate hydrogel combined with a Pickering emulsion of thyme white essential oil

5.1. Introduction

Dengue virus, chikungunya virus, and Zika virus have become global public diseases as their disease vectors, Asian tiger mosquitoes, *Ae. albopictus*, have spread quickly from East Asia to the world [136, 193-195]. Synthetic pesticides have been developed and used to kill the *Ae. albopictus*. However, the pesticides can continuously cause environmental problems and directly damage other organisms because the pesticides are difficult to remove easily. In addition, the increasing resistance of mosquitoes to synthetic pesticides requires the development of more powerful pesticides [196, 197]. Because the continuous use of pesticides can cause serious side effects to the environment, eco-friendly pesticides such as essential oils have been receiving attention as alternative pesticides [198].

Essential oil are secondary metabolic compounds of aromatic plants that have antioxidant, antimicrobial, and larvicidal activity [36-38]. Essential oils extracted by steam distillation are composed of alcohols, aldehydes, ketones, esters, aromatic phenols, lactones, monoterpenes, and sesquiterpenes [39, 40]. In particular, the thyme white essential oil extracted from *Thymus vulgaris* has thymol and carvacrol, which are more fatal to mosquito larvae at relatively low concentrations than other essential oils [199, 200]. It is considered that essential oils do not evolve harmful side effects because, in general, their components are highly volatile and have short residence times in natural environments such as clear water and soil. However, their volatility also means that essential oils need to be released in a controlled, steady manner to have the desired larvicidal effect without being wasted by evaporation.

Pickering emulsions are an associated colloidal system that stabilizes a

two-phase liquid mixture through adsorption of amphiphilic particles at the interface of the two liquids [61]. S-CNCs, which have a high aspect ratio, are suitable particles for making Pickering emulsions [25, 46, 78]. The sulfonate (OSO_3^-) groups introduced at the surface of the CNCs enable the formation of strong emulsion particles [25]. The S-CNCs closely packed at the surface of an oil can reduce its ability to evaporate and can enable the sustained release of the oil through pores at the nanoscale. In addition, the enhanced solubility of essential oil-Pickering emulsions in water effectively improves their mosquito larvicidal performance [41]. Despite the sustained release of essential oils and the high solubility of Pickering emulsions, after the CNC emulsion carriers (diameter of tens of μm) have been dispersed in water and used, it is difficult to remove them from the water. The association of Pickering emulsions with a retrievable macroscale hydrogel is a potential solution to this problem. A hydrogel can easily control the release of chemicals entrapped within it by controlling the degree of gelation and pore size.

SA, a polysaccharide extracted from algae composed of (1-4)-linked β-D-mannuronic acid and α-D-gluronic acid units, is a natural polymer that can form a hydrogel in the presence of divalent cations [44, 45]. Because of their high water solubility and eco-friendly processing [100, 201], SA hydrogels are suitable for use as an environmentally friendly delivery system. Negatively charged S-CNCs at the surface allow essential oil Pickering emulsions to be naturally incorporated with SA in the gelation process. The crystalline fibrous structure of S-CNC reinforces the mechanical properties of the SA hydrogel by forming ionic cross-links through multivalent ions [46, 47]. The release behavior can be controlled by the degree of cross-linking of

SA and S-CNC-Pickering emulsions in the complex to find effective mosquito larvicidal performance [41]. In addition, SA hydrogels incorporated with essential oil-Pickering emulsions can be retrieved after the complete release of essential oils to water, which will reduce the environmental load. The eco-friendly SA-CNC Pickering emulsion hydrogels are one potential method to control the global disease problems by preventing the growth of mosquito larvae in the future.

5.2. Materials and method

5.2.1. Preparation of S-CNC and S-CNC stabilized Pickering emulsion

Preparation of S-CNC and Pickering emulsions was conducted as reported in the previous research [41]. Briefly, 10 g of filter paper was hydrolyzed in 100 mL 60 %(w/w) sulfuric acid at 45 °C for 1 hour [26]. The hydrolyzed paper solution was centrifuged at 6000 rpm for 10 minutes using a high speed, refrigerated centrifuge (VS-24SMTi, Vision Scientific Co., Ltd., Daejeon, Korea). After centrifugation, the solution in the upper region of the centrifuge bottle was collected and dialyzed for 1 week in a cellulose dialysis membrane (MWCO 12-14 kDa, Spectra/Por, Breda, the Netherlands). The dialyzed S-CNC suspension solution was concentrated with a rotary evaporator (N-1000, Eyela, Tokyo, Japan) and stored in a refrigerator until use. The sulfate content of S-CNC samples was determined by conductometric titrations [94, 147, 148]. 35 mg of S-CNC samples were suspended in 15 mL of a 0.01 M hydrochloric acid solution and stirred for 10 minutes. After 10 minutes of stirring, the solution was titrated with 0.01 M NaOH. The conductivity of the solution was measured by a conductometer (FiveGo Cond meter F3, Mettler Toledo, Zürich, Switzerland) during titration.

The S-CNC aqueous solution (1.35%) and thyme white essential oil were mixed at a ratio of 135 mg S-CNC per 1 mL of essential oil, and tip-sonicated (VCX 130, 435-09, Sonics & Materials Inc., Newtown, CT, USA) at 50% amplitudes for 30 seconds to make the Pickering emulsions.

5.2.2. Preparation of SA/Pickering emulsions hydrogel beads

Thyme white Pickering emulsions were added to a 2% SA solution at mixture concentrations of 10, 20, and 30%. A mixture of SA and Pickering emulsions was filled in a 10 mL syringe, which was loaded into a syringe pump (KDS100, KD Scientific Inc., Holliston, MA, USA). The mixture solution was dropped into different concentrations (0.50, 0.75 and 1.0%) of aqueous $CaCl_2$ solutions. Gelation was performed in the gelling solution for 20 minutes. The prepared hydrogel beads were washed with de-ionized (DI) water to remove any salt at the bead surface.

The prepared SA/Pickering emulsions hydrogel beads were stored in pH 7.4 PBS for 2 hours at 37°C to measure the water capacity [206]. After reaching equilibrium swelling, the hydrogel beads were washed with deionized water twice and the swollen weight (W_S) of hydrogel beads was measured. The dried weight (W_D) of hydrogel beads was measured after complete drying in the desiccator. The swelling ratio of SA/Pickering emulsions hydrogel beads was calculated by the Equation (5).

$$\text{Swelling ratio} = (W_S\text{-}W_D)/W_D \qquad \text{Eq. (5)}$$

The visual appearance of the beads was captured with a versatile stereomicroscope (SMZ800N, Nikon, Tokyo, Japan). The encapsulation of thyme white in the Pickering emulsions was visualized by staining the S-CNCs with 1 $\mu l/mg_{CNC}$ Calcofluor White (Sigma-Aldrich) and essential oil with 1.5 $\mu g/\mu l_{oil}$ Nile red (Sigma Aldrich) [79]. The imaging was performed at 638 and 475 nm using a confocal laser scanning microscope (CLSM, LSM719, Carl Zeiss, Overkochen, Germany). The size of the hydrogel beads

was measured with ImageJ software (1.52a, National Institutes of Health, Bethesda, MA, USA). A cross-sectional view of the beads which were stored at -72°C for 24 hours and freeze-dried for 3 days was obtained using a field-emission scanning electron microscope (FE-SEM Supra 55VP, Carl Zeiss, Overkochen, Germany) with a 15 nm platinum coating of the sample surface.

The chemical structure of the composite beads was characterized by Fourier transform infrared spectroscopy (FTIR spectroscopy, Nicolet iS5, Thermo Scientific, Newington, NH, USA) with 32 scans and 2 cm^{-1} resolution, and the crystallinity of the composites was characterized by powder X-ray diffractometry (XRD, D8 Advance, Bruker, Billerica, Massachusetts, USA). The composite beads were dried in an oven overnight to completely remove water and EOs for the characterizations.

The compression modulus of the SA/Pickering emulsions hydrogel beads was obtained with 2.0–2.2 mm diameter of beads using a universal testing analyzer (UTM, GB/LRX Plus, Lloyd, West Sussex, UK) fitted with a 10 N load cell. The compression modulus was determined at 30% strain moving the plate at a rate of 2 mm/minute.

The zeta-potential values of the S-CNC suspensions and Pickering emulsion were measured by a Zetasizer Nano ZS90 analyzer (Malvern Panalytical, U.K.).

5.2.3. *In vitro* thymol releasing test with gas chromatography-mass spectrometry

A group of 10 SA/Pickering emulsions hydrogel beads were immersed in a mixture of 10 mL DI water and 10 mL *n*-hexane, and 1 mL of *n*-hexane supernatant was extracted at different storage times, from 0 to 48 hours. The

amount of essential oils in the extracted *n*-hexane supernatant was measured using a gas chromatography (Agilent 7890B)-mass spectrometer (Agilent 5977B MSD, Agilent Technologies, Santa Clara, CA, USA) (GC-MS) with an HP-5MS column (30 m × 0.25 mm i.d., 0.25 μm film thickness, Agilent, CA, USA). The initial oven temperature was set to 40°C and the temperature was raised to 320°C at a rate of 20°C/minute. Helium was used as the carrier gas and the flow rate was 1.0 mL/minute. Ionization was achieved with 70 eV electrons and scanned in the 40–500 amu range.

5.2.4. Larvicidal activity test

Ae. albopictus was incubated without exposure to pesticides at a temperature of 25°C and a relative humidity of 60%. Larvae were incubated for 16 hours in light and 8 hours in dark. To supply blood to *Ae. albopictus*, live mice in a steel cage were supplied according to the Korea National Institute of Health Institutional Animal Care and Use Committee protocol (KCDC-020-11-2A). The larvae obtained from the adult *Ae. albopictus* were incubated in plastic pans (24×35×5 cm^3) with sterilized food and water at the same temperature and relative humidity. SA/Pickering emulsion hydrogel beads were added to the pans for 48 hours to observe their larvicidal performance. SA/Pickering emulsion 0 hydrogel beads without Pickering emulsions were used as a negative control, and temephos was used as a positive control. Ten larvae were exposed to the SA/Pickering emulsions and incubated with a 16/8 hours light/dark cycle and the degree of larval death was observed until 48 hours after addition of the SA/Pickering emulsions. Each experiment was repeated 4 times.

5.3. Results and discussion

5.3.1. Properties of SA/Pickering emulsions beads

The S-CNCs were strongly adsorbed at the surface of thyme white droplets and their anionic surface prevented the coagulation of droplets (Figure 45A). The zeta potential of S-CNC and Pickering emulsion was determined to be -38.6 ± 1.5 mV and -66.8±1.0 mV, respectively. The OSO_3^- groups at the S-CNC surface provided a colloidal stability of Pickering emulsions due to the electrostatic repulsion of negatively charged Pickering emulsions. The content of the S-CNC for stabilizing thyme white was fixed at S-CNC 135 $mg/mL_{Thyme\ white}$, which had a uniform size distribution of Pickering emulsions. The shape stability as well as size distribution of the spherical droplets was evaluated with dark-field microscopic images and the size of S-CNCs-stabilized Pickering emulsions was 5.27 ± 0.78 μm (Figure 45B and 45C). The shape of Pickering emulsions was maintained for a long time due to the high aspect ratio of S-CNCs forming a compact structure of emulsions.

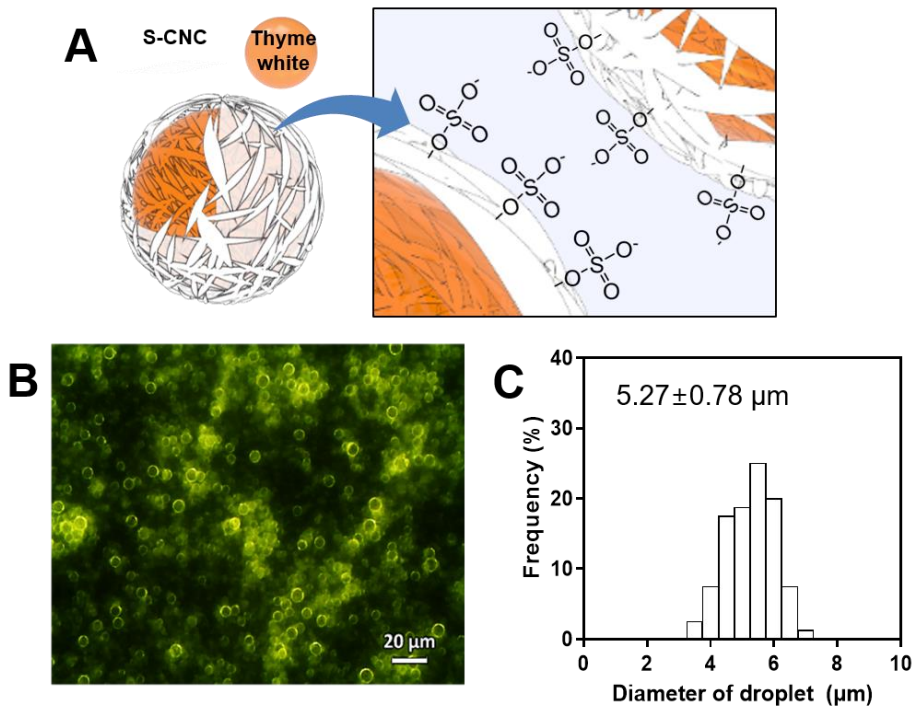

Figure 45. Pickering emulsion of S-CNC and thyme whtie. (A) Schematic of sulfated Pickering emulsion surface. (B) Microscopic image of Pickering emulsions. (C) Size distribution of Pickering emulsions.

Thyme white Pickering emulsions were mixed with SA solution and $CaCl_2$ was added to induce gelation by ionic cross-linking of the solution (Figure 46A). The negatively charged guluronic acids of the SA were bridged by bivalent cations to form a hydrogel [100, 203]. The OSO_3^- groups of at the S-CNC surface were involved in the ionic cross-linking to form an entrapped structure of SA/Pickering emulsions hydrogel. The diameter of the SA/Pickering emulsions hydrogel beads decreased as the concentration of $CaCl_2$ increased due to the more compact structure caused by the increased number of cross-links between Pickering emulsion and SA (Figure 46B). However, the compactness of the SA/Pickering emulsions hydrogel was dominated more by the $CaCl_2$ concentration rather than the Pickering emulsions concentration.

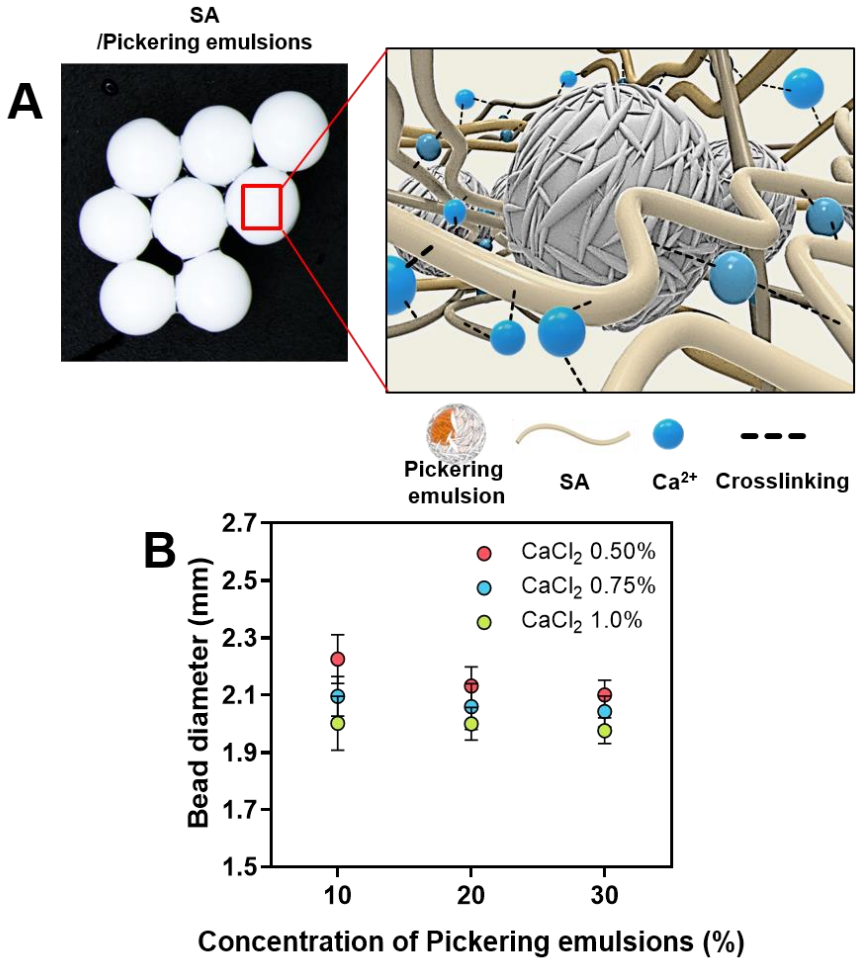

Figure 46. Preparation of SA/Pickering emulsion composite hydrogel beads. (A) Schematic illustration of gelation. (B) The effect of the concentration of Pickering emulsion and $CaCl_2$ on the size variation of the SA/Pickering emulsion beads.

The FTIR spectra of SA and SA/Pickering emulsions hydrogel beads revealed the incorporation of Pickering emulsions with SA (Figure 47A). The peak between 3600 and 3000 cm^{-1} was the hydroxyl group (O-H) stretching vibration in the polysaccharides. As the Pickering emulsions concentration increased, a characteristic peak was observed at 3350 cm^{-1}, which increased as the S-CNC Pickering emulsions concentration increased. A stretching vibration of C-H aliphatic chains of S-CNCs appeared at 2890 cm^{-1} [204], while a peak at 2925 cm^{-1} of SA was observed [205]. The peaks at 1598 and 1419 cm^{-1} in SA were associated with the carboxyl group of SA and these peaks were shifted slightly by addition of Pickering emulsions. As the Pickering emulsion concentration increased, a shoulder peak appeared at 1058 cm^{-1}, which was associated with the C-O stretching of cellulose [153, 205, 206]. The sulfate peak of the original S-CNCs appeared at 1205 cm^{-1}, but was almost screened by the 1800-1270 cm^{-1} peaks of the SA/Pickering emulsions composite beads [26].

Morphologically, the hydrogel beads formed from only SA were amorphous, which is typical in cross-linked hydrogels [100, 207]. The hydrogel beads formed from the mixture solution of SA and Pickering emulsions showed the existence of a crystalline structure in the XRD spectrum (Figure 47B). With the addition of Pickering emulsions to the SA hydrogel, a distinct peak appeared at 22.9^{o} representing the (200) crystal structure of cellulose fibers [26, 208, 209]. This peak indicated that the S-CNCs were incorporated in the SA hydrogel matrix.

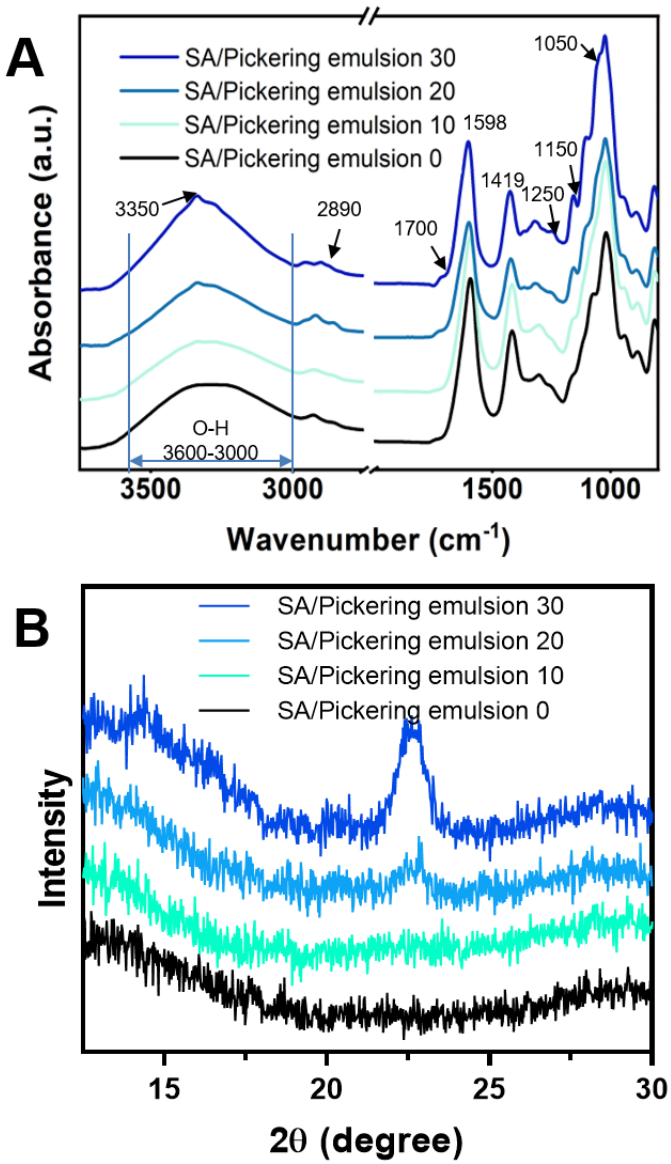

Figure 47. Examination of the incorporation of Pickering emulsions with SA in SA/Pickering emulsion composite hydrogels. (A) FTIR spectra. (B) X-ray diffraction.

The porosity of SA/Pickering emulsion was determined by the swelling ratio according to the amount of Pickering emulsion and $CaCl_2$ concentration used for the ionic crosslinking. The increase of Pickering emulsion content did not show the significant difference in swelling ratio, but the higher concentration of $CaCl_2$ decreased the swelling ratio of the hydrogel beads inferring the decrease of the porosity due to the increased network site of SA (Figure 48A). The compressive strength of the hydrogel beads was characterized by the compression modulus at 30% strain. The compression modulus increased with the addition of Pickering emulsions to SA (Figure 48B). The higher compression modulus of the SA/Pickering emulsion beads was attributed to the flexibility of the SA/Pickering emulsion-networked hydrogel transferring external pressure energy to the other parts of the system. In addition, the flexibility of the organic oil made the hydrogel more elastic and robust [210]. The S-CNCs located at the surface of the Pickering emulsions also attributed as a filler to enhance the toughness. Negatively charged spherical Pickering emulsions (-66.8±1.0 mV) were effectively dispersed in the SA solution and formed a well-mixed composite structure. Such a miscibility was critical to increase the mechanical properties by removing weak points in the composite. Because the SA hydrogel strongly entrapped the oil droplets with densely packed S-CNCs, a mechanical synergistic effect could be expected in both robustness and elasticity [210-213].

Cross-section images of SA/Pickering emulsions hydrogel beads showed that the Pickering emulsions were stably located in the SA hydrogel beads (Figure 49). The SA hydrogel beads without Pickering emulsions decreased in pore size as the concentration of $CaCl_2$ increased. The increase of Pickering emulsions in the SA/Pickering emulsion hydrogel beads formed

an apparent 5–10 μm spherical structure at the pore surface and the cross-sections of the pore walls. The wall thickness became thicker as the concentration of Pickering emulsions increased. The concentrations of $CaCl_2$ and Pickering emulsions were related to the compactness of the network structure of the hydrogel beads. The higher concentration of $CaCl_2$ formed a smaller pore and the higher concentration of Pickering emulsions formed a denser pore structure in the SA/Pickering emulsion composite beads due to the increased networking.

Pickering emulsions were prepared with the S-CNC labeled with Calcofluor White and thyme white labeled with Nile Red to determine the dispersion of Pickering emulsions over the SA hydrogel beads. The labeled Pickering emulsions were incorporated with SA, forming hydrogel beads. The Pickering emulsions were well dispersed over the SA bead, showing the clear, pink color of the SA/Pickering emulsion beads without aggregation (Figure 50A and 50B). Fluorescent colors were emitted from the Pickering emulsions rather than the SA (Figure 50C–50E). The Pickering emulsions composed of thyme white (red) and S-CNCs (blue) were visualized by confocal microscopy. They were well dispersed in the SA matrix without aggregation due to the electrostatic repulsion of the S-CNCs. The Pickering emulsions encapsulated thyme white stably in the SA hydrogel matrix (Figure 50C–50E). The increase of Pickering emulsion concentration reduced the transparency of the SA/Pickering emulsion beads, but the Pickering emulsions were well dispersed over the hydrogel without flocculation.

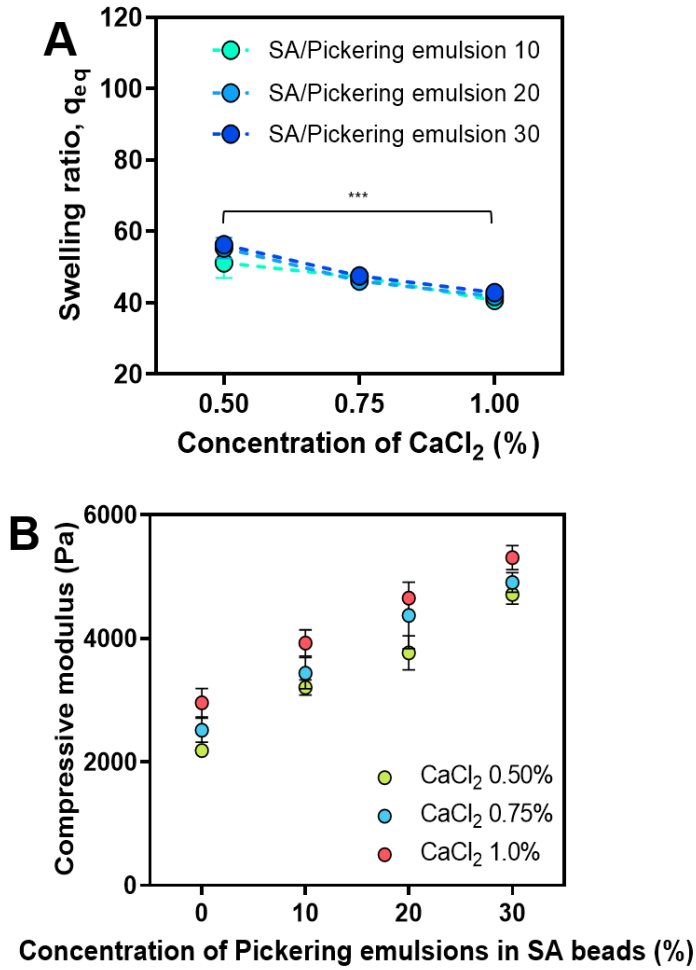

Figure 48. (A) Swelling ratio and (B) compressive strength of SA/Pickering emulsion composite hydrogel beads according to the amount of Pickering emulsion and concentration of the $CaCl_2$ solution.

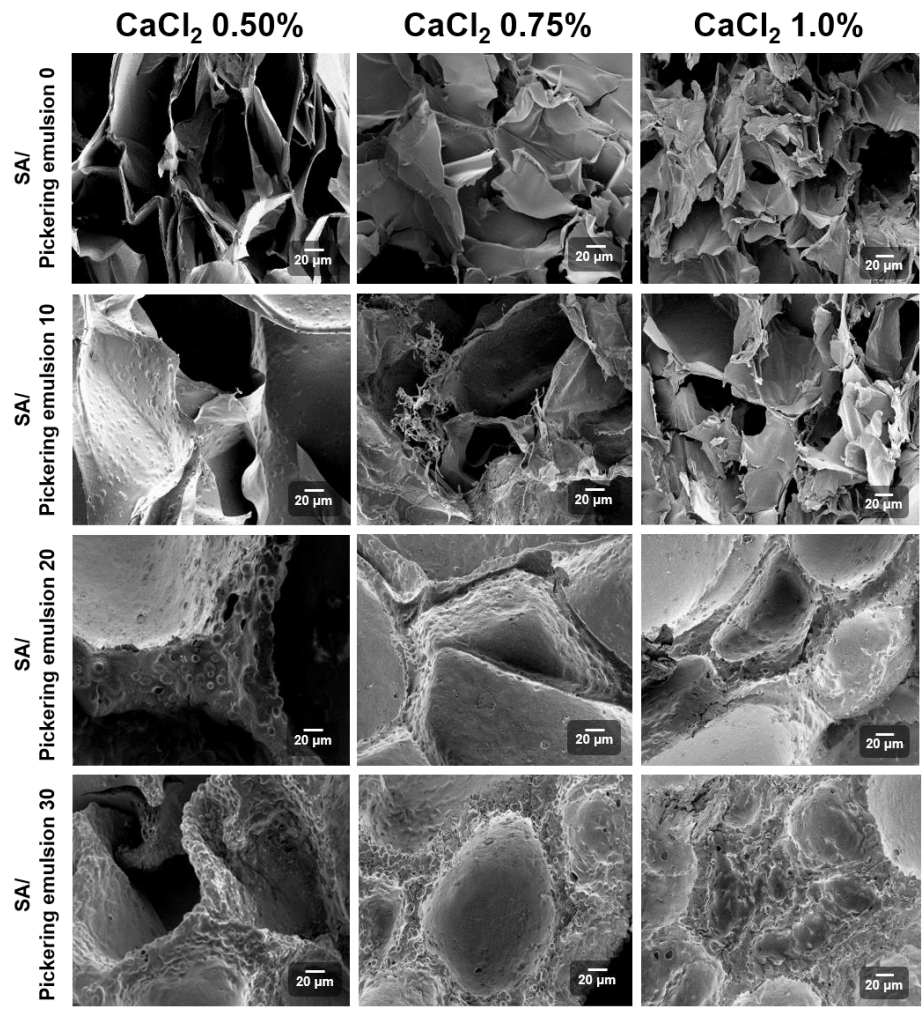

Figure 49. Cross-section images of SA/Pickering emulsion composite hydrogel beads (SA/Pickering emulsion 0, SA/Pickering emulsion 10, SA/Pickering emulsion 20, and SA/Pickering emulsion 30) prepared at concentrations of $CaCl_2$ solution (0.5–1.0%). (Scale bar: 20 μm)

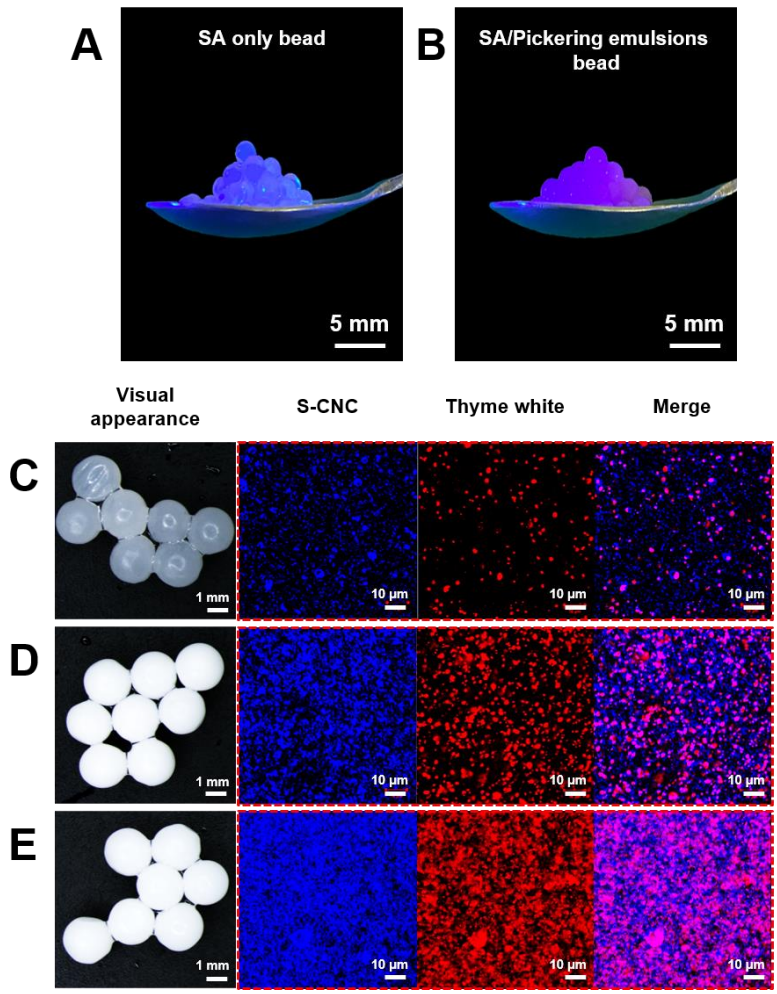

Figure 50. Incorporation of Pickering emulsions in SA hydrogel beads. Picture of (A) SA beads and (B) SA/Pickering emulsions beads where S-CNCs and thyme white were fluorescently labeled. Fluorescence light was illuminated to beads. Confocal images of (C) SA/Pickering emulsion 10 (D) SA/Pickering emulsion 20 and (E) SA/Pickering emulsion 30 beads formed with 0.1% $CaCl_2$ solution. S-CNCs and thyme white were labeled with Calcofluor White and Nile Red, respectively.

5.3.2. Release and larvicidal activities of SA/Pickering emulsions beads

The release profiles of thymol, a significant component of thyme white, were obtained with SA/Pickering emulsion hydrogel beads at different concentrations of Pickering emulsion and $CaCl_2$, as shown in Figure 51. As in Fick's first diffusion law, thymol diffuses from high to low concentration by Brownian motion [214, 215]. Therefore, the thymol diffused out from Pickering emulsion and SA, and the *n*-hexane located outside cumulates thymol as time goes by. The CNC and SA controlled the release rate of the double-entrapped thyme white, and the thyme white was slowly released from inside the SA/Pickering emulsion because a large amount of SA gel network was formed by $CaCl_2$. A relatively high release rate of thymol was determined with SA/Pickering emulsion at lower concentrations of $CaCl_2$ because of the loose structure of the networks. The release rate was closely related to the cross-linking density and porosity. Hydrogels can form a strong polymer network and water-filled permeation channels during the gelation process. Because the release of the thymol occurred through the permeation channels and thymol was released from inside the Pickering emulsion by diffusion, the looser permeation channels released the thymol more effectively. Hydrogel permeability could be estimated from the porosity of the hydrogel, and more release was expected from the SA/Pickering emulsion hydrogel beads prepared at lower $CaCl_2$ and Pickering emulsion concentrations [216-218]. The difference in the release behavior of the SA/Pickering emulsions hydrogel beads corresponded to the porous structure of the beads, as observed in SEM images. Thymol release was continuously observed for 48 hours. The consistent and sustained release of thymol was available with the

SA/Pickering emulsion beads, while the rapid release of thymol was observed with the Pickering emulsions. The sustained release suggested that highly volatile chemicals such as thyme white could be formulated with S-CNCs to form Pickering emulsions and that double core-shell SA/Pickering emulsion hydrogel beads could be a sustainable release system to reduce the waste of highly volatile chemicals.

Because the thyme white is highly volatile, it is impossible to control their concentration in water. Importantly, the larvicidal activity needs an appropriate solubility of the larvicidal reagent in water for a certain duration, and it is critical to increase the solubility of the volatile oil phase in water. The SA/Pickering emulsion beads were perfect to increase the water solubility of thyme white and provide sustained release to control the concentration in water without a rapid release of thyme white over a short time. The mortality of *Ae. albopictus* larvae with storage time was highest in the SA/Pickering emulsions hydrogel beads formed with a 0.50% $CaCl_2$ solution due to its high release rate (Figure 52). SA/Pickering emulsions hydrogel beads formed at 0.75 and 1.0% showed relatively low mortality rate due to a slow release rate of thyme white essential oils. Typically, the mortality rate of *Ae. albopictus* larvae increased gradually with longer storage time of SA/Pickering emulsions in water. The difference of mortality rate could be controlled by simply adjusting the number of SA/Pickering emulsion beads stored in water.

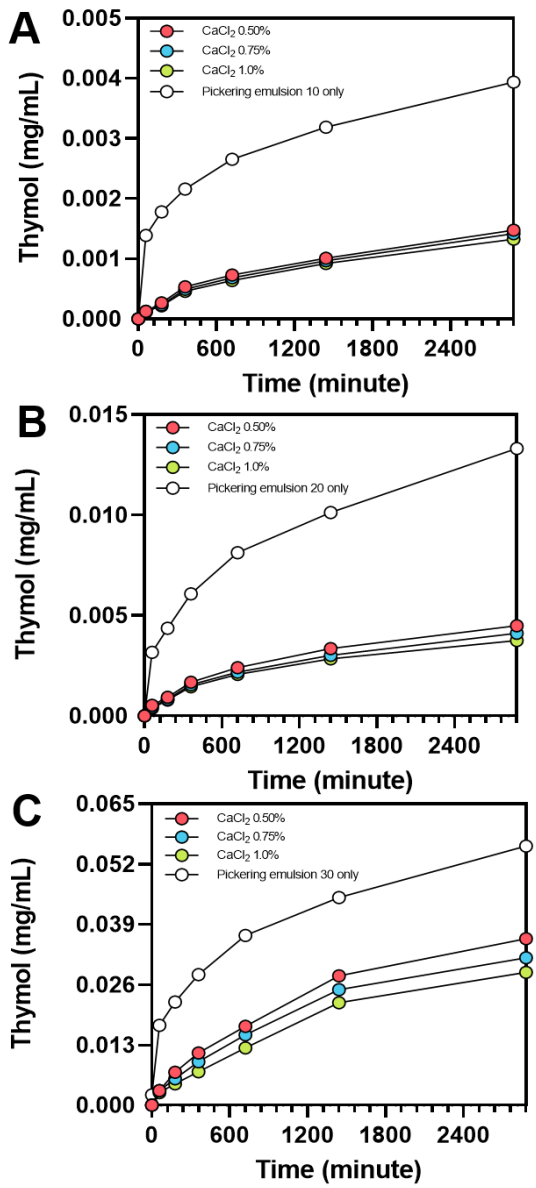

Figure 51. Release of thymol from the SA/Pickering emulsion hydrogel beads. (A) SA/Pickering emulsion 10, (B) SA/Pickering emulsion 20, and (C) SA/Pickering emulsion 30.

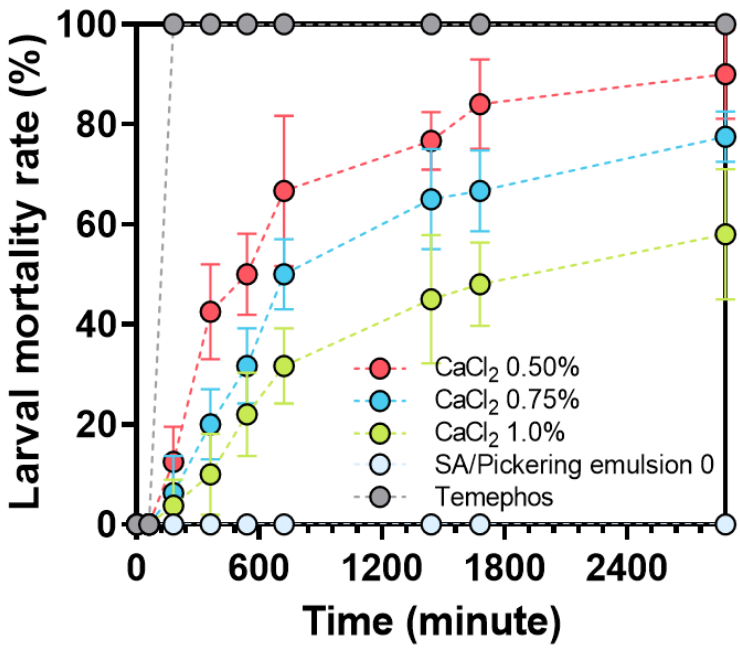

Figure 52. Larvicidal activity of SA/Pickering emulsion hydrogel beads prepared at the different $CaCl_2$ solution concentration.

The larvicidal activity of SA/Pickering emulsion hydrogel beads could be controlled by the number of beads used for investigation. The larvicidal activity against *Ae. albopictus* larvae was effective when at least 50 hydrogel beads were used for the formation of SA/Pickering emulsion 30 at 0.75 or 0.1% $CaCl_2$ while SA/Pickering emulsion 30 hydrogel beads with 0.5% $CaCl_2$ were effective with lower number of beads due to their higher release rate (Table 13). As shown by a homogeneity analysis, the group of SA/Pickering emulsions hydrogel beads was consistent with the $CaCl_2$ concentration. The SA/Pickering emulsions double *C. officinale* RE-shell structure with sustainability could be stored longer than the existing Pickering emulsions-only systems. The SA/Pickering emulsions composites could be easily removed from water after use, and they maintained larvicidal performance even after 48 hours.

Table 13. Larvicidal activities of SA/Pickering emulsion 30 hydrogel beads against *Ae. albopictus.*

Formulation	Conc. of $CaCl_2$ (%)	Larvicidal Activity (%, Mean ± S.E, N=4)[1]		
		70[2]	50	35
SA/ Pickeirng emulsion30	0.50	100a	100a	90.0±8.94ab
	0.75	100a	100a	77.5±5.00bc
	1.0	100a	100a	62.5±13.0c
SA/Pickering emulsion 0		0d	0d	0d
Temephos[3]		100a	100a	100a

[1] Means within a column followed by same letters are not significantly different (P = 0.05, Scheffe's test).
[2] Number of SA/Pickering emulsions hydrogel beads used
[3] Used at a concentration of 10 ppm in all tests

5.4. Summary

Highly volatile thyme white was entrapped primarily by S-CNCs and secondarily by SA to reduce the volatility of the essential oils and sustain their controlled release. The incorporation of Pickering emulsions with SA was confirmed with FTIR and XRD characterizations. The release of essential oils from the SA-Pickering emulsions was varied by the gelling conditions, such as Pickering emulsion and $CaCl_2$ concentrations, because the cross-linking density of the composite hydrogels determined their release behavior. Thymol was released in a controlled manner from SA-Pickering emulsions hydrogel beads without a severe initial discharge of essential oils. The sustained release of thymol was effective in the enhancement of larvicidal activity.

VI. Conclusion

The first aim of this research is to observe the charge effects of ionic CNCs at the Pickering emulsion method. The desulfation controlled the surface charge of CNCs with a low concentration of HCl. As desulfation proceeded, the surface of the S-CNC was substituted from sulfate groups to hydroxyl groups, and the dS-CNCs became relatively hydrophobic and de-ionized. The dS-CNCs with different negativity showed the surface charge effect on encapsulation of four nonpolar liquids and two polar liquids. The emulsion stability verified that highly charged S-CNC and dS-CNC (5H) were insufficient as emulsifying agents and required a reducing the surface charge. However, dS-CNC (30H) formed irreversibly packed emulsion droplets with high stability for long-term storage. Consequently, when the CNCs encapsulate the lipophilic liquids with low surface tension or high polarity, the surface charge of the CNC affects to form of Pickering emulsion. It can encapsulate the lipophilic liquids with appropriate control of the CNC's surface charges.

After confirming Pickering emulsion formation by controlling CNC's surface charge, five different essential oils (nutmeg, massoia, *P. kadsura* SE, *C. officinale* RE, and thyme white) were encapsulated by S-CNC to enhance antibacterial and larvicidal activity. The results showed that essential oils could be stably encapsulated and well-dispersed in water by the Pickering emulsions method despite low surface tension and high volatility. S-CNC/essential oil Pickering emulsions showed excellent antimicrobial activity against gram-positive and gram-negative microorganisms, and encapsulated essential oils maintained antimicrobial activity until 25 days. In addition, larvicidal activities of the S-CNC/essential oil Pickering emulsions were stronger than those of crude essential oils. The thyme white Pickering

emulsion enhanced their larvicidal activity 2.6-fold more than crude thyme white. In addition, nutmeg Pickering emulsion showed 2.1-fold, *P. kadsura* SE Pickering emulsion showed 1.7-fold, massoia Pickering emulsion showed 1.3-fold, and *C. officinale* RE Pickering emulsion showed 1.1-fold more active than crude essential oils. These enhancements of larvicidal activities of Pickering emulsion indicate that S-CNC-stabilized Pickering emulsions are suitable for essential oils as a larvicide against mosquito larvae and bactericide against harmful microorganisms.

Thyme white, which showed high antimicrobial and larvicidal activities, was also entrapped primarily by CNCs and secondary by SA to reduce the volatility of the essential oils and sustain their controlled release. Double entrapped thyme white could be controlled their release profile with a multi-layered membrane caused by SA networking and Pickering encapsulation. The release of essential oils from the SA-Pickering emulsions was varied by the gelling conditions, such as Pickering emulsion and $CaCl_2$ concentrations, because the composite hydrogels' cross-linking density determined their release behavior. The release of essential oils from the SA-Pickering emulsions was varied by the gelling conditions, such as Pickering emulsions and $CaCl_2$ concentrations, because the composite hydrogels' cross-linking density and diffusion rate determined their release behavior. Moreover, Pickering emulsified thyme white enhanced SA hydrogel beads' compressive modulus, allowing them to maintain their shape even at high water pressure. Thyme white was released in a controlled manner from SA-Pickering emulsions hydrogel beads without a severe initial discharge of thymol. The composite materials improved their larvicidal activity more than Pickering emulsions at the low concentration of thyme white, and sustained release effectively enhanced larvicidal activity.

VII. Reference

[1] Pickering, S.U., Cxcvi. *Journal of the Chemical Society, Transactions*, **1907**, 91(0), 2001-2021.

[2] Ramsden, W., Separation of solids in the surface-layers of solutions and 'suspensions'(observations on surface-membranes, bubbles, emulsions, and mechanical coagulation).—Preliminary account. *Proceedings of the Royal Society of London*, **1904**, 72(477-486), 156-164.

[3] Torres, L., R. Iturbe, M. Snowden, B. Chowdhry, and S. Leharne, Preparation of o/w emulsions stabilized by solid particles and their characterization by oscillatory rheology. *Colloids and Surfaces A: Physicochemical and Engineering Aspects*, **2007**, 302(1-3), 439-448.

[4] Wu, F., J. Deng, L. Hu, Z. Zhang, H. Jiang, Y. Li, Z. Yi, and T. Ngai, Investigation of the stability in Pickering emulsions preparation with commercial cosmetic ingredients. *Colloids and Surfaces A: Physicochemical and Engineering Aspects*, **2020**, 602, 125082.

[5] Wei, Y.-s., Z.-c. Niu, F.-q. Wang, K. Feng, M.-h. Zong, and H. Wu, A novel Pickering emulsion system as the carrier of tocopheryl acetate for its application in cosmetics. *Materials Science and Engineering: C*, **2020**, 109, 110503.

[6] Simovic, S., N. Ghouchi-Eskandar, and C. Prestidge, Pickering emulsions for dermal delivery. *Journal of Drug Delivery Science and Technology*, **2011**, 21(1), 123-133.

[7] Hua, L., J. Deng, Z. Wang, Y. Wang, B. Chen, Y. Ma, X. Li, and B. Xu,

Improving the functionality of chitosan-based packaging films by crosslinking with nanoencapsulated clove essential oil, *International Journal of Biological Macromolecules*, **2021**, 192, 627-634.

[8] Zhu, J.-Y., C.-H. Tang, S.-W. Yin, and X.-Q. Yang, Development and characterization of novel antimicrobial bilayer films based on Polylactic acid (PLA)/Pickering emulsions, *Carbohydrate Polymers*, **2018,** 181, 727-735.

[9] Rehman, A., S.M. Jafari, R.M. Aadil, E. Assadpour, M.A. Randhawa, and S. Mahmood, Development of active food packaging via incorporation of biopolymeric nanocarriers containing essential oils, *Trends in Food Science and Technology*, **2020**, 101, 106-121.

[10] Zhou, T., Z. Huang, F. Wan, and Y. Sun, Carbon quantum dots-stabilized Pickering emulsion to prepare NIR light-responsive PLGA drug delivery system, *Materials Today Communications*, **2020**, 23, 100951.

[11] Elmotasem, H., H.K. Farag, and A.A. Salama, *In vitro* and *in vivo* evaluation of an oral sustained release hepatoprotective caffeine loaded w/o Pickering emulsion formula–Containing wheat germ oil and stabilized by magnesium oxide nanoparticles, *International Journal of Pharmaceutics*, **2018**, 547(1-2), 83-96.

[12] Bergfreund, J., Q. Sun, P. Fischer, and P. Bertsch, Adsorption of charged anisotropic nanoparticles at oil–water interfaces. *Nanoscale Advances*, **2019**. 1(11). 4308-4312.

[13] Pang, K., B. Ding, X. Liu, H. Wu, Y. Duan, and J. Zhang, High-yield preparation of a zwitterionically charged chitin nanofiber and its application in a doubly pH-responsive Pickering emulsion, *Green Chemistry*, **2017**,

19(15), 3665-3670.

[14] Aveyard, R., J.H. Clint, D. Nees, and V.N. Paunov, Compression and structure of monolayers of charged latex particles at air/water and octane/water interfaces, *Langmuir*, **2000**, 16(4), 1969-1979.

[15] Mazeau, K. and L. Heux, Molecular dynamics simulations of bulk native crystalline and amorphous structures of cellulose, *The Journal of Physical Chemistry B*, **2003**, 107(10), 2394-2403.

[16] Maurer, R.J., A.F. Sax, and V. Ribitsch, Molecular simulation of surface reorganization and wetting in crystalline cellulose I and II, *Cellulose*, **2013**, 20(1), 25-42.

[17] Kalashnikova, I., H. Bizot, B. Cathala, and I. Capron, Modulation of cellulose nanocrystals amphiphilic properties to stabilize oil/water interface. *Biomacromolecules*, **2012**, 13(1), 267-275.

[18] Chen, L.H. and P.S. Doyle, Design and use of a thermogelling methylcellulose nanoemulsion to formulate nanocrystalline oral dosage forms. *Advanced Materials*, **2021**, 33(29), 2008618.

[19] Shin, J., S.-M. Seo, I.-K. Park, and J. Hyun, Larvicidal composite alginate hydrogel combined with a Pickering emulsion of essential oil, *Carbohydrate Polymers*, **2021**, 254, 117381.

[20] Liu, B., T. Li, W. Wang, L.M. Sagis, Q. Yuan, X. Lei, M.A.C. Stuart, D. Li, C. Bao, and J. Bai, Corncob cellulose nanosphere as an eco-friendly detergent. *Nature Sustainability*, **2020**, 3(6), 448-458.

[21] Bertsch, P., M. Diener, J. Adamcik, N. Scheuble, T. Geue, R. Mezzenga, and P. Fischer, Adsorption and interfacial layer structure of unmodified nanocrystalline cellulose at air/water interfaces, *Langmuir*, **2018**, 34(50), 15195-15202.

[22] Jiang, F. and Y.-L. Hsieh, Holocellulose nanocrystals: amphiphilicity, oil/water emulsion, and self-assembly, *Biomacromolecules*, **2015**, 16(4), 1433-1441.

[23] Tsuji, T., K. Tsuboi, S. Yokota, S. Tagawa, and T. Kondo, Characterization of an amphiphilic Janus-type surface in the cellulose nanofibril prepared by aqueous counter collision, *Biomacromolecules*, **2021**, 22(2), 620-628.

[24] Bergfreund, J., S. Siegenthaler, V. Lutz-Bueno, P. Bertsch, and P. Fischer, Surfactant adsorption to different fluid interfaces. *Langmuir*, **2021**, 37(22), 6722-6727.

[25] Cherhal, F., F. Cousin, and I. Capron, Structural description of the interface of Pickering emulsions stabilized by cellulose nanocrystals, *Biomacromolecules*, **2016**, 17(2), 496-502.

[26] Lu, P. and Y.-L. Hsieh, Preparation and properties of cellulose nanocrystals: rods, spheres, and network, *Carbohydrate Polymers*, **2010**, 82(2), 329-336.

[27] Fleming, K., D.G. Gray, and S. Matthews, Cellulose crystallites, *Chemistry*, **2001**, 7(9), 1831-5.

[28] Bondeson, D., A. Mathew, and K. Oksman, Optimization of the isolation

of nanocrystals from microcrystalline cellulose by acid hydrolysis, *Cellulose*, **2006**, 13(2), 171-180.

[29] Elazzouzi-Hafraoui, S., Y. Nishiyama, J.-L. Putaux, L. Heux, F. Dubreuil, and C. Rochas, The shape and size distribution of crystalline nanoparticles prepared by acid hydrolysis of native cellulose, *Biomacromolecules*, **2008**, 9(1), 57-65.

[30] Tang, J., M.F.X. Lee, W. Zhang, B. Zhao, R.M. Berry, and K.C. Tam, Dual responsive Pickering emulsion stabilized by poly [2-(dimethylamino) ethyl methacrylate] grafted cellulose nanocrystals, *Biomacromolecules*, **2014**, 15(8), 3052-3060.

[31] Song, M.-L., H.-Y. Yu, L.-M. Chen, J.-Y. Zhu, Y.-Y. Wang, J.-M. Yao, Z. Zou, and K.C. Tam, Multibranch strategy to decorate carboxyl groups on cellulose nanocrystals to prepare adsorbent/flocculants and Pickering emulsions, *ACS Sustainable Chemistry and Engineering*, **2019**, 7(7), 6969-6980.

[32] Nigmatullin, R., M.A. Johns, J.C. Muñoz-García, V. Gabrielli, J. Schmitt, J. Angulo, Y.Z. Khimyak, J.L. Scott, K.J. Edler, and S.J. Eichhorn, Hydrophobization of cellulose nanocrystals for aqueous colloidal suspensions and gels, *Biomacromolecules*, **2020**, 21(5), 1812-1823.

[33] Vanderfleet, O.M., J. Winitsky, J. Bras, J. Godoy-Vargas, V. Lafitte, and E.D. Cranston, Hydrothermal treatments of aqueous cellulose nanocrystal suspensions: effects on structure and surface charge content, *Cellulose*, **2021**. 28(16), 10239-10257.

[34] Wang, D., T. Yang, J. Li, J. Zhang, J. Yu, X. Zhang, and J. Zhang,

Thermostable and redispersible cellulose nanocrystals with thixotropic gelation behavior by a facile desulfation process, *ACS Sustainable Chemistry and Engineering*, **2020,** 8(31), 11737-11746.

[35] Abitbol, T., A. Palermo, J.M. Moran-Mirabal, and E.D. Cranston, Fluorescent labeling and characterization of cellulose nanocrystals with varying charge contents, *Biomacromolecules*, **2013**, 14(9), 3278-3284.

[36] Isman, M.B., Plant essential oils for pest and disease management, *Crop Protection*, **2000**, 19(8-10), 603-608.

[37] Mossa, A.-T.H., Green pesticides: essential oils as biopesticides in insect-pest management, *Journal of Environmental Science and Technology*, **2016**, 9(5), 354.

[38] Hung, N.H., L.T. Huong, N.T. Chung, N.T.H. Thuong, P. Satyal, N.A. Dung, T.A. Tai, and W.N. Setzer, *Callicarpa* species from central Vietnam: essential oil compositions and mosquito larvicidal activities, *Plants*, **2020**, 9(1), 113.

[39] Brahmi, F., A. Abdenour, M. Bruno, P. Silvia, P. Alessandra, F. Danilo, Y.-G. Drifa, E.M. Fahmi, M. Khodir, and C. Mohamed, Chemical composition and *in vitro* antimicrobial, insecticidal and antioxidant activities of the essential oils of *Mentha pulegium* L. and *Mentha rotundifolia* (L.) Huds growing in Algeria, *Industrial Crops and Products*, **2016**, 88, 96-105.

[40] Wannes, W.A., B. Mhamdi, J. Sriti, M.B. Jemia, O. Ouchikh, G. Hamdaoui, M.E. Kchouk, and B. Marzouk, Antioxidant activities of the essential oils and methanol extracts from myrtle (*Myrtus communis* var. *italica* L.) leaf, stem and flower, *Food and Chemical Toxicology*, **2010,** 48(5),

1362-1370.

[41] Shin, J., K. Na, S. Shin, S.-M. Seo, H.J. Youn, I.-K. Park, and J. Hyun, Biological activity of thyme white essential oil stabilized by cellulose nanocrystals, *Biomolecules*, **2019**, 9(12), 799.

[42] Seo, S.-M., J. Shin, J.-W. Lee, J. Hyun, and I.-K. Park, Larvicidal activities of *Piper kadsura* (Choisy) Ohwi extract and its constituents against *Aedes albopictus*, toxicity to non-target organisms and development of cellulose nanocrystal-stabilized Pickering emulsion, *Industrial Crops and Products*, **2021**, 162, 113270.

[43] Seo, S.-M., J.-W. Lee, J. Shin, J.-H. Tak, J. Hyun, and I.-K. Park, Development of cellulose nanocrystal-stabilized Pickering emulsions of massoia and nutmeg essential oils for the control of *Aedes albopictus, Scientific Reports*, **2021**, 11(1), 1-12.

[44] Draget, K.I., K. Steinsvåg, E. Onsøyen, and O. Smidsrød, Na- and K-alginate; effect on Ca^{2+}-gelation, *Carbohydrate Polymers*, **1998**, 35(1-2), 1-6.

[45] Klöck, G., A. Pfeffermann, C. Ryser, P. Gröhn, B. Kuttler, H.-J. Hahn, and U. Zimmermann, Biocompatibility of mannuronic acid-rich alginates, *Biomaterials*, **1997**, 18(10), 707-713.

[46] Calabrese, V., J.C. Courtenay, K.J. Edler, and J.L. Scott, Pickering emulsions stabilized by naturally derived or biodegradable particles, *Current Opinion in Green and Sustainable Chemistry*, **2018**, 12, 83-90.

[47] Huq, T., S. Salmieri, A. Khan, R.A. Khan, C. Le Tien, B. Riedl, C.

Fraschini, J. Bouchard, J. Uribe-Calderon, and M.R. Kamal, Nanocrystalline cellulose (NCC) reinforced alginate based biodegradable nanocomposite film, *Carbohydrate Polymers*, **2012**, 90(4), 1757-1763.

[48] Dickinson, E., Emulsion stability, in *Food Hydrocolloids*, **1994**, *Springer*, 387-398.

[49] Friberg, S.E., Emulsion stability, in *Emulsions—A Fundamental and Practical Approach*, **1992**, *Springer*, 1-24.

[50] Tadros, T.F., Emulsion formation and stability, **2013**, *John Wiley & Sons*, 1-5.

[51] Frith, W., R. Pichot, M. Kirkland, and B. Wolf, Formation, stability, and rheology of particle stabilized emulsions: influence of multivalent cations, *Industrial & Engineering Chemistry Research*, **2008**, 47(17), 6434-6444.

[52] Dickinson, E., C. Ritzoulis, and M.J. Povey, Stability of emulsions containing both sodium caseinate and Tween 20, *Journal of Colloid and Interface Science*, **1999**, 212(2), 466-473.

[53] Saito, H., A. Kawagishi, M. Tanaka, T. Tanimoto, S. Okada, H. Komatsu, and T. Handa, Coalescence of lipid emulsions in floating and freeze–thawing processes: examination of the coalescence transition state theory*, Journal of Colloid and Interface Science*, **1999**, 219(1), 129-134.

[54] Yamak, H.B., Emulsion polymerization: Effects of polymerization variables on the properties of vinyl acetate based emulsion polymers, in *Polymer Science*. **2013**, *Intech Open*, 35-72.

[55] Fluksman, A. and O. Benny, A robust method for critical micelle concentration determination using coumarin-6 as a fluorescent probe, *Analytical Methods*, **2019**, 11(30), 3810-3818.

[56] Mondal, S. and S. Ghosh, Role of curcumin on the determination of the critical micellar concentration by absorbance, fluorescence and fluorescence anisotropy techniques, *Journal of Photochemistry and Photobiology B: Biology*, **2012**, 115, 9-15.

[57] Bergfreund, J., S. Siegenthaler, V. Lutz-Bueno, P. Bertsch, and P. Fischer, Surfactant adsorption to different fluid interfaces, *Langmuir*, **2021**, 37(22), 6722–6727.

[58] Gadelha, G., M.S. Nawaz, N.P. Hankins, S.J. Khan, R. Wang, and C.Y. Tang, Assessment of micellar solutions as draw solutions for forward osmosis, *Desalination*, **2014**, 354, 97-106.

[59] Jiao, J., D.G., Rhodes and D.J. Burgess, Multiple emulsion stability: pressure balance and interfacial film strength, *Journal of Colloid and Interface Science*, **2002**, 250(2), 444-450.

[60] Xiao, J. and W. Li, Study on osmotic pressure of non-ionic and ionic surfactant solutions in the micellar and microemulsion regions, *Fluid Phase Equilibria*, **2008**, 263(2), 231-235.

[61] Osanloo, M., A. Amani, H. Sereshti, M.R. Abai, F. Esmaeili, and M.M. Sedaghat, Preparation and optimization nanoemulsion of Tarragon (*Artemisia dracunculus*) essential oil as effective herbal larvicide against *Anopheles stephensi, Industrial Crops and Products*, **2017**, 109, 214-219.

[62] Aswathanarayan, J.B. and R.R. Vittal, Nanoemulsions and their potential applications in food industry. *Frontiers in Sustainable Food Systems*, **2019**. 3. 95.

[63] Low, L.E., S.P. Siva, Y.K. Ho, E.S. Chan, and B.T. Tey, Recent advances of characterization techniques for the formation, physical properties and stability of Pickering emulsion, *Advances in Colloid and Interface Science*, **2020**, 277, 102117.

[64] Pal, R., Modeling of sedimentation and creaming in suspensions and Pickering emulsions, *Fluids*, **2019**, 4(4), 186.

[65] Su, H., C.-A.H. Price, L. Jing, Q. Tian, J. Liu, and K. Qian, Janus particles: design, preparation, and biomedical applications, *Materials Today Bio*, **2019**, 4, 100033.

[66] Jeffrey, G.A. and L.M. Wingert, Carbohydrate liquid crystals, *Liquid Crystals*, **1992**, 12(2), 179-202.

[67] Uraki, Y., Y. Usukura, T. Kishimoto, and M. Ubukata, Amphiphilicity of a lignin-carbohydrate complex, *Wood Research and Technology Holzforschung*, **2006**, 60(6), 659-664.

[68] Chen, T., P.J. Colver, and S.A. Bon, Organic–inorganic hybrid hollow spheres prepared from TiO_2-stabilized Pickering emulsion polymerization, *Advanced Materials*, **2007**, 19(17), 2286-2289.

[69] Wang, H., L. Zhao, G. Song, G. Tang, and X. Shi, Organic–inorganic hybrid shell microencapsulated phase change materials prepared from SiO_2/TiC-stabilized Pickering emulsion polymerization. *Solar Energy*

Materials and Solar Cells, **2018**, 175, 102-110.

[70] Chang, F., C. Vis, M. Bergmeijer, S. Howes, and P. Bruijnincx, Bifunctional Janus silica spheres for Pickering interfacial tandem catalysis, *Chem Sus Chem*, **2021**, 14(23), 5328-5335.

[71] Archer, R.J., A.J. Parnell, A.I. Campbell, J.R. Howse, and S.J. Ebbens, A Pickering emulsion route to swimming active Janus colloids, *Advanced Science*, **2018**, 5(2), 1700528.

[72] Yang, Y., Z. Fang, X. Chen, W. Zhang, Y. Xie, Y. Chen, Z. Liu, and W. Yuan, An overview of Pickering emulsions: solid-particle materials, classification, morphology, and applications, *Frontiers in Pharmacology*, **2017**, 8, 287.

[73] Binks, B.P., Particles as surfactants—similarities and differences, *Current Opinion in Colloid & Interface Science*, **2002**, 7(1-2), 21-41.

[74] Zhou, W., J. Cao, W. Liu, and S. Stoyanov, How rigid rods self-assemble at curved surfaces, *Angewandte Chemie*, **2009**, 121(2), 384-387.

[75] Daware, S.V. and M.G. Basavaraj, Emulsions stabilized by silica rods via arrested demixing, *Langmuir*, **2015**, 31(24), 6649-6654.

[76] Kaku, Y., S. Fujisawa, T. Saito, and A. Isogai, Synthesis of chitin nanofiber-coated polymer microparticles via Pickering emulsion, *Biomacromolecules*, **2020**, 21(5), 1886-1891.

[77] Luu, X.-C. and A. Striolo, Ellipsoidal Janus nanoparticles assembled at spherical oil/water interfaces, *The Journal of Physical Chemistry B*, **2014**,

118(47), 13737-13743.

[78] Capron, I., O.J. Rojas, and R. Bordes, Behavior of nanocelluloses at interfaces, *Current Opinion in Colloid & Interface Science*, **2017**, 29, 83-95.

[79] Bai, L., S. Huan, W. Xiang, and O.J. Rojas, Pickering emulsions by combining cellulose nanofibrils and nanocrystals: phase behavior and depletion stabilization, *Green Chemistry*, **2018**, 20(7), 1571-1582.

[80] Li, X., H. Li, Q. Xiao, L. Wang, M. Wang, X. Lu, P. York, S. Shi, and J. Zhang, Two-way effects of surfactants on Pickering emulsions stabilized by the self-assembled microcrystals of α-cyclodextrin and oil, *Physical Chemistry Chemical Physics*, **2014**, 16(27), 14059-14069.

[81] Tang, C., S. Spinney, Z. Shi, J. Tang, B. Peng, J. Luo, and K.C. Tam, Amphiphilic cellulose nanocrystals for enhanced Pickering emulsion stabilization, *Langmuir*, **2018**, 34(43), 12897-12905.

[82] Pandey, A., M. Derakhshandeh, S.A. Kedzior, B. Pilapil, N. Shomrat, T. Segal-Peretz, S.L. Bryant, and M. Trifkovic, Role of interparticle interactions on microstructural and rheological properties of cellulose nanocrystal stabilized emulsions, *Journal of Colloid and Interface Science*, **2018**, 532, 808-818.

[83] Ahsan, H.M., X. Zhang, Y. Li, B. Li, and S. Liu, Surface modification of microcrystalline cellulose: Physicochemical characterization and applications in the stabilization of Pickering emulsions, *International Jjournal of Biological Macromolecules*, **2019**, 132, 1176-1184.

[84] Varanasi, S., L. Henzel, L. Mendoza, R. Prathapan, W. Batchelor, R.

Tabor, and G. Garnier, Pickering emulsions electrostatically stabilized by cellulose nanocrystals, *Frontiers in Chemistry*, **2018**, 6, 409.

[85] Tian, S., W. Gao, Y. Liu, and W. Kang, Study on the stability of heavy crude oil-in-water emulsions stabilized by two different hydrophobic amphiphilic polymers, *Colloids and Surfaces A: Physicochemical and Engineering Aspects*, **2019**, 572, 299-306.

[86] Lu, Y., X. Qian, W. Xie, W. Zhang, J. Huang, and D. Wu, Rheology of the sesame oil-in-water emulsions stabilized by cellulose nanofibers, *Food Hydrocolloids*, **2019**, 94, 114-127.

[87] Barnes, H.A., J.F. Hutton, and K. Walters, An introduction to rheology, Vol. 3., **1989**, *Elsevier*, 1-8.

[88] Wang, M., X. Wang, K. Zhang, M. Wu, Q. Wu, J. Liu, J. Yang, and J. Zhang, Nano-hydroxyapatite particle brushes via direct initiator tethering and surface-initiated atom transfer radical polymerization for dual responsive Pickering emulsion, *Langmuir*, **2020**, 36(5), 1192-1200.

[89] Goi, Y., S. Fujisawa, T. Saito, K. Yamane, K. Kuroda, and A. Isogai, Dual functions of tempo-oxidized cellulose nanofibers in oil-in-water emulsions: a pickering emulsifier and a unique dispersion stabilizer, *Langmuir*, **2019**, 35(33), 10920-10926.

[90] Moon, R.J., A. Martini, J. Nairn, J. Simonsen, and J. Youngblood, Cellulose nanomaterials review: structure, properties and nanocomposites, *Chemical Society Reviews*, **2011**, 40(7), 3941-3994.

[91] Siró, I. and D. Plackett, Microfibrillated cellulose and new

nanocomposite materials: a review, *Cellulose*, **2010**, 17(3), 459-494.

[92] Ren, G., M.R. Rosquete, A.G. Peralta, S. Pattathil, M.G. Hahn, T. Wilkop, and G. Drakakaki, Isolation and glycomic analysis of Trans-Golgi network vesicles in Plants, in *Plant Endosomes*. **2020**, *Springer*, 153-167.

[93] Trache, D., A.F. Tarchoun, M. Derradji, T.S. Hamidon, N. Masruchin, N. Brosse, and M.H. Hussin, Nanocellulose: from fundamentals to advanced applications, *Frontiers in Chemistry*, **2020**, 8, 392.

[94] Kalashnikova, I., H. Bizot, P. Bertoncini, B. Cathala, and I. Capron, Cellulosic nanorods of various aspect ratios for oil in water Pickering emulsions, *Soft Matter*, **2013**, 9(3), 952-959.

[95] Li, T., C. Chen, A.H. Brozena, J. Zhu, L. Xu, C. Driemeier, J. Dai, O.J. Rojas, A. Isogai, and L. Wågberg, Developing fibrillated cellulose as a sustainable technological material, *Nature*, **2021**, 590(7844), 47-56.

[96] Bogolitsyn, K., A. Parshina, and L. Aleshina, Structural features of brown algae cellulose, *Cellulose*, **2020**, 27(17), 9787-9800.

[97] Zanchetta, E., E. Damergi, B. Patel, T. Borgmeyer, H. Pick, A. Pulgarin, and C. Ludwig, Algal cellulose, production and potential use in plastics: challenges and opportunities, *Algal Research*, **2021**, 56, 102288.

[98] Jonjaroen, V., S. Ummartyotin, and S. Chittapun, Algal cellulose as a reinforcement in rigid polyurethane foam, *Algal Research*, **2020**, 51, 102057.

[99] Castro, C., R. Zuluaga, J.-L. Putaux, G. Caro, I. Mondragon, and P. Gañán, Structural characterization of bacterial cellulose produced by

Gluconacetobacter swingsii sp. from Colombian agroindustrial wastes, *Carbohydrate Polymers*, **2011**, 84(1), 96-102.

[100] Park, M., D. Lee, and J. Hyun, Nanocellulose-alginate hydrogel for cell encapsulation, *Carbohydrate Polymers*, **2015**, 116, 223-228.

[101] Joseleau, J.-P., V. Chevalier-Billosta, and K. Ruel, Interaction between microfibrillar cellulose fines and fibers: influence on pulp qualities and paper sheet properties, *Cellulose*, **2012**, 19(3), 769-777.

[102] Wu, C.-N., T. Saito, S. Fujisawa, H. Fukuzumi, and A. Isogai, Ultrastrong and high gas-barrier nanocellulose/clay-layered composites, *Biomacromolecules*, **2012**, 13(6), 1927-1932.

[103] Shin, S., H. Kwak, and J. Hyun, Transparent cellulose nanofiber based open cell culture platform using matrix-assisted 3D printing, *Carbohydrate Polymers*, **2019**, 225, 115235.

[104] Isogai, A., T. Saito, and H. Fukuzumi, TEMPO-oxidized cellulose nanofibers, *Nanoscale*, **2011**, 3(1), 71-85.

[105] Vanderfleet, O.M., D.A. Osorio, and E.D. Cranston, Optimization of cellulose nanocrystal length and surface charge density through phosphoric acid hydrolysis, *Philosophical Transactions of the Royal Society A: Mathematical, Physical and Engineering Sciences*, **2018**, 376(2112), 20170041.

[106] Yang, B., Z. Dai, S.-Y. Ding, and C.E. Wyman, Enzymatic hydrolysis of cellulosic biomass, *Biofuels*, **2011**, 2(4), 421-449.

[107] Zhao, Q., G. Sun, K. Yan, A. Zhou, and Y. Chen, Novel bio-antifelting agent based on waterborne polyurethane and cellulose nanocrystals, *Carbohydrate Polymers*, **2013**, 91(1), 169-174.

[108] Williams, N.X., G. Bullard, N. Brooke, M.J. Therien, and A.D. Franklin, Printable and recyclable carbon electronics using crystalline nanocellulose dielectrics, *Nature Electronics*, **2021**, 4(4), 261-268.

[109] Lindman, B., G. Karlström, and L. Stigsson, On the mechanism of dissolution of cellulose, *Journal of Molecular Liquids*, **2010**, 156(1), 76-81.

[110] Glasser, W.G., R.H. Atalla, J. Blackwell, R.M. Brown, W. Burchard, A.D. French, D.O. Klemm, and Y. Nishiyama, About the structure of cellulose: debating the Lindman hypothesis, *Cellulose*, **2012**, 19(3), 589-598.

[111] Park, S., J.O. Baker, M.E. Himmel, P.A. Parilla, and D.K. Johnson, Cellulose crystallinity index: measurement techniques and their impact on interpreting cellulase performance, *Biotechnology for Biofuels*, **2010**, 3(1), 1-10.

[112] Moreau, C., A. Villares, I. Capron, and B. Cathala, Tuning supramolecular interactions of cellulose nanocrystals to design innovative functional materials, *Industrial Crops and Products*, **2016**, 93, 96-107.

[113] Bruel, C., J.R. Tavares, P.J. Carreau, and M.-C. Heuzey, The structural amphiphilicity of cellulose nanocrystals characterized from their cohesion parameters, *Carbohydrate Polymers*, **2019**, 205, 184-191.

[114] Gestranius, M., P. Stenius, E. Kontturi, J. Sjöblom, and T. Tammelin, Phase behaviour and droplet size of oil-in-water Pickering emulsions

stabilised with plant-derived nanocellulosic materials, *Colloids and Surfaces A: Physicochemical and Engineering Aspects*, **2017**, 519, 60-70.

[115] Kannam, S.K., D.P. Oehme, M.S. Doblin, M.J. Gidley, A. Bacic, and M.T. Downton, Hydrogen bonds and twist in cellulose microfibrils, *Carbohydrate Polymers*, **2017**, 175, 433-439.

[116] Azzam, F., L. Heux, J.-L. Putaux, and B. Jean, Preparation by grafting onto, characterization, and properties of thermally responsive polymer-decorated cellulose nanocrystals, *Biomacromolecules*, **2010**, 11(12), 3652-3659.

[117] Matthews, J.F., M. Bergenstråhle, G.T. Beckham, M.E. Himmel, M.R. Nimlos, J.W. Brady, and M.F. Crowley, High-temperature behavior of cellulose I, *The Journal of Physical Chemistry B*, **2011**, 115(10), 2155-2166.

[118] Kumar, A., Y.S. Negi, V. Choudhary, and N.K. Bhardwaj, Characterization of cellulose nanocrystals produced by acid-hydrolysis from sugarcane bagasse as agro-waste, *Journal of Materials Physics and Chemistry*, **2014**, 2(1), 1-8.

[119] Jiang, F., A.R. Esker, and M. Roman, Acid-catalyzed and solvolytic desulfation of H_2SO_4-hydrolyzed cellulose nanocrystals, *Langmuir*, **2010**, 26(23), 17919-17925.

[120] Wang, D., T. Yang, J. Li, J. Zhang, J. Yu, X. Zhang, and J. Zhang, Thermostable and redispersible cellulose nanocrystals with thixotropic gelation behavior by a facile desulfation process, *ACS Sustainable Chemistry & Engineering*, **2020**, 8(31), 11737-11746.

[121] Kim, D.W., J. Shin, and S.Q. Choi, Nano-dispersed cellulose nanofibrils-PMMA composite from Pickering emulsion with tunable interfacial tensions, *Carbohydrate Polymers*, **2020**, 247, 116762.

[122] Liu, X., X. Qi, Y. Guan, Y. He, S. Li, H. Liu, L. Zhou, C. Wei, C. Yu, and Y. Chen, Transparent and strong polymer nanocomposites generated from Pickering emulsion gels stabilized by cellulose nanofibrils, *Carbohydrate Polymers*, **2019**, 224, 115202.

[123] Fingas, M., Handbook of oil spill science and technology. **2014**, *John Wiley & Sons*, 39-49.

[124] Mariod, A.A., M.E.S. Mirghani, and I. Hussein, Unconventional oilseeds and oil sources. **2017**, *Academic Press Cambridge, MA, USA*, 293-297.

[125] Fingas, M., Introduction to oil chemistry and properties, in *Oil Spill Science and Technology*, **2011**, *Elsevier*. 51-59.

[126] Hirasaki, G.J., S.-W. Lo, and Y. Zhang, NMR properties of petroleum reservoir fluids, *Magnetic Resonance Imaging*, **2003**, 21(3-4), 269-277.

[127] Akmaz, S., A.C. Alpak, M. Haktanır, and M. Yaşar, Comparison of molecular properties of saturate and aromatic fractions of Turkish and Iraqi crude oil residues, *Journal of Petroleum Science and Engineering*, **2020**, 195, 107923.

[128] Zheljazkov, V.D., C.L. Cantrell, T. Astatkie, and E. Jeliazkova, Distillation time effect on lavender essential oil yield and composition, *Journal of Oleo Science*, **2013**, 62(4), 195-199.

[129] Cassel, E., R. Vargas, N. Martinez, D. Lorenzo, and E. Dellacassa, Steam distillation modeling for essential oil extraction process, *Industrial Crops and Products*, **2009**, 29(1), 171-176.
[130] Mejri, J., A. Aydi, M. Abderrabba, and M. Mejri, Emerging extraction processes of essential oils: a review, *Asian Journal of Green Chemistry*, **2018**, 2(3), 246-267.

[131] Chávez-González, M.L., L. Sepúlveda, D.K. Verma, H.A. Luna-García, L.V. Rodríguez-Durán, A. Ilina, and C.N. Aguilar, Conventional and emerging extraction processes of flavonoids, *Processes*, **2020**, 8(4), 434.

[132] Grande-Tovar, C.D., C. Chaves-Lopez, A. Serio, C. Rossi, and A. Paparella, Chitosan coatings enriched with essential oils: effects on fungi involved in fruit decay and mechanisms of action, *Trends in Food Science & Technology*, **2018**, 78, 61-71.

[133] Peng, Y. and Y. Li, Combined effects of two kinds of essential oils on physical, mechanical and structural properties of chitosan films, *Food Hydrocolloids*, **2014**, 36, 287-293.

[134] Zhou, Y., S. Sun, W. Bei, M.R. Zahi, Q. Yuan, and H. Liang, Preparation and antimicrobial activity of oregano essential oil Pickering emulsion stabilized by cellulose nanocrystals, *International Journal of Biological Macromolecules*, **2018**, 112, 7-13.

[135] Al-Jumaili, A., A. Kumar, K. Bazaka, and M.V. Jacob, Plant secondary metabolite-derived polymers: a potential approach to develop antimicrobial films, *Polymers*, **2018**, 10(5), 515.

[136] Bonizzoni, M., G. Gasperi, X. Chen, and A.A. James, The invasive mosquito species *Aedes albopictus*: current knowledge and future perspectives, *Trends in Parasitology*, **2013**, 29(9), 460-468.

[137] Organization, W.H., Global insecticide use for vector-borne disease control: a 10-year assessment [2000-2009], **2011**, *World Health Organization*, 1-49.

[138] Vontas, J., E. Kioulos, N. Pavlidi, E. Morou, A. Della Torre, and H. Ranson, Insecticide resistance in the major dengue vectors *Aedes albopictus* and *Aedes aegypti, Pesticide Biochemistry and Physiology*, **2012**, 104(2), 126-131.

[139] Anadu, D., H. Anaso, and O. Onyeka, Acute toxicity of the insect larvicide abate®(temephos) on the fish *tilapia melanopleura* and the dragonfly larvae *neurocordelia virginiensis, Journal of Environmental Science & Health Part B*, **1996**, 31(6), 1363-1375.

[140] Abban, E. and J. Samman, Preliminary observations on the effect of the insect larvicide abate on fish catches in the river Oti, Ghana, *Environmental Pollution Series A, Ecological and Biological*, **1980**, 21(4), 307-311.

[141] Jantan, I.b., M.F. Yalvema, N.W. Ahmad, and J.A. Jamal, Insecticidal activities of the leaf oils of eight *Cinnamomum*. species *Against Aedes aegypti*. and *Aedes albopictus. Pharmaceutical Biology*, **2005**, 43(6), 526-532.

[142] Cheng, S.S., H.T. Chang, C.Y. Lin, P.S. Chen, C.G. Huang, W.J. Chen, and S.T. Chang, Insecticidal activities of leaf and twig essential oils from *Clausena excavata* against *Aedes aegypti* and *Aedes albopictus* larvae, *Pest Management Science: Formerly Pesticide Science*, **2009**, 65(3), 339-343.

[143] Benelli, G., G. Flamini, G. Fiore, P.L. Cioni, and B. Conti, Larvicidal and repellent activity of the essential oil of *Coriandrum sativum* L.(Apiaceae) fruits against the filariasis vector *Aedes albopictus* Skuse (Diptera: Culicidae), *Parasitology Research*, **2013**, 112(3), 1155-1161.

[144] Conti, B., G. Benelli, G. Flamini, P.L. Cioni, R. Profeti, L. Ceccarini, M. Macchia, and A. Canale, Larvicidal and repellent activity of *Hyptis suaveolens* (Lamiaceae) essential oil against the mosquito *Aedes albopictus* Skuse (Diptera: Culicidae), *Parasitology Research*, **2012**, 110(5), 2013-2021.

[145] Govindarajan, M., R. Sivakumar, M. Rajeswary, and K. Yogalakshmi, Chemical composition and larvicidal activity of essential oil from *Ocimum basilicum* (L.) against *Culex tritaeniorhynchus*, *Aedes albopictus* and *Anopheles subpictus* (Diptera: Culicidae), *Experimental Parasitology*, **2013**, 134(1),7-11.

[146] Zhang, H., Y. Qian, S. Chen, and Y. Zhao, Physicochemical characteristics and emulsification properties of cellulose nanocrystals stabilized O/W pickering emulsions with high $-OSO_3^-$ groups, *Food Hydrocolloids*, **2019**, 96, 267-277.

[147] da Silva Perez, D., S. Montanari, and M.R. Vignon, TEMPO-mediated oxidation of cellulose III, *Biomacromolecules*, **2003**, 4(5), 1417-1425.

[148] Tang, Z., W. Li, X. Lin, H. Xiao, Q. Miao, L. Huang, L. Chen, and H. Wu, TEMPO-oxidized cellulose with high degree of oxidation, *Polymers*, **2017**, 9(9), 421.

[149] Ruan, C., Y. Zhu, X. Zhou, N. Abidi, Y. Hu, and J.M. Catchmark, Effect of cellulose crystallinity on bacterial cellulose assembly, *Cellulose*, **2016**,

23(6), 3417-3427.

[150] Kralchevsky, P., R. Miller, and F. Ravera, Colloid and interface chemistry for nanotechnology. Vol. 4., **2016**, *CRC Press*, 77-110.

[151] Kassab, Z., E. Syafri, Y. Tamraoui, H. Hannache, and M. El Achaby, Characteristics of sulfated and carboxylated cellulose nanocrystals extracted from Juncus plant stems, *International Journal of Biological Macromolecules*, **2020**, 154, 1419-1425.

[152] Torlopov, M.A., I.S. Martakov, V.I. Mikhaylov, P.V. Legki, Y.A. Golubev, E.F. Krivoshapkina, C. Tracey, P.A. Sitnikov, and E.V. Udoratina, Manipulating the colloidal properties of (non-) sulfated cellulose nanocrystals via stepwise surface cyanoethylation/carboxylation, *European Polymer Journal*, **2019**, 115, 225-233.

[153] Criado, P., C. Fraschini, M. Jamshidian, S. Salmieri, N. Desjardins, A. Sahraoui, and M. Lacroix, Effect of cellulose nanocrystals on thyme essential oil release from alginate beads: Study of antimicrobial activity against *Listeria innocua* and ground meat shelf life in combination with gamma irradiation, *Cellulose*, **2019**, 26(9), 5247-5265.

[154] Börjesson, M., K. Sahlin, D. Bernin, and G. Westman, Increased thermal stability of nanocellulose composites by functionalization of the sulfate groups on cellulose nanocrystals with azetidinium ions, *Journal of Applied Polymer Science*, **2018**, 135(10), 45963.

[155] Sakkayawong, N., P. Thiravetyan, and W. Nakbanpote, Adsorption mechanism of synthetic reactive dye wastewater by chitosan, *Journal of Colloid and Interface Science*, **2005**, 286(1), 36-42.

[156] Delgado, E.J. and G.A. Diaz, A molecular structure based model for predicting surface tension of organic compounds, *SAR and QSAR in Environmetal Research*, **2006**, 17(5), 483-96.

[157] Shibuichi, S., T. Yamamoto, T. Onda, and K. Tsujii, Super water-and oil-repellent surfaces resulting from fractal structure, *Journal of Colloid and Interface Science*, **1998**, 208(1), 287-294.

[158] Guarda, A., J.F. Rubilar, J. Miltz, and M.J. Galotto, The antimicrobial activity of microencapsulated thymol and carvacrol*, International Journal of Food Microbiology*, **2011**, 146(2), 144-150.

[159] Rasooli, I., M.B. Rezaei, and A. Allameh, Ultrastructural studies on antimicrobial efficacy of thyme essential oils on *Listeria monocytogenes, International Journal of Infectious Diseases*, **2006**, 10(3), 236-241.

[160] Marino, M., C. Bersani, and G. Comi, Antimicrobial activity of the essential oils of *Thymus vulgaris* L. measured using a bioimpedometric method, *Journal of Food Protection*, **1999**, 62(9), 1017-1023.

[161] Burt, S., Essential oils: their antibacterial properties and potential applications in foods—a review, *International Journal of Food Microbiology*, **2004**, 94(3), 223-253.

[162] Wei, Y.P., F. Cheng, G. Hou, and S.F. Sun, Amphiphilic cellulose: Surface activity and aqueous self-assembly into nano-sized polymeric micelles, *Reactive & Functional Polymers*, **2008**, 68(5), 981-989.

[163] Kalashnikova, I., H. Bizot, B. Cathala, and I. Capron, New Pickering emulsions stabilized by bacterial cellulose nanocrystals, *Langmuir*, **2011**,

27(12), 7471-7479.

[164] Cunha, A.G., J.B. Mougel, B. Cathala, L.A. Berglund, and I. Capron, Preparation of double Pickering emulsions stabilized by chemically tailored nanocelluloses, *Langmuir*, **2014**, 30(31), 9327-9335.

[165] Jiménez Saelices, C. and I. Capron, Design of Pickering micro-and nanoemulsions based on the structural characteristics of nanocelluloses, *Biomacromolecules*, **2018**, 19(2), 460-469.

[166] Saidane, D., E. Perrin, F. Cherhal, F. Guellec, and I. Capron, Some modification of cellulose nanocrystals for functional Pickering emulsions, *Philosophical Transactions of the Royal Society A: Mathematical, Physical and Engineering Sciences*, **2016**, 374(2072), 20150139.

[167] Jimenez-Saelices, C., B. Seantier, Y. Grohens, and I. Capron, Thermal superinsulating materials made from nanofibrillated cellulose-stabilized Pickering emulsions, *ACS Applied Materials & Interfaces*, **2018**, 10(18), 16193-16202.

[168] Bai, L., L.G. Greca, W. Xiang, J. Lehtonen, S. Huan, R.W.N. Nugroho, B.L. Tardy, and O.J. Rojas, Adsorption and assembly of cellulosic and lignin colloids at oil/water interfaces, *Langmuir*, **2018**, 35(3), 571-588.

[169] Habibi, M.H. and R. Sheibani, Removal of 2-mercaptobenzoxazole from water as model of odorous mercaptan compounds by a heterogenous photocatalytic process using Ag-ZnO nanocomposite coated thin film on glass plate, *Bulletin of Environmental Contamination and Toxicology*, **2010**, 85(6), 589-592.

[170] Shin, S. and J. Hyun, Matrix-assisted three-dimensional printing of cellulose nanofibers for paper microfluidics. *ACS Applied Materials & Interfaces*, **2017**, 9(31), 26438-26446.

[171] Saelices, C.J. and I. Capron, Design of Pickering micro- and nanoemulsions based on the structural characteristics of nanocelluloses, *Biomacromolecules*, **2018**, 19(2), 460-469.

[172] Wiegand, I., K. Hilpert, and R.E. Hancock, Agar and broth dilution methods to determine the minimal inhibitory concentration (MIC) of antimicrobial substances, *Nature Protocols*, **2008**, 3(2), 163-175.

[173] Cheng, S., C. Lin, M. Chung, Y. Liu, C. Huang, and S. Chang, Larvicidal activities of wood and leaf essential oils and ethanolic extracts from *Cunninghamia konishii* Hayata against the dengue mosquitoes, *Industrial Crops and Products*, **2013**, 47, 310-315.

[174] Lee, D.C. and Y.-J. Ahn, Laboratory and simulated field bioassays to evaluate larvicidal activity of *Pinus densiflora* hydrodistillate, its constituents and structurally related compounds against *Aedes albopictus*, *Aedes aegypti* and *Culex pipiens pallens* in relation to their inhibitory effects on acetylcholinesterase activity, *Insects*, **2013**, 4(2), 217-229.

[175] Seo, S.-M., C.-S. Jung, J. Kang, H.-R. Lee, S.-W. Kim, J. Hyun, and I.-K. Park, Larvicidal and acetylcholinesterase inhibitory activities of Apiaceae plant essential oils and their constituents against *Aedes albopictus* and formulation development, *Journal of Agricultural and Food Chemistry*, **2015**, 63(45), 9977-9986.

[176] Govindarajan, M., M. Rajeswary, S. Hoti, A. Bhattacharyya, and G.

Benelli, Eugenol, *α*-pinene and *β*-caryophyllene from *Plectranthus barbatus* essential oil as eco-friendly larvicides against malaria, dengue and Japanese encephalitis mosquito vectors, *Parasitology Research*, **2016**, 115(2), 807-815.

[177] Bhardwaj, A., D. Kumar Tewary, R. Kumar, V. Kumar, A. Kumar Sinha, and A. Shanker, Larvicidal and structure–activity studies of natural phenylpropanoids and their semisynthetic derivatives against the tobacco armyworm *Spodoptera litura* (F_{AB}.)(Lepidoptera: Noctuidae), *Chemistry & Biodiversity*, **2010**, 7(1), 168-177.

[178] Du, S.S., K. Yang, C.F. Wang, C.X. You, Z.F. Geng, S.S. Guo, Z.W. Deng, and Z.L. Liu, Chemical constituents and activities of the essential oil from *Myristica fragrans* against cigarette beetle *Lasioderma serricorne, Chemistry & Biodiversity*, **2014**, 11(9), 1449-1456.

[179] Hammond, D.G. and I. Kubo, Structure–activity relationship of alkanols as mosquito larvicides with novel findings regarding their mode of action, *Bioorganic & Medicinal Chemistry*, **1999**, 7(2), 271-278.

[180] Seo, S.-M., J. Kim, E. Kim, H.-M. Park, Y.-J. Kim, and I.-K. Park, Structure− activity relationship of aliphatic compounds for nematicidal activity against pine wood nematode (*Bursaphelenchus xylophilus*), *Journal of Agricultural and Food Chemistry*, **2010**, 58(3), 1823-1827.

[181] Park, I.-K., S.-G. Lee, S.-C. Shin, J.-D. Park, and Y.-J. Ahn, Larvicidal activity of isobutylamides identified in *Piper nigrum* fruits against three mosquito species, *Journal of Agricultural and Food Chemistry*, **2002**, 50(7), 1866-1870.

[182] Miyakado, M., I. Nakayama, H. Yoshioka, and N. Nakatani, The

Piperaceae amides I: Structure of pipercide, a new insecticidal amide from *Piper nigrum* L, *Agricultural and Biological Chemistry*, **1979**, 43(7), 1609-1611.

[183] Miyakado, M., I. Nakayama, and H. Yoshioka, Insecticidal joint action of pipercide and co-occurring compounds isolated from *Piper nigrum* L, *Agricultural and Biological Chemistry*, **1980**, 44(7), 1701-1703.

[184] Navickiene, H.M.D., J.E. Miranda, S.A. Bortoli, M.J. Kato, V.S. Bolzani, and M. Furlan, Toxicity of extracts and isobutyl amides from *Piper tuberculatum*: potent compounds with potential for the control of the velvetbean caterpillar, *Anticarsia gemmatalis*, *Pest Management Science: Formerly Pesticide Science*, **2007**, 63(4), 399-403.

[185] Ladeira Macedo, A., T. Carvalho Costa dos Santos, A. Leda Valverde, D. de Lima Moreira, and T. Rocha Alves Vasconcelos, An overview of neolignans of the genus *Piper* L.: isolation methods and biological activities, *Mini Reviews in Medicinal Chemistry*, **2017**, 17(8), 693-720.

[186] Chauret, D.C., C.B. Bernard, J.T. Arnason, T. Durst, H. Krishnamurty, P. Sanchez-Vindas, N. Moreno, L. San Roman, and L. Poveda, Insecticidal neolignans from *Piper decurrens*, *Journal of Natural Products*, **1996**, 59(2), 152-155.

[187] Narciso, J.O.A., R.O. de Araújo Soares, J.R. dos Santos Mallet, A.É. Guimarães, M.C. de Oliveira Chaves, J.M. Barbosa-Filho, and M. Maleck, Burchellin: study of bioactivity against *Aedes aegypti*, *Parasites & Vectors*, **2014**, 7(1), 1-10.

[188] Matsui, K. and K. Munakata, The structure of piperenone, a new insect

antifeeding substance from *Piper futokadzura*, *Tetrahedron Letters*, **1975**, 16(24), 1905-1908.

[189] Tang, C., Y. Chen, J. Luo, M.Y. Low, Z. Shi, J. Tang, Z. Zhang, B. Peng, and K.C. Tam, Pickering emulsions stabilized by hydrophobically modified nanocellulose containing various structural characteristics, *Cellulose*, **2019**, 26(13-14), 7753-7767.

[190] Ziaee, E., M. Razmjooei, E. Shad, and M.H. Eskandari, Antibacterial mechanisms of *Zataria multiflora* Boiss. essential oil against *Lactobacillus curvatus*, *LWT-Food Science and Technology*, **2018**, 87, 406-412.

[191] War, A.R., M.G. Paulraj, T. Ahmad, A.A. Buhroo, B. Hussain, S. Ignacimuthu, and H.C. Sharma, Mechanisms of plant defense against insect herbivores, *Plant Signaling & Behavior*, **2012**, 7(10), 1306-1320.

[192] Senthil-Nathan, S., A review of resistance mechanisms of synthetic insecticides and botanicals, phytochemicals, and essential oils as alternative larvicidal agents against mosquitoes. *Frontiers in Physiology*, **2020**, 10, 1591.

[193] Kraemer, M.U., M.E. Sinka, K.A. Duda, A.Q. Mylne, F.M. Shearer, C.M. Barker, C.G. Moore, R.G. Carvalho, G.E. Coelho, W. Van Bortel, G. Hendrickx, F. Schaffner, I.R. Elyazar, H.J. Teng, O.J. Brady, J.P. Messina, D.M. Pigott, T.W. Scott, D.L. Smith, G.R. Wint, N. Golding, and S.I. Hay, The global distribution of the arbovirus vectors *Aedes aegypti* and *Ae. albopictus*. *Elife*, **2015**, 4, e08347.

[194] Sanborn, M.A., T.A. Klein, H.-C. Kim, C.K. Fung, K.L. Figueroa, Y. Yang, E.A. Asafo-adjei, R.G. Jarman, and J. Hang, Metagenomic analysis reveals three novel and prevalent mosquito viruses from a single pool of

Aedes vexans nipponii collected in the Republic of Korea, *Viruses*, **2019**, 11(3), 222.

[195] Tyler, K.L., Emerging viral infections of the central nervous system: part 1, *Archives of Neurology*, **2009**, 66(8), 939-948.

[196] Nauen, R., Insecticide resistance in disease vectors of public health importance, *Pest Management Science: Formerly Pesticide Science*, **2007**, 63(7), 628-633.

[197] Nkya, T.E., I. Akhouayri, W. Kisinza, and J.-P. David, Impact of environment on mosquito response to pyrethroid insecticides: facts, evidences and prospects, *Insect Biochemistry and Molecular Biology*, **2013**, 43(4), 407-416.

[198] Wang, Z., H. Perumalsamy, X. Wang, and Y.-J. Ahn, Toxicity and possible mechanisms of action of honokiol from *Magnolia denudata* seeds against four mosquito species, *Scientific Reports*, **2019**, 9(1), 1-19.

[199] Pavela, R., Insecticidal activity of some essential oils against larvae of *Spodoptera littoralis*, *Fitoterapia*, **2005**, 76(7-8), 691-696.

[200] Tabari, M.A., M.R. Youssefi, F. Maggi, and G. Benelli, Toxic and repellent activity of selected monoterpenoids (thymol, carvacrol and linalool) against the castor bean tick, *Ixodes ricinus* (Acari: Ixodidae), *Veterinary Parasitology*, **2017**, 245, 86-91.

[201] Yang, J.M. and H.C. Chiu, Preparation and characterization of polyvinyl alcohol/chitosan blended membrane for alkaline direct methanol fuel cells, *Journal of Membrane Science*, **2012**, 419, 65-71.

[202] Lee, S., H. Tae, and C.S. Ki, Fabrication of schizophyllan hydrogel via orthogonal thiol-ene photopolymerization, *Carbohydrate Polymers*, **2017**, 167, 270-279.

[203] Lin, N., C.c. Bruzzese, and A. Dufresne, TEMPO-oxidized nanocellulose participating as crosslinking aid for alginate-based sponges, *ACS Applied Materials & Interfaces*, **2012**, 4(9), 4948-4959.

[204] Fujisawa, S., Y. Okita, H. Fukuzumi, T. Saito, and A. Isogai, Preparation and characterization of TEMPO-oxidized cellulose nanofibril films with free carboxyl groups, *Carbohydrate Polymers*, **2011**, 84(1), 579-583.

[205] Huq, T., B. Riedl, J. Bouchard, S. Salmieri, and M. Lacroix, Microencapsulation of nisin in alginate-cellulose nanocrystal (CNC) microbeads for prolonged efficacy against *Listeria monocytogenes*, *Cellulose*, **2014**, 21(6), 4309-4321.

[206] Guidetti, G., S. Atifi, S. Vignolini, and W.Y. Hamad, Flexible photonic cellulose nanocrystal films, *Advanced Materials*, **2016**, 28(45), 10042-10047.

[207] Thakur, S., B. Sharma, A. Verma, J. Chaudhary, S. Tamulevicius, and V.K. Thakur, Recent progress in sodium alginate based sustainable hydrogels for environmental applications, *Journal of Cleaner Production*, **2018**, 198, 143-159.

[208] Huang, B., M. Liu, Z. Long, Y. Shen, and C. Zhou, Effects of halloysite nanotubes on physical properties and cytocompatibility of alginate composite hydrogels, *Materials Science and Engineering: C*, **2017**, 70, 303-310.

[209] Fan, Q., C. Jiang, W. Wang, L. Bai, H. Chen, H. Yang, D. Wei, and L.

Yang, Eco-friendly extraction of cellulose nanocrystals from grape pomace and construction of self-healing nanocomposite hydrogels, *Cellulose*, **2020**, 27(5), 2541-2553.

[210] Zhang, X.Z., Y.X. Wang, X.G. Luo, A. Lu, Y. Li, B. Li, and S.L. Liu, O/W Pickering emulsion templated organo-hydrogels with enhanced mechanical strength and energy storage capacity. *ACS Applied Bio Materials*, **2019**, 2(1). 480-487.

[211] Tanpichai, S., S.K. Biswas, S. Witayakran, and H. Yano, Optically transparent tough nanocomposites with a hierarchical structure of cellulose nanofiber networks prepared by the Pickering emulsion method, *Composites Part A: Applied Science and Manufacturing*, **2020**, 132, 105811.

[212] Zhao, S., Z. Wang, H. Kang, W. Zhang, J. Li, S. Zhang, L. Li, and A. Huang, Construction of bioinspired organic-inorganic hybrid composite by cellulose-induced interfacial gelation assisted with Pickering emulsion template, *Chemical Engineering Journal*, **2019**, 359, 275-284.

[213] Zou, S., Z. Wei, Y. Hu, Y. Deng, Z. Tong, and C. Wang, Macroporous antibacterial hydrogels with tunable pore structures fabricated by using Pickering high internal phase emulsions as templates, *Polymer Chemistry*, **2014**, 5(14), 4227-4234.

[214] Tawakkal, I.S., M.J. Cran, and S.W. Bigger, Release of thymol from poly (lactic acid)-based antimicrobial films containing kenaf fibres as natural filler, *LWT-Food Science and Technology*, **2016**, 66, 629-637.

[215] Ramos, M., A. Beltrán, M. Peltzer, A.J. Valente, and M. del Carmen Garrigós, Release and antioxidant activity of carvacrol and thymol from

polypropylene active packaging films, *LWT-Food Science and Technology*, **2014**, 58(2), 470-477.

[216] Graham, N. and M. McNeill, Hydrogels for controlled drug delivery. *Biomaterials*, **1984**, 5(1), 27-36.

[217] Kahya, N. and F.B. Erim, Surfactant modified alginate composite gels for controlled release of protein drug, *Carbohydrate Polymers*, **2019**, 224, 115165.

[218] Lee, K.Y. and D.J. Mooney, Hydrogels for tissue engineering, *Chemical Reviews*, **2001**, 101(7), 1869-1880.

초 록

이온성 셀룰로오스 나노결정(CNC)은 친유성 액체를 담지할 수 있는 피커링 입자이다. CNC는 황산으로 가수분해하여 표면에 sulfate 그룹이 도입되었고, 그로 인해 화학적으로 음전하를 띤 CNC (S-CNC)가 제조되었다. S-CNC의 양친매성 특성에도 불구하고 표면 에너지가 낮고 극성이 높은 오일을 유화하기 위해서는 표면 치환도의 조절을 통해 표면 음전하의 조절이 필요하다. S-CNC의 탈황은 CNC의 추가적인 가수분해를 막기 위해 낮은 농도의 염산 용액을 사용하여 진행되었으며 반응 시간에 따른 탈황된 S-CNC (dS-CNC)이 제조되었다. S-CNC의 탈황 반응으로부터 감소된 CNC의 표면 전하는 CNC에 상대적으로 상대적으로 높은 소수성 친화도를 부여한다. 표면 전하가 감소한 CNC의 유화 양상을 확인하기 위해 표면 장력이 낮은 6가지 다른 오일이 선택되었다. 에멀젼의 콜로이달 안정성은 CNC/오일 피커링 에멀젼의 에멀젼 분획, 입자 크기 및 표면 장력에 의해 평가되었다.

6가지 오일에 대한 CNC의 표면 전하 효과를 확인한 후, 5가지 다른 고휘발성 및 소수성 에센셜 오일을 양친매성 CNC에 의해 캡슐화하여 항유충 및 항균 효과를 관찰할였다. 염색 용액을 통한 표지를 통해 공초점 현미경 이미지를 관찰하여 CNC가 에센셜 오일을 안정적으로 감싸고 있음을 확인하였다. CNC의 양은 에센셜 오일 피커링 에멀젼의 액적 크기 분포에 영향을

미쳤고, 유변학적 특성과 표면장력에 의해 피커링 에멀젼의 유화 안정성이 확인되었다. 에센셜 오일 및 에멀젼의 항균 활성은 대장균(*E. coli*) 및 황색 포도상구균(*S. aureus*)의 최소 억제 농도 및 최소 살균 농도에 의해 평가되었으며 지속 가능성 또한 평가되었다. 살유충 활성은 모기 유충인 *Aedes albopictus* (Skuse) (*Ae. albopictus*) 애벌레에 대하여 평가되었다.

피커링 에멀젼을 하이드로젤로 담지하는 과정은 에센셜 오일의 방출 거동을 조절하고 회수성을 용이하게 하여 조금 더 친환경적인 도입을 가능하게 한다. 마이크로 사이즈의 피커링 에멀젼은 알긴산 나트륨(SA)에 담지되었다. 화학 및 물리적 특성 분석을 통해 SA-CNC/에센셜 오일 피커링 에멀젼 복합 하이드로겔 비드의 특성을 관찰하였다. 복합체의 시간에 따른 에센셜 오일 활성은 thymol의 방출 거동을 통해 평가되었다. SA-피커링 에멀젼 복합 하이드로겔 비드의 살유충 활성은 모기 유충인 *Ae. albopictus* 장구벌레로 평가되었다.

색인어: 셀룰로오스 나노결정, 표면 전하 효과, 탈황반응, 피커링 에멀젼, 에센셜 오일, 유충 제거 활성, 항균 활성

학번: 2017-21230